Meadowlark

the clean, green, flying machine

A highly efficient, highly profitable, hybrid-electric aircraft giving customers a jet experience without the emissions.

Zane Black
1340030

Olivia Caudillo
1422281

Matthew Donnelly
1230108

Olivia Hughes
1422975

KU
THE UNIVERSITY OF
KANSAS

Haley Anne Mahusay
14222310

Anna Parnell
1387737

Caroline Smith
1340124

Hannah Wilson
1315218

Advisor: Dr. Ron Barrett-Gonzalez

Compliance Matrix

	Requirement	Compliance	Page
Entry Into Service	2035 for airplane	2035	3
Engines	Existing engines or one that reflects a 2034-certified technology level	PW121 with provisions for future expansion	42
Electric Power	Use of electric motors, controllers, and batteries that would be in service by 2034	Use of electric motors, controllers, and batteries that would be in service by 2034	42
Block Fuel Reduction	20%+ block fuel reduction on 500 nmi mission and emissions reduction vs. current turboprops	20%+ reduction using 36% electric	36
Passenger Capacity (with 30 in. seat pitch)	50 +0/-4 passengers	50 passengers	38
Range	1,000 nmi	1,000 nmi	32
Cruise Speed	Minimum cruise speed of 275 KTAS (350 KTAS target)	393 KTAS	25
Seat Width	Minimum seat with of 17.2 in. (18 in. target) and arm rest width of 2 in.	18 in. seat width 2 in. arm rest width	40
Cross-Section	Standup height similar to competitive aircraft. Baggage compartment is tall enough to be serviced ergonomically. Aisle width of at least 18 in.	Standup height similar to competitive aircraft. Baggage compartment is tall enough to be serviced ergonomically. Aisle width of at least 18 in.	39
Wing Span	Minimum wing span 24 m (target 36 m)	60 ft (18.30 m)	37
Approach Speed	Category C (<141 kts)	141 kts	31
Takeoff Field Length	4,500 ft over a 50 ft obstacle to a runway with dry pavement (ISA + 18°F)	3,300 ft	78
Landing Field Length	4,500 ft over a 50 ft obstacle to a runway with dry pavement (ISA + 18°F) at maximum landing weight	3,300 ft	78
Takeoff and Landing Performance	5,000 ft above mean sea level (ISA + 18°F)	Takes off 5,000 ft above mean sea level	78
Distance to Climb	Less than 200 nmi	Less than 200 nmi	25
Cruise Altitude	FL280 or more	FL300	31
Fuel Burn	Competitive with similar aircraft for 500 nmi	Competitive with similar aircraft for 500 nmi	36
Climb Gradient Requirements	Meet 14 CFR 25.121 Climb Gradient Requirements	Meets 14 CFR 25.121 Climb Gradient Requirements	27
Crew Number	2 pilots and 1 cabin crew for every 50 passengers	2 pilots 1 cabin crew	9
Pilot and Baggage Weight	Pilot/Crew Weight of 190 lb Baggage weight per pilot of 30 lb and volume of at least 4 ft^3 per person	660 lb 4 ft^3 cargo volume	24
Passenger and Baggage Weight	Passenger weight of 200 lb Baggage weight per passenger of 40 lb and 5 ft^3	12,000 lb 5 ft^3 cargo volume	24
Flying Quality	Meets CFR Part 25	Class 1 Flying Quality	73-75

Table of Contents

List of Figures

List of Tables

Acknowledgements

Zane Black

I would like to acknowledge my parents, Ian and Stephanie, as well as my brother Reece, for their continued support of me in my academic endeavors.

Olivia Caudillo

I would like to acknowledge my mom and dad, Irene and Ryan, my sister, Sophia, my brother, Julian, and my grandparents for supporting me in my academic career.

Matthew Donnelly

I would like to acknowledge my parents, Mick and Chris, my four siblings, Kevin, Katie, Claire, and Nathan, and my girlfriend, Grace, for their never-ending support on any path I choose to take.

Olivia Hughes

I would like to acknowledge my parents, Tim and Rita, and my sister, Greta, for always supporting me in everything I do.

Haley Anne Mahusay

I would like to acknowledge my family, the professors I've had at KU, and my high school yearbook teacher, Cherié Burgett, who introduced me to graphic design.

Anna Parnell

I'd like to acknowledge my parents, Jonathan and Lisa, my brothers, Jacob & Brandon, and my best friends, Halle, Caroline, Matt, and AJ, for their continuous love and support throughout my academic career. I'd also like to especially dedicate this work to my granddad, Dr. Darrell Parnell, for showing me how the skies declare the glory of God.

Cary Smith

I would like to acknowledge my mom, Jen, my dad, Mark, my sister, Maddy, my grandparents, Meme, Dor, Grandma, Grandpa, my boyfriend, McCoy, and my best friends, Anna, Halle, Matt, and AJ for always supporting me and making me laugh.

Hannah Wilson

I would like to acknowledge my mom, Beth, my dad, Jeremy, my step-dad, Dave, and my sisters, Emma and Mara, for their constant support throughout my academic career.

List of Symbols

Symbol	Definition	Units
a_{lat}	Lateral Acceleration	ft/s^2 (m/s^2)
a_{vert}	Vertical Acceleration	ft/s^2 (m/s^2)
A	Aspect Ratio	(~)
b	Wing Span	ft (m)
c_r	Root Chord	ft (m)
c_t	Tip Chord	ft (m)
C_D	Drag Coefficient	(~)
C_{D0}	Zero-Lift Drag Coefficient	(~)
$C_{l\beta}$	Rolling Moment Coefficient due to Side Slip Angle	(~)
$C_{l\dot{\beta}}$	Rolling Moment Coefficient due to Side Slip Rate	rad^{-1}
$C_{l\delta\alpha}$	Rolling Moment Coefficient due to Aileron Deflection Angle	rad^{-1}
$C_{l\delta r}$	Rolling Moment Coefficient due to Rudder Deflection Angle	rad^{-1}
C_{lp}	Rolling Moment Coefficient Due to Roll Rate	rad^{-1}
C_{lr}	Rolling Moment Coefficient Due to Yaw Rate	rad^{-1}
C_L	Lift Coefficient	(~)
$C_{L\alpha}$	Lift Coefficient due to AOA	(~)
$C_{L\alpha dyn}$	Dynamic Lift Coefficient due to AOA	(~)
$C_{L\alpha h}$	Lift Coefficient Due to AOA on Horizontal Tail	(~)
$C_{L\alpha w}$	Lift Coefficient due to AOA on Wing	(~)
$C_{L\alpha wf}$	Lift Coefficient due to AOA for Wing-Fuselage	(~)
C_{Lmax}	Maximum Lift Coefficient	(~)
$C_{LmaxClean}$	Clean Maximum Lift Coefficient	(~)

C_{LmaxL} ..... Landing Maximum Lift Coefficient ..... (~)
C_{LmaxTO} ..... Takeoff Maximum Lift Coefficient ..... (~)
$C_{n\beta}$ ..... Yawing Moment Coefficient due to Sideslip ..... deg^{-1}
$C_{n\beta wf}$ ..... Yawing Moment Coefficient due to Sideslip ..... deg^{-1}
$C_{n\delta\alpha}$ ..... Yawing Moment Coefficient due to Aileron Deflection Angle ..... rad^{-1}
$C_{n\delta r}$ ..... Yawing Moment Coefficient due to Rudder Deflection Angle ..... rad^{-1}
C_{np} ..... Yawing Moment Coefficient due to Roll Rate ..... rad^{-1}
C_{nr} ..... Yawing Moment Coefficient due to Yaw Rate ..... rad^{-1}
C_p ..... Brake Specific Fuel Consumption ..... lbs/hp·hr (g/kW·hr)
C_{ride} ..... Ride Comfort Index ..... (~)
$C_{y\beta}$ ..... Side Force Coefficient due to Side Slip Angle ..... (~)
$C_{y\hat{\beta}}$ ..... Side Force Coefficient due to Side Slip Rate ..... rad^{-1}
$C_{y\delta\alpha}$ ..... Side Force Coefficient due to Aileron Deflection Angle ..... rad^{-1}
$C_{y\delta r}$ ..... Side Force Coefficient due to Rudder Deflection Angle ..... rad^{-1}
C_{yp} ..... Side Force Coefficient due to Roll Rate ..... rad^{-1}
C_{yr} ..... Side Force Coefficient due to Yaw Rate ..... rad^{-1}
D_f ..... Fuselage Diameter ..... ft (m)
Do ..... Tire Outer Diameter ..... ft (m)
e ..... Oswald Efficiency Factor ..... (~)
E_{ltr} ..... Loiter Time ..... sec
h ..... Altitude ..... ft (m)
h_{cg} ..... Z-Location of CG ..... ft (m)
i_h ..... Incidence Angle of the Horizontal Tail ..... °
i_w ..... Wing Incidence Angle ..... °
Kt ..... Touchdown Kinetic Energy ..... ft-lbf (Nm)
l_f ..... Fuselage Length ..... ft (m)
l_m ..... Length of Main Gear from CG ..... ft (m)
l_n ..... Length of Nose Gear from CG ..... ft (m)
L/D_{cr} ..... Cruise Lift-to-Drag Ratio ..... (~)
L/D_{ltr} ..... Loiter Lift-to-Drag Ratio ..... (~)
$\bar{q}$ ..... Dynamic Pressure ..... lbs/ft^2 (Pa)
M_{ff} ..... Mission Fuel Fraction ..... (~)
N ..... Load Factor ..... g's
Ng ..... Landing Gear Load Factor ..... (~)
P_m ..... Main Gear Load ..... lbf (N)
P_{max} ..... Maximum Tire Loading ..... lbf (N)
P_n ..... Nose Gear Load ..... lbf (N)
Pm_{dynt} ..... Dynamic Main Gear Load ..... lbf (N)
PM_{max} ..... Maximum Static Main Gear Load ..... lbf (N)
PM_{min} ..... Minimum Static Main Gear Load ..... lbf (N)
Pn_{dynt} ..... Dynamic Nose Gear Load ..... lbf (N)
PN_{max} ..... Maximum Static Nose Gear Load ..... lbf (N)
PN_{min} ..... Minimum Static Nose Gear Load ..... lbf (N)
R ..... Density ..... $slug/ft^3$ (kg/m^3)
rcl ..... Tire Clearance Radius ..... ft (m)
rsl ..... Static Loaded Radius ..... ft (m)
R ..... Range ..... (m)
R_{cr} ..... Cruise Range ..... nmi (m)
s_t ..... Allowable Tire Deflection ..... ft (m)
ss ..... Strut Stroke Deflection ..... ft (m)
S ..... Wing Area ..... ft^2 (m^2)
S_h ..... Horizontal Tail Area ..... ft^2 (m^2)
S_v ..... Vertical Tail Area ..... ft^2 (m^2)
S_{TOFL} ..... Takeoff Distance ..... ft (m)
S_{TOG} ..... Takeoff Ground Distance ..... ft (m)

S_{wetfus} ..... Wetted Fuselage Area ..... ft^2 (m^2)
t_{2s} ..... Spiral Mode Time to Double Amplitude ..... s
t_r ..... Root Thickness ..... ft (m)
t_R ..... Roll Mode Time to Double Amplitude ..... s
t_t ..... Tip Thickness ..... ft (m)
T ..... Thrust ..... lbf (N)
$T_{altitude}$ ..... Thrust at Altitude ..... lbf (N)
t/c ..... Thickness Ratio ..... (~)
$(t/c)_r$ ..... Root Thickness to Chord Ratio ..... (~)
$(t/c)_t$ ..... Tip Thickness to Chord Ratio ..... (~)
$(t/c)_w$ ..... Wing Thickness to Chord Ratio ..... (~)
T/W ..... Thrust-to-Weight Ratio ..... (~)
$(T/W)_{TO}$ ..... Takeoff Thrust-to-Weight Ratio ..... (~)
U ..... Perturbation Speed ..... KTAS (m/s)
V ..... Speed ..... KTAS (m/s)
V_{at} ..... Approach Speed ..... KTAS (m/s)
V_{cr} ..... Cruise Speed ..... KTAS (m/s)
V_{ltr} ..... Loiter Speed ..... KTAS (m/s)
V_{max} ..... Max Speed ..... KTAS (m/s)
V_{SL} ..... Landing Speed ..... KTAS (m/s)
V_{WF} ..... Wing Fuel Volume ..... ft^3 (m^3)
$\bar{V}_h$ ..... Horizontal Tail Volume Coefficient ..... (~)
$\bar{V}_v$ ..... Vertical Tail Volume Coefficient ..... (~)
w_t ..... Touchdown Rate ..... ft/s (m/s)
w_{tire} ..... Tire Width ..... ft (m)
wd ..... Tire Clearance Width ..... ft (m)
W ..... Weight ..... lbs (kg)
W_{ar} ..... Arm Rest Width ..... ft (m)
W_e ..... Empty Weight ..... lbs (kg)
W_f ..... Fuel Weight ..... lbs (kg)
W_i ..... Aisle Width ..... ft (m)
W_L ..... Landing Weight ..... lbs (kg)
W_{oe} ..... Operating Empty Weight ..... lbs (kg)
W_{to} ..... Takeoff Weight ..... lbs (kg)
W_{pl} ..... Payload Weight ..... lbs (kg)
W_s ..... Seat Width ..... ft (m)
W/S ..... Wing Loading ..... lbs/ft^2 (kg/m^2)
$(W/S)_{TO}$ ..... Takeoff Wing Loading ..... lbs/ft^2 (kg/m^2)
X_h ..... CG to the Quarter-Chord of the MGC on the Horizontal Tail ..... ft (m)
$\bar{X}_{ach}$ ..... AC Location of Horizontal Tail from LE to Wing MGC ..... ft (m)
$\bar{X}_{acw}$ ..... AC Location from LE of the Wing MGC ..... ft (m)
X_v ..... CG to the Quarter-Chord of the MGC on the Vertical Tail ..... ft (m)

Greek Symbol ..... **Definition** ..... **Units**

$\delta\varepsilon h/\delta\alpha$ ..... Downwash on Horizontal Tail due to AOA ..... °
$\Delta\bar{X}_{acf}$ ..... Munk Shift ..... ft (m)
$\Delta\bar{X}_{acA}$ ..... AC Location of the Aircraft from the LE of the Wing MGC ..... ft (m)
h_p ..... Propeller Efficiency ..... (~)
α ..... Angle of Attack ..... °
β ..... Sideslip Angle ..... °
δ ..... Change in Altitude ..... ft (m)
δα ..... Change in Aileron Deflection Angle ..... rad
δr ..... Change in Rudder Deflection Angle ..... rad
ζ_{dr} ..... Dutch Roll Damping Coefficient ..... (~)

ζ_{ph}	Phugoid Damping Coefficient	(~)
ζ_{sp}	Short Period Damping Coefficient	(~)
η_s	Shock Absorption Efficiency for Oleo-pneumatic	(~)
η_t	Shock Absorption Efficiency for Tires	(~)
Λ	Sweep Angle	^{o}
$\Lambda_{c1/4}$	Quarter Chord Sweep Angle	^{o}
Λ_h	Sweep Angle of the Horizontal Tail	^{o}
Λ_v	Sweep Angle of Vertical Tail	^{o}
λ	Taper Ratio	(~)
λ_w	Wing Taper Ratio	(~)
ρ	Density	lbs/ft^3 (kg/m^3)
σ	Air Density Ratio	(~)
σ_w	Isotropic Gust	ft/s (m/s)
τ_w	Wing Thickness to Chord Ratio	(~)
ψ	Dihedral Angle	^{o}
ψ_v	Dihedral Angle of Vertical Tail	^{o}
ω_{ndr}	Dutch Roll Natural Frequency	rad/s
ω_{nph}	Phugoid Natural Frequency	rad/s
ω_{nsp}	Short Period Natural Frequency	rad/s

List of Acronyms

Acronyms	Definition	Units
AAA	Advanced Aircraft Analysis	(ft)
AC	Aerodynamic Center	(ft)
ACES	Aircraft Cleaning Expert System	(~)
AEI	All Engines Inoperative	(~)
AIAA	American Institute of Aeronautics and Astronautics	(~)
AO	Ancillary Objective	(~)
APU	Auxiliary Power Unit	(~)
C	Calculated	(~)
CAD	Computer Aided Design	(~)
CFR	Code of Federal Regulations	(~)
CG	Center of Gravity	(ft)
CPU	Central Processing Unit	(~)
CRJ	Canadair Regional Jet	(~)
CONOPS	Concept of Operations	(~)
DOC	Direct Operating Cost	($)
E	Estimation	(~)
EIS	Entry into Service	(~)
ELT	Emergency Locator Transmitter	(~)
EOS	End of Service	(~)
ESC	Electronic Speed Control	(~)
FAA	Federal Aviation Administration	(~)
FAR	Federal Acquisition Regulation	(~)
FL	Flight Level	(ft)
GW	Gross Weight	(lb)
iGOAT	Intelligent Ground Operations Aircraft Tug	(~)
M	Mandatory Requirement	(~)
MGC	Mean Geometric Chord	(ft)
MTOW	Maximum Takeoff Weight	(lb)
NLF	Natural Laminar Flow	(~)
O	Objective	(~)
OEI	One Engine Inoperative	(~)
OF	Objective Function	(~)

PEEK .....Polyether Ether Ketone ..... (~)
P&WC.....Pratt & Whitney Canada ..... (~)
R.....Requirement..... (~)
RE .....Roskam Estimation ..... (~)
RFP .....Request for Proposal ..... (~)
RJ ..... Regional Jet ..... (~)
RTP ..... Regional Turboprop..... (~)
STAMPED..... Statistical Time and Market Predictive Engineering Design..... (~)
T .....Tradeable Requirement ..... (~)
TCAS .....Traffic Alert and Collision Avoidance System ..... (~)

1 Introduction, Concept of Operations, Mission Profile and Specification

The objective of this report is to design and document a 50-passenger hybrid-electric regional turboprop. The American Institute of Aeronautics and Astronautics (AIAA) Request for Proposal (RFP) was written because the current regional turboprop market is commonly based off older designs. Over the next 20 years, around 2,000 regional planes are expected to be built, specifically in the 50-seat range. The hybrid-electric nature of the propulsion system allows for lower direct emissions. [1] Figure 1-1 is the concept of operations, or CONOPS, which depicts general characteristics and the mission of the Meadowlark aircraft as described in the RFP as well as additional advanced technologies.

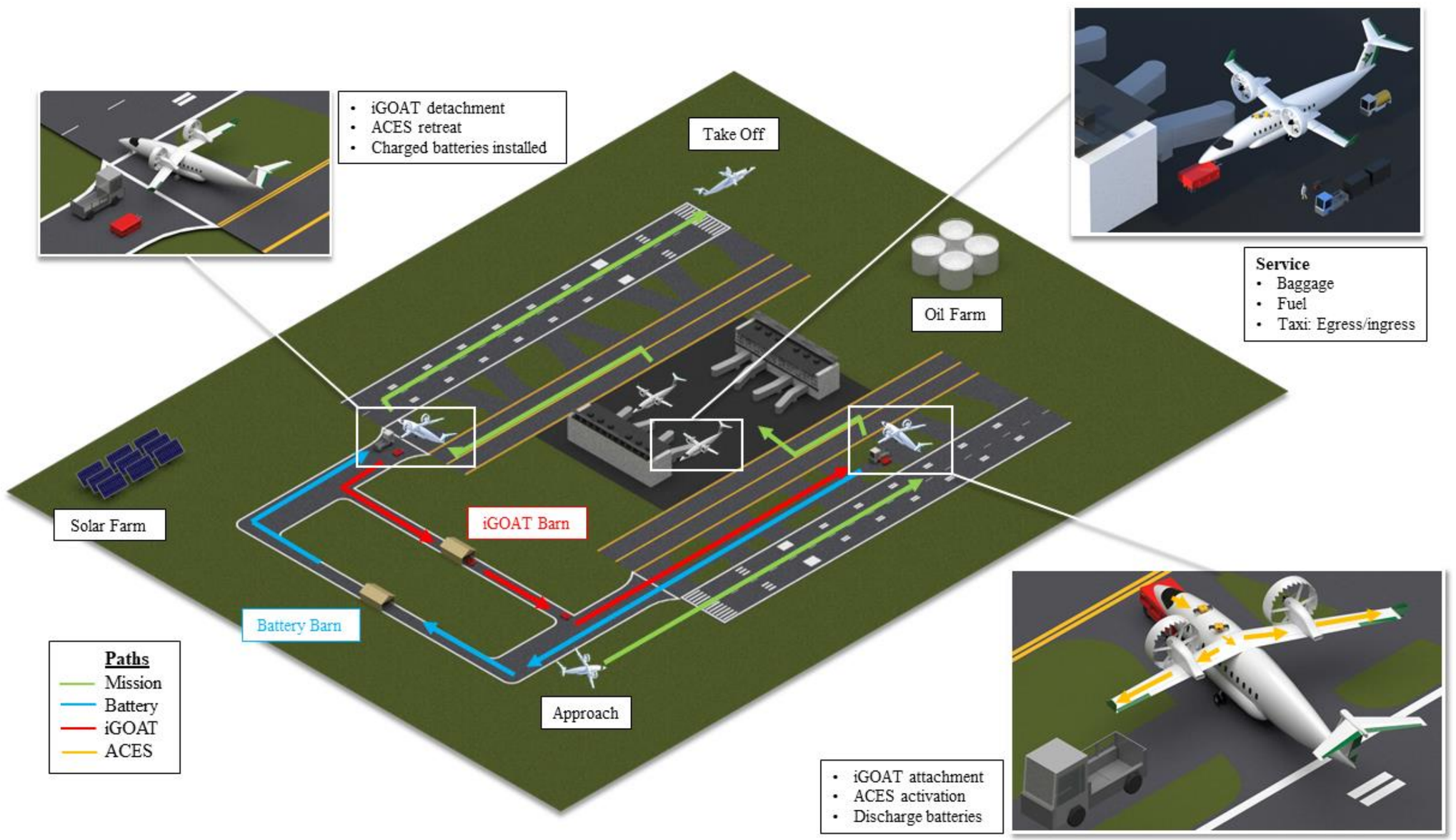

Figure 1-1: Concept of Operations

Table 1.1 contains the design specifications for the hybrid-electric regional turboprop in the RFP. The specifications are outlined below.

Table 1.1: Mission Specification [1]

Aircraft Specifications and Service Life	
Passenger Capacity	(M) 50 +0/-4 in a single class arrangement with 30 inch seat pitch
Design Range	(M) 1,000 nmi with full passengers
Seat and Arm Rest Width	(M) >17.2 inches, (T) target of 18 inches, (M) 2 inch arm rest width
Cross Section	(M) Aisle stand up height similar to competitive aircraft, (M) Baggage compartment tall enough for ergonomic servicing, (M) >18 inch aisle width
Wing Span	(M) <36 m or (T) <24 m
Certification	(M) Certified by 2035 for airplane, certified by 2034 for any new engines (M) Capable of flight in known icing conditions (M) Meets applicable certification rules in Federal Aviation Administration 14 Code of Federal Regulations (CFR) Part 25 (T) Provide systems and avionics architecture that will enable autonomous operations
Performance Requirements	
Approach Speed	(M) Category C <141 kts
Takeoff Field Length	(M) <4,500 ft over a 50 ft obstacle with a runway of dry pavement
Landing Field Length	(M) <4,500 ft over 50 ft obstacle with a runway of dry pavement at maximum landing weight
Takeoff and Landing Altitude	(M) Performance should be shown 5,000 ft above mean sea level
Distance to Climb	(M) <200 nmi to climb to initial cruising altitude
Cruising Altitude and Speed	(M) >FL280 (Flight Level), >275 KTAS Target 350 KTAS
Fuel Burn	(M) 20% reduction in block fuel on a 500 nmi mission vs. current turboprops
Climb Gradient Requirements	(M) Meet 14 CFR 25.121 Climb Gradient Requirements
Payload Requirements	
Crew	(M) 2 pilots and 1 cabin crew member for every 50 passengers
Pilot and Baggage Weights	Pilot/crew weight of 190 lbs, 30 lbs and 4 cubic feet of baggage per person
Passenger and Baggage Weights	200 lbs per passenger, 40 lbs and 5 cubic feet of baggage per passenger

Figure 1-2 shows the mission profile of the Meadowlark aircraft, which splits the aircraft's mission into seven mission phases. The lengths of these phases are arbitrary and track the flow of the mission.

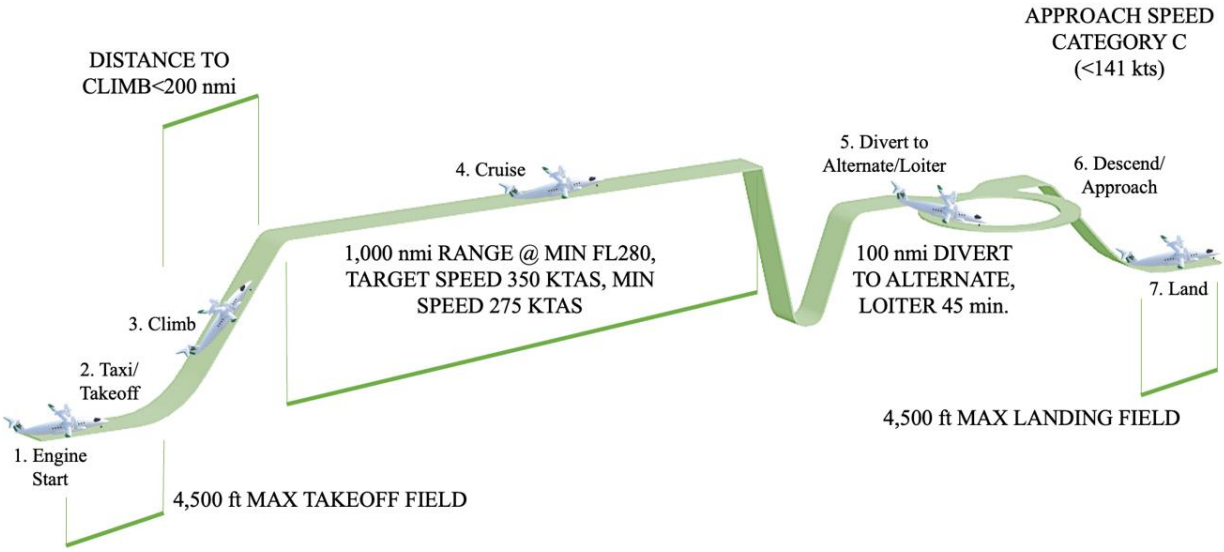

Figure 1-2: Mission Profile

2 Historical Review

The current regional aircraft market consists of jets and turboprops, both of which are important when looking at relevant aircraft for the Meadowlark. Three jets and twelve turboprops were studied to gain a better understanding of the market.

ATR 42-600

Figure 2-1: ATR 42-600 [2]

The ATR 42-600 is the current ATR 42 series aircraft that seats 48 people. The aircraft is powered by two PW127XT-M engines. This program was launched in late 2007 and the first flight took place two and a half years later in 2010. The ATR 42-X00 family consists of 42-200, 42-300, 42-320, 42-400, 42-500, and 42-600S, the short takeoff and landing version of the 42-600. [2] The program is still in service, with 497 aircraft build as of January 2023. [3]

ATR 72-600

Figure 2-2: ATR 72-600 [2]

The ATR 72-600 houses 72 passengers. Like the ATR 42-600, this aircraft is powered by two PW127XT-M engines that can run completely on sustainable aviation fuel. [4] The ATR 72 program was started in 1986 and was delivered in October of 1989. The program continued growing and the ATR 72-600 had its first flight in July of 2009. This aircraft has variations that include the 72-600F, a freighter aircraft for FedEx. [5]

Fokker F-27

The Fokker F-27 Friendship was initiated as a replacement for piston-engine aircraft such as the Douglas DC-3 in the post-war era. The original design fit only 32 seats but was expanded to accommodate 40 passengers in the final design. The original F-27 variant was fitted with Rolls-Royce Dart 511 engines and made its first flight in 1955. Over the 26 years it was in production, over 700 F-27 were built between the Netherlands and the United States and numerous editions including the F27-500 which could fit up to 52 passengers. Upon the development of the F-50 in 1987, the F-27 naturally began being phased out of production. [6]

Figure 2-4: Fokker F-27 [7]

Fokker F-50

Derived from the F-27, the Fokker F-50 completed its maiden flight in December of 1985. This turboprop transport aircraft accommodates 2 crew members and 58 passengers. Powered by two PW125B turboprop engines, the F-50 has a maximum speed of 287 kts. Production of the F-50 ended in 1996 when Fokker went bankrupt with the last aircraft delivered to Ethiopian Airlines in May 1997. In total, 213 F-50s were produced and 168 currently remain operational. [7]

Figure 2-3: Fokker F-50 [7]

EADS CASA C-295

The EADS CASA C-295 (now Airbus C295) was initiated November 1996 for the Spanish Air Force. It is presently used primarily as a military transport aircraft in countries such as Spain, Egypt, Poland, Brazil, Portugal, and others. Other than transport missions, it is also commonly used for medical evacuations, cargo drops, and maritime patrols. Powered by two PW127G turboprop engines, the C-295 can carry 2 crew members and 73 passengers or troops. [8]

Figure 2-5: EADS CASA C-295 [8]

BAe ATP

The BAe ATP is a 64-passenger aircraft that was announced in early 1984, had its first flight in 1986 and entered service in 1988. This aircraft houses 2 PW126A turboprops with six blade composite propellers. There were 63 ATPs built before a redesign and new engine choices (PW127D engines) created the Bae Jetstream 61 in 1994 where 4 were built. The

Figure 2-6: BAe ATP [9]

BAe ATP is still flown, primarily in Sweden as a cargo aircraft. The cargo conversion of this aircraft was first flown in mid-2002. [9]

Saab 2000

Designed with two Rolls-Royce AE 2100P engines and carrying 50-58 passengers, the Saab 2000 first flew in 1992 and entered service in 1994. The successful precursor– the smaller Saab-Fairchild 340 designed to carry just 30-36 passengers –inspired the Swiss company to expand, designing a larger regional turboprop. The Saab 2000 became popular with regional airlines, companies, and private individuals. A total of 63 aircraft were produced with the last Saab 2000 delivered in 1999. Today only 10 remain active, with 4 of them belonging to the Pakistan Air Force. [10]

Figure 2-7: Saab 2000 [10]

Bombardier Dash 8 Q300

The Bombardier Dash 8 Q300 series was first announced in the middle of 1985, and the program moved quickly into motion in the spring of 1986. The first flight for the Q300 series was on the 15th of May in 1987. The Q300 most notably differed from the Q200 by the extended wingtips, and larger interior spaces such as the galley and lavatory. The aircraft was fully certified on the 14th of February in 1989. As of 2006 a total of 243 orders were placed for the Q300. [11]

Figure 2-8: Bombardier Dash 8 Q300 [11]

Bombardier Q400

The Bombardier Dash 8 models were renamed as only Q-series turboprops (Q200, Q300, and Q400). After the production of the first three series aircraft ended in 2008, the Q400 production ramped up. [12] The Q400 seats around 76 passengers and houses two Pratt and Whitney PW150A engines that allow the aircraft to go faster than the previous series of aircraft. The Q400 is extremely successful and has transported more than 400 million passengers as of 2017. [13]

Figure 2-9: Bombardier Q400 [12]

Hawker Siddeley HS 748

The Hawker Siddeley HS 748 is a twin-engine turboprop first developed in the 1950s to be a replacement for the DC-3. The first prototype flew on 24th June 1960. The aircraft seats thirty-six passengers and was originally designed to be a commercial airliner by the British company Avro. [14] However, the aircraft was also often modified by different governments to be utilized as a trainer in the respective navy or air force. Hawker Siddeley eventually manufactured 380 total planes of this design through the year 1988, and the aircraft is still used in some facets today. [15]

Figure 2-10: Hawker Siddeley HS 748 [14]

Handley Page Dart Herald 200

The Handley Page Dart 200 was yet again designed to be a replacement to the DC-3 focused on incorporating newer engine technology of the time. The first prototype flew in 1955, but the Rolls-Royce Dart engine moved the path of the prototype in a new direction and the first flight with the Dart engines was in 1958. The 200 series version was sold during the early 1960s and featured seating of up to 56 compared to the 47 in the 100 series. Dart Heralds have flown a minimum of 2,000 total hours. [16]

Figure 2-11: Handley Page Dart Herald 200 [17]

Embraer EMB 120 Brasilia

The Embraer EMB 120 Brasilia is considered a successful regional turboprop first introduced in 1985. The company has sold 329 EMB 120 Brasilia aircraft in total. At the time of its release, the EMB 120 Brasilia was the fastest turboprop of its kind. The aircraft also had the shortest takeoff range and sat up to 40 people. With the 350 kt cruise speed, and 25,353 lb. maximum take-off weight, the aircraft performed well in the market. "At present, the EMB-120 Brasilia commands a 24% share of the worldwide sales market, in the 21-40 seat category." [18]

Figure 2-12: Embraer EMB 120 Brasilia [19]

Embraer ERJ 145

The Embraer ERJ 145 is a 50-seat passenger airliner that first flew in August of 1995. The turbojet is one of three variants and is the largest of the three. The aircraft has a range of 2,963km and can fly at a maximum speed of 833km/h. The Embraer ERJ

Figure 2-13: Embraer ERJ 145 [20]

145 rears its performance from the two Rolls-Royce AE 3007A engines mounted near the empennage of the aircraft. Their largest customer is ExpressJet Airlines who have ordered 244 total ERJ 145 turbojets. [20]

Bombardier CRJ 700

The Bombardier CRJ 700 is a regional turbojet developed in 1997 that seats between 70 and 78 passengers. The first flight for the CRJ 700 was in 1999 and it was the main competitor to the ERJ 145. The CRJ 700 maximum cruise speed is 829 km/h and the range is 2,553 km. The turbojet aircraft utilizes two CF35-8C5B1 engines from General Electric. Sky West has purchased 102 of these Bombardier CRJ 700s and the aircraft was successful in the market. [21]

Figure 2-15: Bombardier CRJ 700 [21]

Embraer E170

The Embraer E170 is a 70-passenger commercial jet designed after the ERJ-145 and took its maiden flight in February 2002. The E170 has two General Electric CF34-8E engines mounted under the wings giving it a range of 3,889 km with cruise speeds of Mach 0.75. One key design feature that led to the success of the E170 is the "double-bubble" fuselage, providing more volume in the passenger cabin and easier access to overhead compartments. While only 191 E170s were sold, it was a predecessor for other successful aircraft in the Embraer E-Jet family. [22]

Figure 2-14: Embraer E170 [22]

3 Design Optimization Function, Economics Model, Life-Cycle Cost Minimization and Weights

3.1 Design Optimization Function

To assess different designs, a design optimization function is created and the RFP requirements (R_i), design objectives (O_j), and objectives based on ancillary objectives (AO_k) are inserted into the function. Once configurations are determined, they will all be ranked on these weighting functions. The design optimization function can be seen in the equation below.

$$\boldsymbol{OF} = \left(\prod_{i=1}^{20} \boldsymbol{R_i}\right)\left(\sum_{n=1}^{4} \boldsymbol{O_j}\right)\left(\sum_{k=1}^{7}(\boldsymbol{AO_k} * \boldsymbol{weight})\right) \quad \textbf{Equation 3-1}$$

The requirement weighting functions were directly based off of the RFP [1]. Requirements must be completed to have a successful design, which is why they are treated as binary. Design objectives are also found in the RFP, though they are configuration advancements, and are not necessary to meet. The

$$R_i(binary) = \begin{cases} 0 \; is \; criterion \; not \; met \\ 1 \; if \; criterion \; met \end{cases} \quad \textbf{Equation 3-2}$$

equations for the requirements and design objectives are seen in the equations below. Ancillary objectives, on the other hand, are additional design considerations that allow for the aircraft to be more competitive. Each ancillary objective was given a weight from 0 to 1 based on the importance of meeting that objective. After configurations are established, each will be ranked on the 20 requirements, 4 design objectives, and 10 chosen ancillary objectives. These will then be put into the optimization function and a final design value will be found for each configuration. The list of requirements, design objectives, and ancillary objectives are seen in Table 3.1, Table 3.2, and Table 3.3, respectively.

$$O_j = \begin{cases} 0 \text{ if worst at meeting objective} \\ \text{Linear variation if neither best or worst} \\ 1 \text{ if best in meeting objective} \end{cases} \quad \textbf{Equation 3-3}$$

Table 3.1: Design Objectives

Label	Requirement
R_1	50 +0/-4 in a single class arrangement with 30 inch seat pitch
R_2	1,000 nmi range (R) with full passengers
R_3	Seat width (W_s) >17.2 inches
R_4	Arm rest width (W_{ar}) >2 inches
R_5	Aisle stand up height similar to competitive aircraft
R_6	Baggage compartment tall enough for ergonomic servicing
R_7	Aisle width (W_i) >18 inches
R_8	Wingspan (b) <36 m
R_9	Able to be certified by 2035
R_{10}	Capable of flight in known icing conditions
R_{11}	Takeoff field length (TOFL) <4,500 ft over 50 ft obstacle dry pavement
R_{12}	Landing field length (LFL) <4,500 ft over 50 ft obstacle dry pavement
R_{13}	Performance should be shown 5,000 ft above mean sea level
R_{14}	Distance to climb <200 nmi to initial cruise altitude
R_{15}	Approach speed (V_{at}) category C, <141 kts
R_{16}	Cruise altitude >FL280
R_{17}	Cruise speed (V_{cr}) >275 KTAS
R_{18}	20% reduction in block fuel on 500 nmi mission
R_{19}	Meet 14 CFR 25.121 Climb Gradient Requirements
R_{20}	2 pilots and 1 cabin crew member for every 50 passengers

Table 3.2: Design Objectives

Label	Objective
O_1	Target cruise speed of 350 KTAS
O_2	Target seat width of 18 inches
O_3	Minimize wingspan
O_4	Autonomous capabilities

Table 3.1: Ancillary Objectives

Label	Objective	Weight
AO_1	Door width large enough for standard wheelchair	0.8
AO_2	Large tray-tables for an average laptop	0.5
AO_3	Ground turn less than 8 minutes	1
AO_4	European standards for cargo bay	0.7
AO_5	Multiple doors for simultaneous loading and off boarding docks	0.6
AO_6	Allow for engine diameter growth and powerplant upgrades	1
AO_7	Minimal interference with ground traffic	0.5
AO_8	Batteries are on outer mold line of fuselage	0.9
AO_9	Allow for battery pack changes as they improve over time	1
AO_{10}	Ease of meeting Stage 5+ noise regulations	0.9

3.2 Regional Aircraft Fleet Operation Norms, Turnaround Time

Figure 3-1 show the aircraft routes of three major airline companies: American Airlines, United Airlines and Delta Airlines. The blue circles represent large hubs and airports within the routes that contain thirty or more direct destinations. The yellow circles represent hubs airports that have between seven to thirty direct flights. All red circles represent airports that have fewer than seven direct destinations. The data collected and routes shown were influenced by seasonal demand and customer demand. Along with demand, the type of aircraft and the maximum number of passengers on board likely contribute to the route selection for the airlines.

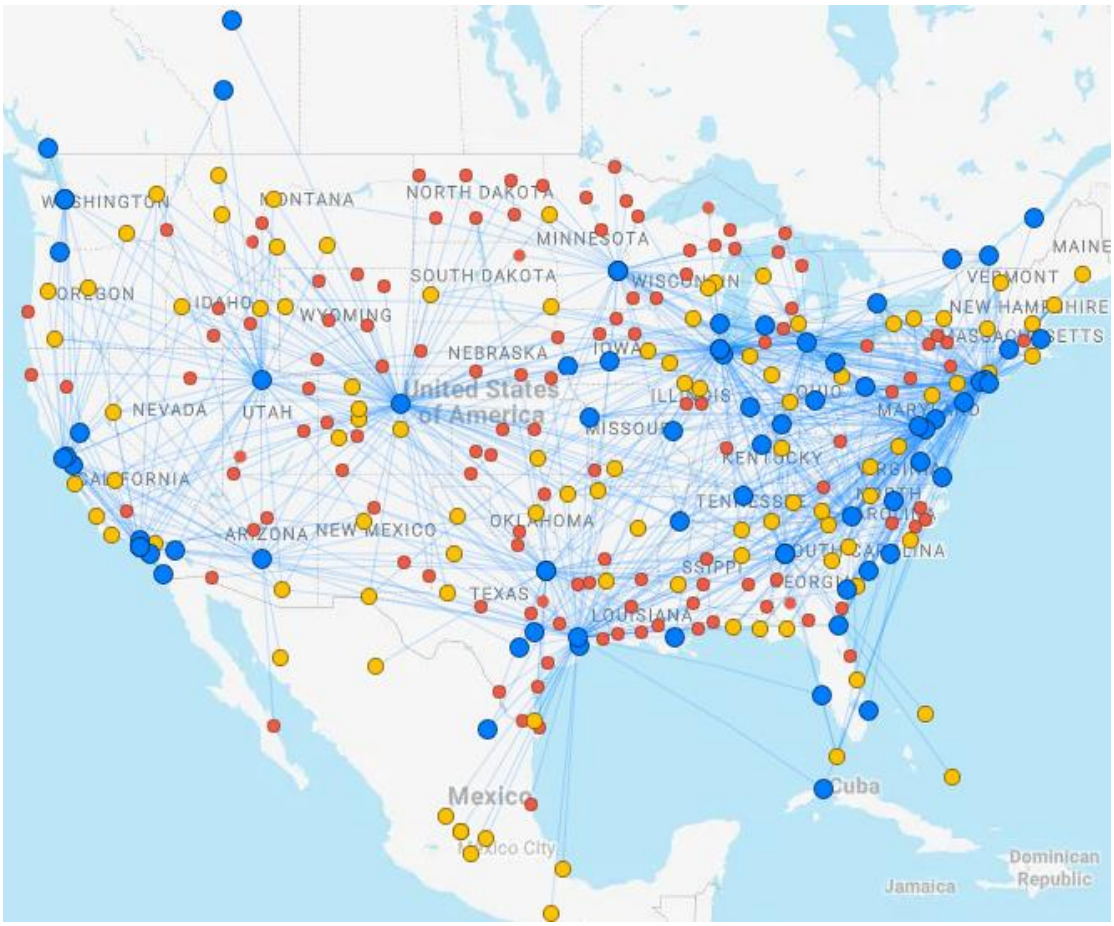

Figure 3-1: Route Flights for June 1, 2023 for Several Airlines

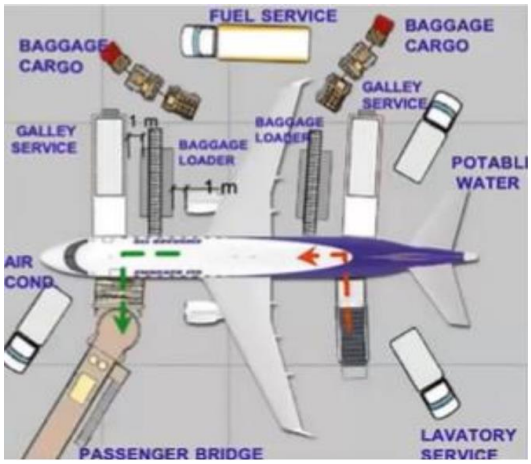

Figure 3-2: Embraer 170/190 Ground Operations Example Diagram [24]

Due to their higher speeds, regional jets can have 1 to 5 legs per day [23], which is more than the typical regional turboprop. The Embraer 170/190 regional jet's ground operations example is seen in Figure 3-2. The positioning of every aspect of the ground operations is crucial to ground turn time and how many aircraft can fit at an airport. Combining and eliminating services can lessen turn time, which is better for customers, the airline company, and the airport. The proposed turnaround time for the Meadowlark aircraft is seen in comparison to a typical regional jet rapid turn, seen in Figure 3-3.

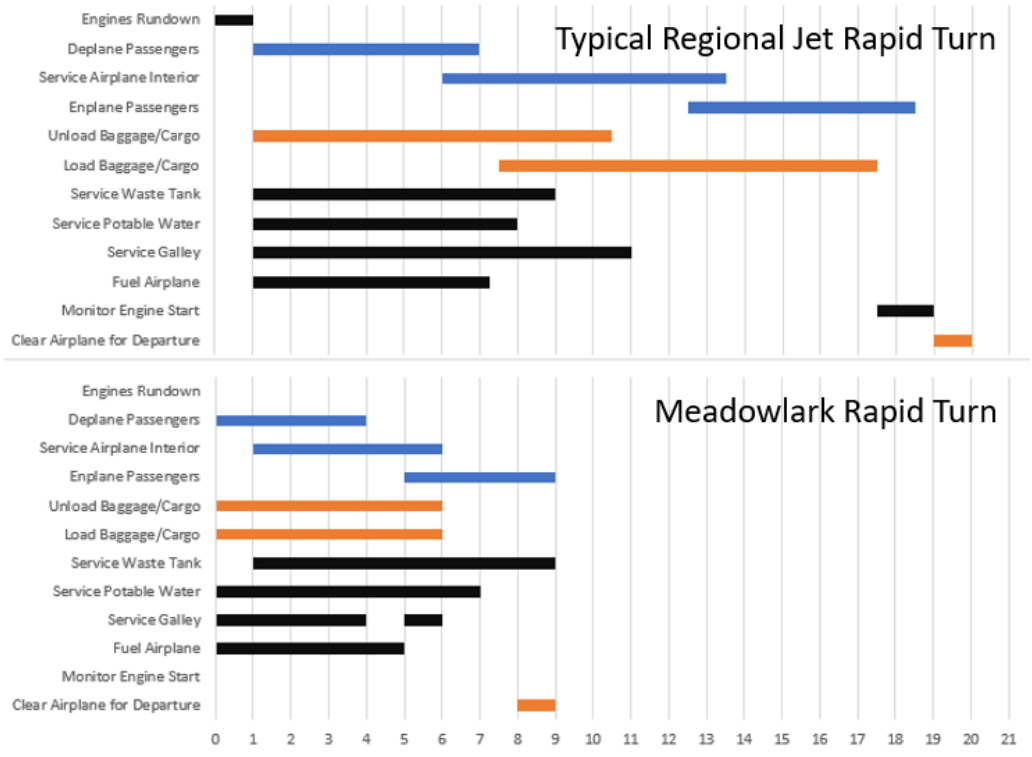

Figure 3-3: Turn Time for Typical Regional Aircraft vs. Meadowlark

The minute gap from minute 4 to minute 5 is the full-cabin sterilization system, which will be discussed in following sections.

3.3 The 50-Passenger Regional Aircraft Market

Over the course of the past decade, regional aircraft demand has changed greatly across the world. Currently, there are two regional jet (RJ) aircraft which are still in production and in widespread use, the Canadair Regional Jet (CRJ) and the Embraer 135. As for regional turboprops, the De Havilland Canada DHC-8 and the Avions Regional Transport ATR 42 are among the most popular regional turboprops (RTP) in the world today [25]. The global distribution of 50-seat regional aircraft may be seen in Figure 3-4.

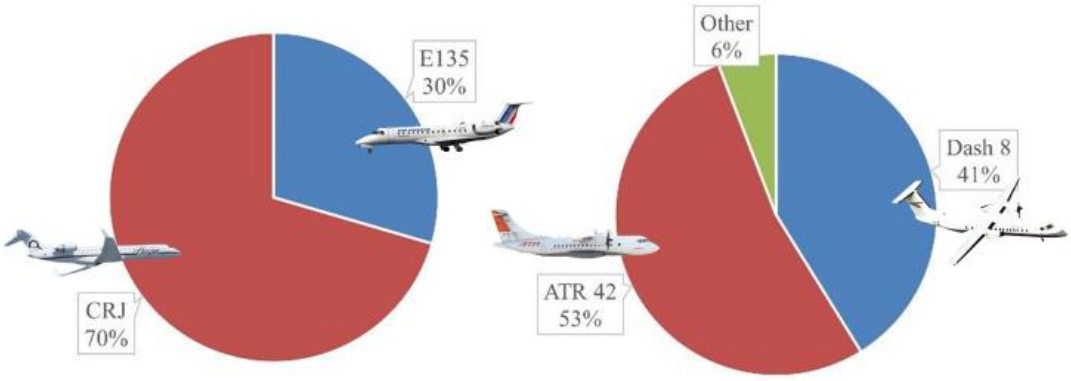

Figure 3-4: 2023 50 Seat Regional Aircraft Global Ownership [25]

In terms of preference by continent, North America heavily favors regional jets, while the rest of the world prefers turbojets, as shown in Figure 3-5.

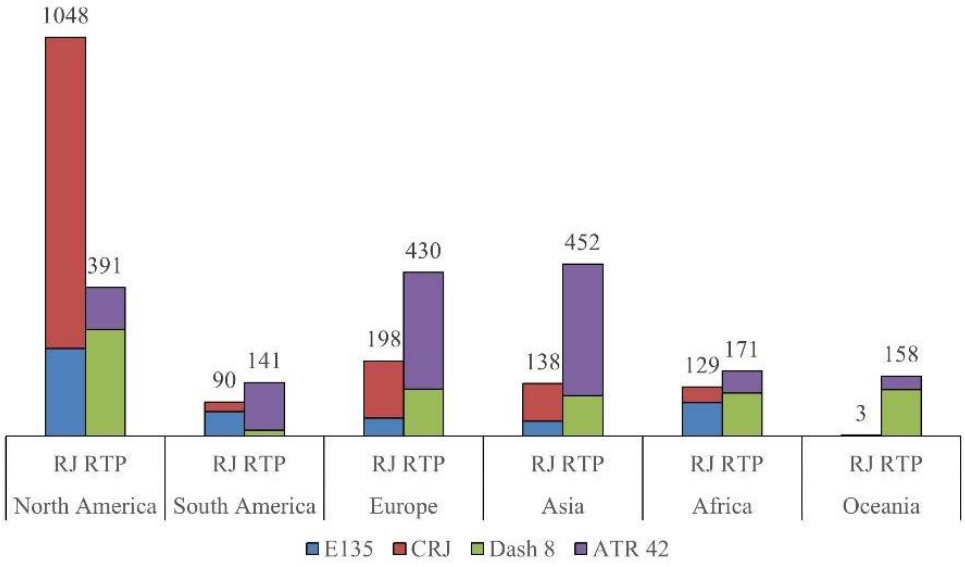

Figure 3-5: 2023 Regional Aircraft Fleets by Continent [25]

Considering these statistics, it was determined that offering an aircraft which is a hybrid in two senses: propulsion and configuration, would be the best suited aircraft for the global market in 2035. As seen in Figure 3-6, the regional aircraft fleet has grown substantially over the past 20 years, and as such it can be inferred that demand will continue to grow.

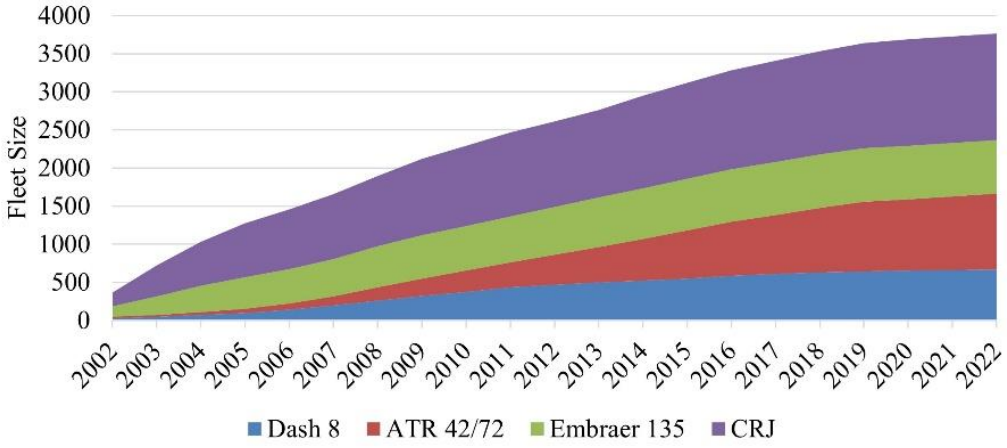

Figure 3-6: 20-Year Regional Aircraft Fleet Growth [25]

3.4 Regional Aircraft Market, Payload-Range, Operating Expenses, Carbon Footprint

Figure 3-7 shows the payload-range diagrams for the Bae ATP (1986), Bombardier Q-400 (1998), ATR 72-600 (2009), Bombardier CRJ-700 (1999), Embraer E170 (2002), and the Embraer ERJ 145 (1995). where MTOW means maximum takeoff weight. These regional jets and turboprop planes shown in the payload-range diagram have a seating capacity of 50-70 people. Figure 3-8 shows the amount American Airlines spent on direct operating cost (DOC) over the span of 28 years. Every year, the amount spent on DOC rises significantly, so by 2035, it can be assumed that the amount to be spent on DOC will greatly exceed $50,000,000.

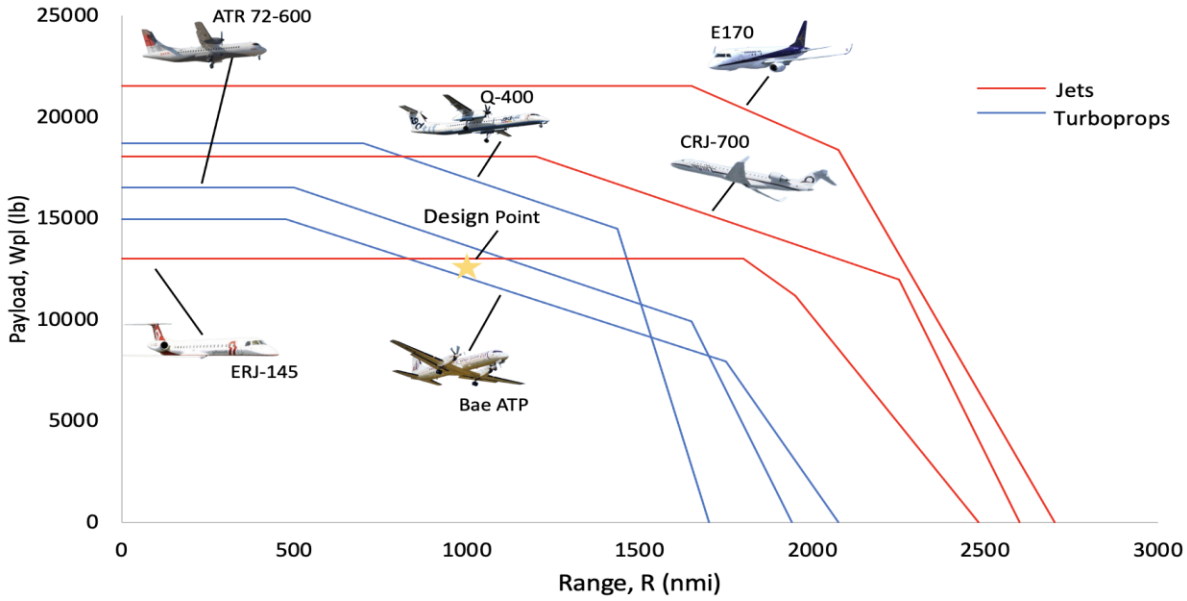

Figure 3-7: STAMPED Payload Range Diagrams

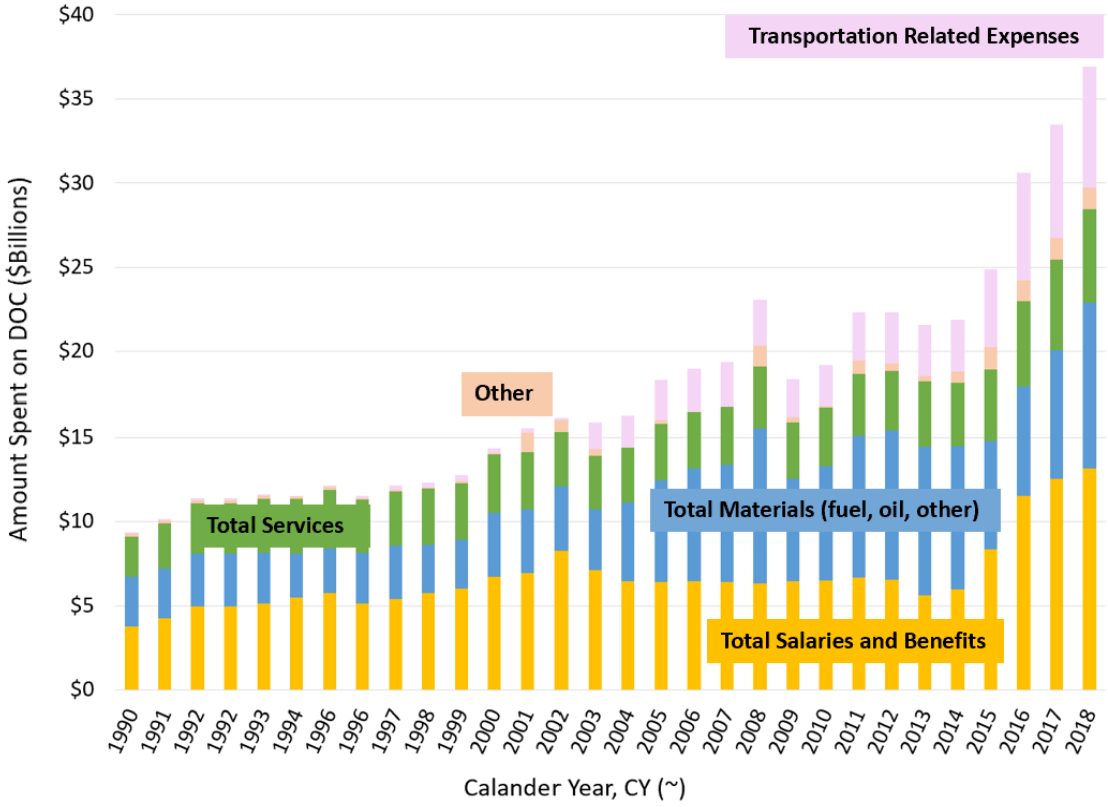

Figure 3-8:American Airlines Total Cost [25]

Figure 3-9 shows an in-depth cost breakdown of the DOC of American Airlines in 2018. The most significant cost comes from salaries and benefits, while materials, which includes fuel, is another significant cost. Both costs contribute to over 50% of the total cost. The lowest percentage cost is the total services.

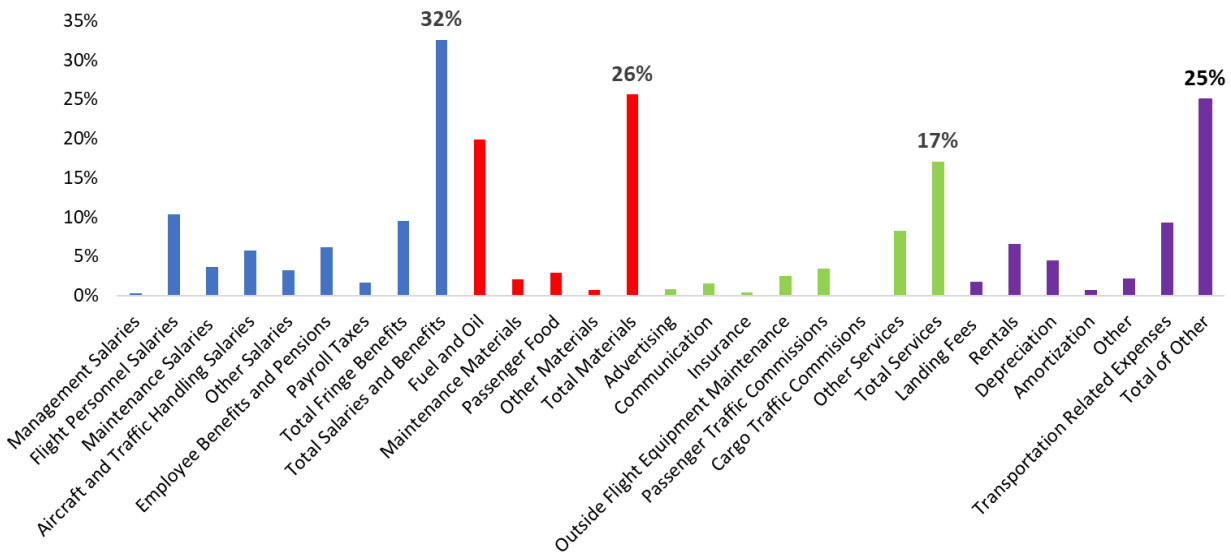

Figure 3-9: 2018 American Airlines DOC by Percentage [25]

Figure 3-10 shows the cost percentage breakdown comparison between a conventional aircraft, SUGAR Volt, and Meadowlark. of DOC American Airlines in 2019. For the three aircrafts, the total salaries and benefits and total materials are the most different between all three. Compared to the conventional aircraft, the SUGAR Volt has a higher personnel cost, especially with flight personal salaries and fringe benefits. With the Meadowlark, the flight personnel, aircraft, and traffic handing costs decrease due to the advanced technologies used, as shown in Figure 1-1.

These technologies are discussed further in Chapter 5. Along with personnel cost, the fuel and oil decrease between the three aircrafts. It is assumed that the SUGAR Volt decreases in fuel cost by about 30%, while the Meadowlark decreases fuel cost up to 35%, depending on electric percentage airline utilize. Overall, to eliminate these costs, the team will implement solutions that will decrease time spent on the runway burning fuel and install automated devices to do jobs that employees are currently doing.

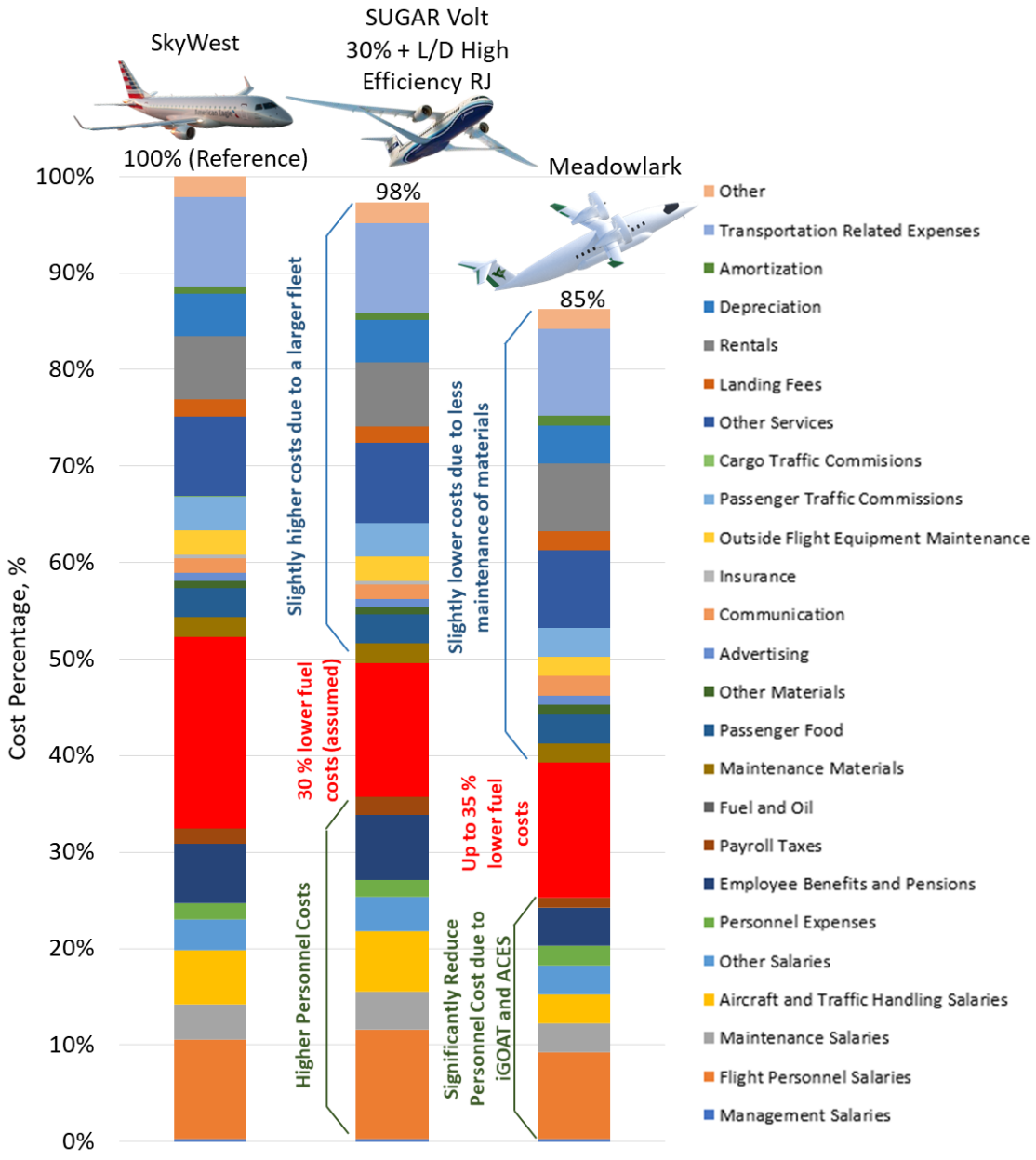

Figure 3-10: DOC of Conventional, SUGAR Volt, and Meadowlark [26][27]

4 STAMPED Analysis of Aircraft Regional Market

To predict how the market has been trending and what designs will be like in 2035, Statistical Time and Market Predictive Engineering Design (STAMPED) techniques were used. This allows for a general understanding of the market's existing aircraft in the regional turboprop and jet category and projection into the future. The trends are found for empty weight to takeoff weight ratio, cruise speed, wing loading, and aspect ratio.

4.1 Empty Weight to Takeoff Weight Ratio

Empty weight (W_e) to takeoff weight (W_{to}) ratio is plotted in Figure 4-1 below. The average regional turboprop aircraft in 2035 will feature an empty weight to takeoff weight ratio of roughly 0.575.

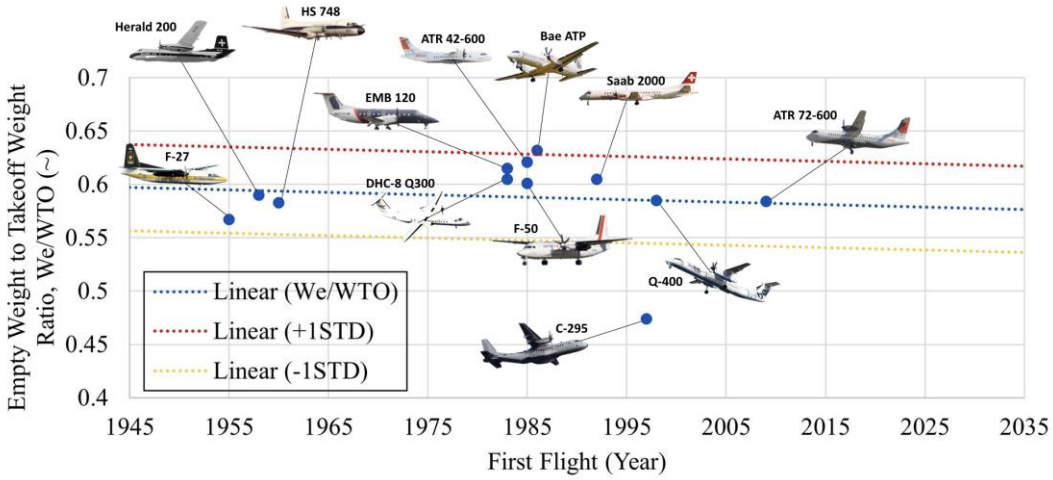

Figure 4-1: W_e/W_{to} of Regional Aircraft

4.2 Cruise Speed

Cruise speed (V_{cr}) is plotted in Figure 4-2 below. The average regional turboprop aircraft in 2035 will feature a cruise speed of roughly 300 kts, while a contemporary regional jet would be about 490 kts.

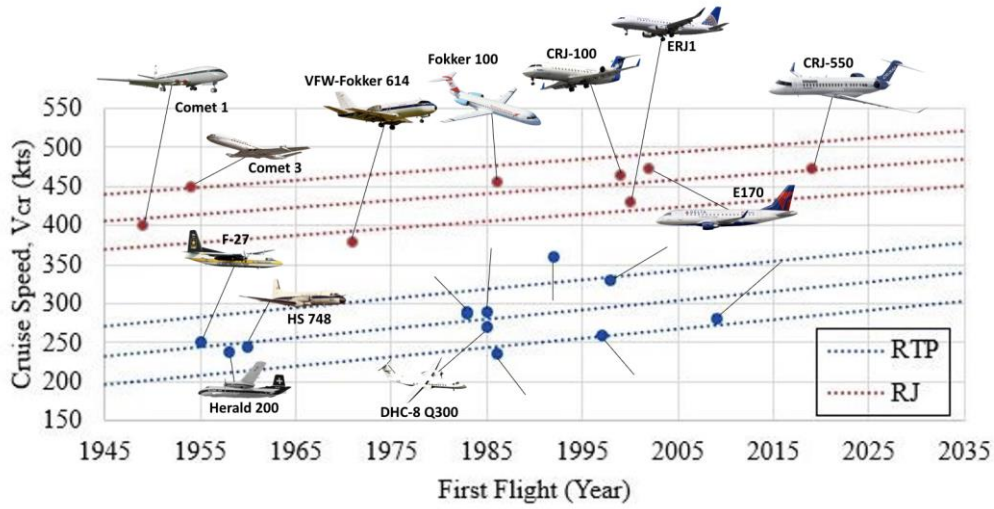

Figure 4-2: Cruise Speed of Regional Aircraft

4.3 Wing Loading

Wing loading (W/S) is plotted in Figure 4-3 below. The average regional turboprop aircraft in 2035 will feature a wing loading of roughly 85 lbf/ft^2, while a contemporary regional jet would be about 110 lbf/ft^2.

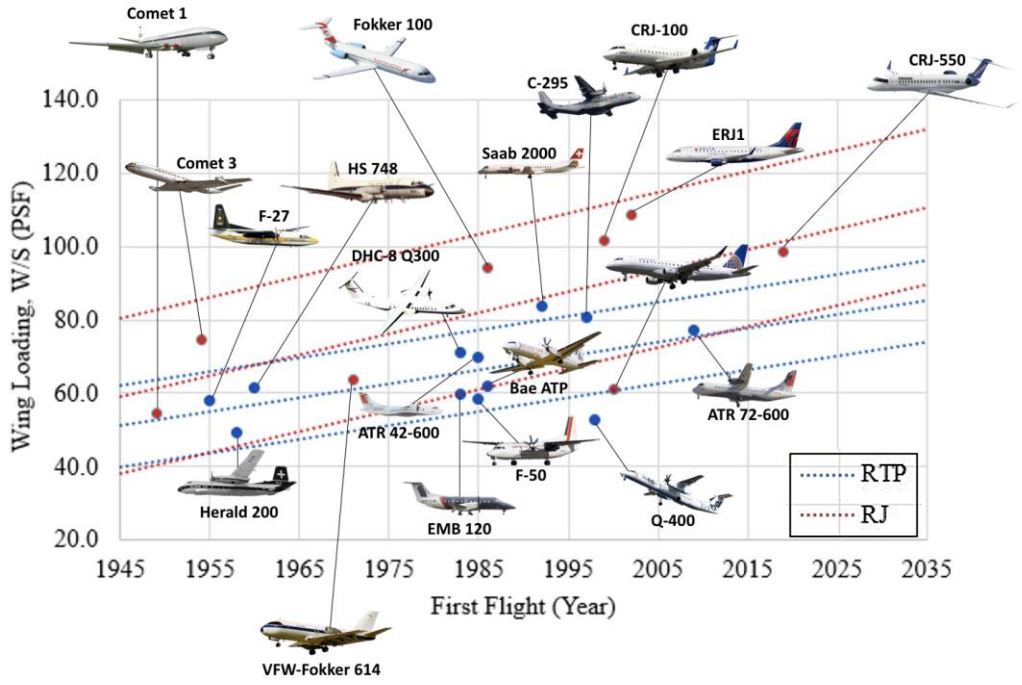

Figure 4-3: 50-Seat Regional Aircraft Wing Loading Trends

4.4 Aspect Ratio

Aspect ratio (A) is plotted in Figure 4-4. The average regional turboprop aircraft in 2035 will feature an aspect ratio of roughly 12, while a contemporary regional jet would be about 9.5.

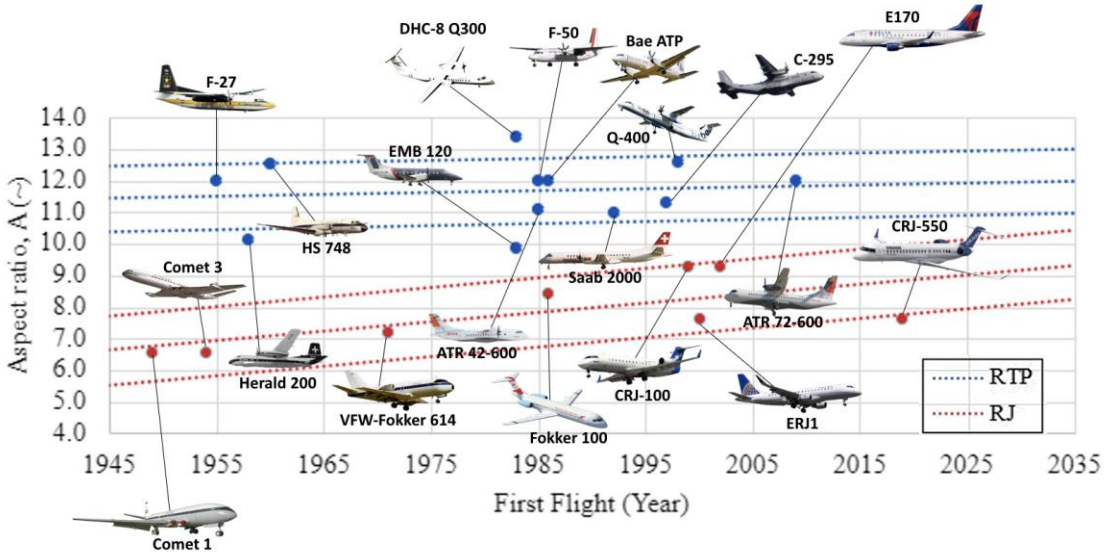

Figure 4-4 50-Seat Regional Aircraft Aspect Ratio Trends

5 Advanced Technology

This chapter will discuss an overview of the advanced technology.

5.1 Overview of Advanced Technology

Below is a catechism table for the three advanced technologies that this aircraft system will have. These are found in Table 5.1.

Table 5.1: Catechisms for Advanced Technologies

What is it called?	NLF	Natural laminar flow (NLF) fuselage and surfaces
	iGOAT	intelligent Ground Operations Aircraft Tug (iGOAT)
	ACES	Aircraft Cleaning Expert System (ACES)
What are these trying to do?	NLF	Improving efficiency and performance of the aircraft by reducing aerodynamic drag
	iGOAT	Reducing the number of ground walkers needed by an airport and allow for less fuel, and therefore less weight and emissions, for the aircraft
	ACES	Working as cleaners for the wings and fuselage of Meadowlark, making sure that the NLF remains effective with every flight
How does this currently get done?	NLF	NLF aircraft have been highly researched and NLF fuselages have been incorporated into some aircraft, like the Piaggio P180, though this is one of the only fuselages like this.
	iGOAT	Aircraft tugs exist in many airports and autonomous, electric aircraft tugs have been designed in companies like Mototok and the startup Moonware. [28][29]
	ACES	Though dependent on the airline, aircraft are externally cleaned between six and eight weeks. [30]
What limits does this present?	NLF	Manufacturing costs are higher when dealing with NLF surfaces.
	iGOAT	These tugs do not exist for specific aircraft and only have one job, making airlines less likely to utilize them.
	ACES	Aircraft fly through all types of dirt and debris which sticks to the wings and fuselage. This increases the aerodynamic drag.
What is new about this approach?	NLF	There are not many aircraft that incorporate both an NLF fuselage, wings, and *winglets*. Meadowlark will have all of these.
	iGOAT	While the iGOAT is also autonomous and electric, it will also power the aircraft on the ground and house the ACES.
	ACES	With the ACES, aircraft can be cleaned between every flight while passengers are deboarding and boarding. Cleaning of the aircraft in between each flight, along with the NLF fuselage, will improve the aerodynamic qualities.
Why, at this time, can this approach succeed?	NLF	The demand of NLF fuselages is high due to the improved aerodynamic and fuel efficiencies in a search for a greener future.
	iGOAT	On a similar note as a greener future, the iGOAT will result in less necessary fuel for takeoff weight and will be completely electric.
	ACES	A cleaner aircraft will result in a more efficient flight, less fuel is required, and higher speeds can be achieved.
What difference does this approach offer?	NLF	There is not much different than what has been done before, but aircraft do not tend to use more than one type of NLF surface.
	iGOAT	There are no tugs that are fully electric, autonomous, and serve more of a purpose than just tugging aircraft around.
	ACES	There are no aircraft that have individual cleaners that will, not only clean the aircraft after most flights, but also be active at the terminals while passengers are deboarding and boarding.

5.2 Operational and Physical Description and Concept of Operations

5.2.1 Intelligent Ground Operations Aircraft Tug

The iGOAT is the most versatile tool of the Meadowlark system. The iGOAT will be a smart, self-driving system given tasks from a new command center on site at the airport. The intelligent or autonomous portion of the system will increase productivity and decrease personnel costs. The iGOAT will have redundancy built into its mechanical and electrical systems to minimize failures, and the ground operations tower will have full control over the iGOATs, pausing all motion if necessary. It functions as the tug, and it charges and stores the ACES, as shown in Figure 5-1.

Figure 5-1: iGOAT Model with ACES

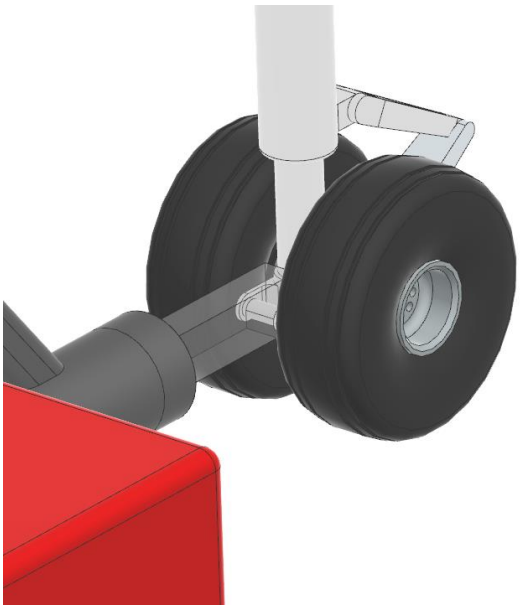

Figure 5-2: iGOAT Attachment to Nose Landing Gear

Once the Meadowlark lands, the iGOAT will leave a special housing unit at one end of the airport. The iGOAT will then attach itself to a power plant at the nose of the aircraft through a bay at the nose gear as shown in Figure 5-2. This will result in the Meadowlark not burning any block fuel during taxi to the terminal while simultaneously keeping the core of the engine running for a fast turn time. The iGOAT will continue to supply power to the aircraft during the entirety of the turnaround time, and will taxi the Meadowlark to takeoff. As explained in the CONOPS, there will never be chance of interference with normal aircraft operations, as the iGOAT will make use of its own routes when not connected to a Meadowlark. The minimization of fuel burn on the ground will decrease overall emissions and promote a fully clean airport. It is understood that the infrastructure to support the iGOAT cannot be fully available at all airports by the EIS date, and it should be noted that without the iGOAT the Meadowlark aircraft can still complete the mission. The iGOAT operations would grow and expand over the aircraft lifespan as the aircraft is also designed to adapt as well.

5.2.2 Aircraft Cleaning Expert System

Once the iGOAT is attached to the Meadowlark, the ACES will crawl up the nose gear and then onto the fuselage, making their way down the fuselage and to the nose gear. A model of the ACES can be seen in Figure 5-3. ACES will utilize strong suction to make their way onto the aircraft. The ACES have six fully rotatable arms to allow it to crawl wherever it needs to go. They will be individually hooked up to water lines through a hole in the side of their body, which will provide them with the water to mix with their high-concentrate, aircraft-grade soap that is housed within the system. Though the skin will be made from composites, there are products that specialize in cleaning of composites, such as Composiclean. [31] This soap will be housed in a containment unit in the center of the ACES which can be inserted and screwed in on the top of the body. This combination of water and aircraft-grade soap will be deposited onto the skin and there are four scrubber brushes that will rotate and wash away dirt, debris, and bugs that would have ruined the positive effects of the NLF fuselage. Clean water will then run to wash away any soap residue.

Figure 5-3: ACES Model

The ACES movement can be seen in Figure 5-4. The ACES will move off of the iGOAT and attach to the front upper and lower part of the aircraft. As they clean the surface, they begin to move towards the wing. At the fuselage-wing intersection, the ACES will the wing, with a main focus of the leading edge. Afterwards, they will head back to the iGOAT and clean the surfaces. The ACES will primarily clean the forward 50-60% of the aircraft.

Figure 5-4: ACES Concept of Operations

5.3 State of the Art of the Advanced Technologies

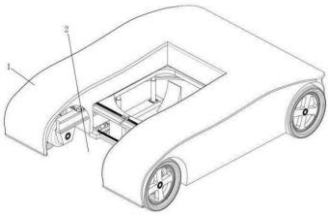

Figure 5-5: Green Airport Intelligence Aircraft Tractor [32]

There are several advanced technologies that can contribute to the advancement in performance regarding the iGOAT and ACES. The combination of the ideas which currently exists and the iGOAT and ACES will continue to improve the overall productivity of the system. One example is the green airport intelligence aircraft tractor [32]. Figure 5-5 shows the design of the green airport intelligence aircraft tractor. It is an environmentally friendly, energy saving, low operation cost vehicle and electrical control system. The technology allows for the movement of the aircraft front, back, and side-to-side. The systems designed for this vehicle can be implemented and improved on by the iGOAT.

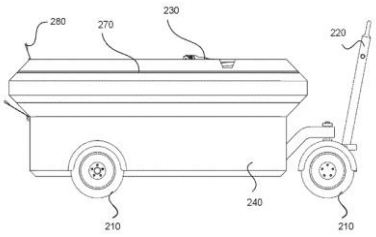

Figure 5-6: Aircraft Charging Unit [31] Figure 5-7: Aircraft Charging Unit [33]

Another technology that can be utilized is the Aircraft Charging Unit created by Brian Hinman and Tabetha Hinman. [33] The technology includes a current transducer with a power source, solid state converter that is compatible with aircrafts near or at the gate terminal and configured to provide power to the aircraft. Figure 5-6 shows the Aircraft Charging Unit.

With the ACES, there are current technology that can contribute to the advancement of performance. A recent technology is from The Boeing Company called Walking Robot [34]. The technology involves a walking robot arm that focuses on current issues involving drilling, inspection, and

fastening for manufacturing and maintenance purposes. To move across the aircraft surface, the robot uses suction cups to secure to the surface. Figure 5-8 shows how the Walking Robots would look like on the exterior surface of the aircraft when building and a detailed drawing.

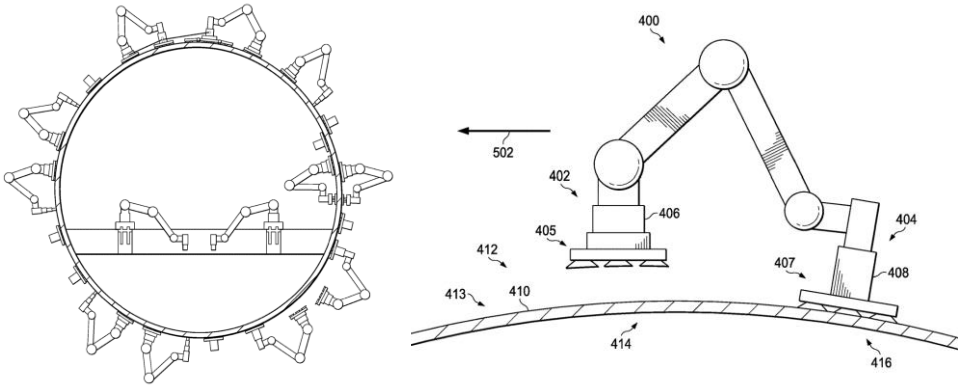

Figure 5-8: Walking Robot Exterior and Detailed Drawing [32]

6 Weight Sizing

This chapter performs Class II weight sizing. The fuel fractions are determined using Jan Roskam's *Airplane Design Part I.* [35] The identified values which are calculated to be one are special cases made possible due to the use of the iGOAT. The ability to save fuel for this part of the mission profile lowers the total weight as well as emissions. The fuel fractions are tabulated in Table 6.1.

Table 6.1: Mission Fuel Fractions

W_{i+1}/W_i	Segment	Fuel Fraction [RE]-Roskam Estimation [E]- Estimation [C]- Calculated
W_1/W_{TO}	Engine Start, Warm Up	1 [iGOAT powered] [E]
W_2/W_1	Taxi	1 [iGOAT powered] [E]
W_3/W_2	Take-off	0.996 [RE]
W_4/W_3	Climb	0.985 [RE]
W_5/W_4	Cruise	.97 [C]
W_6/W_5	Climb to Alternate	.98 [E]
W_7/W_6	Divert to Alternate	.98 [E]
W_8/W_7	Loiter	.993 [C]
W_9/W_8	Descent	1 [Battery powered] [E]
W_{10}/W_9	Landing, Taxi, Shutdown	1 [iGOAT powered] [E]
M_{ff}	Mission Fuel Fraction	.9075 [C]

The mission fuel fraction is used to find the total fuel needed. From this and knowing the payload weight, the following weight values, takeoff weight, W_{TO}, empty weight, W_E, payload weight, W_{PL}, and fuel weight, W_F,

are found to be the values below. The payload weight accounts for all pilots and crew members weights and baggage, as well as 50 passengers and baggage requirements.

$$W_{TO} = 36{,}000\ lb \qquad W_E = 18{,}600\ lb \qquad W_{PL} = 12{,}660\ lb \qquad W_F = 4{,}580\ lb$$

7 Wing and Powerplant Sizing

To perform the wing and powerplant sizing, the lift coefficients were estimated using data from similar aircraft and factoring in the features of Meadowlark such as natural laminar flow wings and fuselage. Other important parameters that were estimated were the wing area, takeoff thrust and takeoff power. After these estimations, the design point was chosen based on the boundaries put forth on the carpet diagram and the wing loading and thrust-to-weight ratio under the limiting flight condition found by the equation shown. Keeping the design point as close to these boundaries as possible is vital for optimizing the wing and powerplant sizes, leading them to be smaller and thereby having higher performance.

$$\frac{W}{S}|lim = \frac{1}{2}\rho V^2 C_{Lmax}|_{LimitingFlightCondition}$$ **Equation 7-1**

7.1 Takeoff and Landing Sizing

The takeoff sizing for the powerplant and wing were found using the two equations shown below. The takeoff size is dependent on the takeoff distance of 4,500 feet. When solving for the thrust-to-weight ratio for takeoff, the independent variable in the equation is the wing loading. Wing loadings from values of zero to 200 were used to calculate the takeoff values. Sigma (σ) represents the air density ratio of 0.683 that was found at 5,000 feet above sea level. Four C_{LmaxTO} values are used to find the boundaries of the design points. These values are 3.7, 3.8, 3.9, and 4.

$$(\frac{T}{W})_{TO} = \frac{37.6(\frac{W}{S})_{TO}(\frac{lb}{ft^2})}{S_{TOFL}(ft)\sigma C_{LmaxTO}}$$ **Equation 7-2**

$$\frac{W}{S} = \frac{\frac{1}{2}\rho V_{SL}^2 C_{Lmax}|_L}{(\frac{W_L}{W_{TO}})}$$ **Equation 7-3**

After finding the thrust-to-weight ratios, the wing loading is found using the equation to the right. Three C_{LmaxL} values were used to find these boundaries and determine the wing loading and therefore the wing area needed. The C_{LmaxL} values were required to achieve the field length of 4,500 feet at standard sea-level conditions.

7.2 Climb Sizing

There are five configurations for the aircraft's flight phases. Each of these phases has a different amount of drag depending on the use of landing gear and flaps. The drags are shown visually in a drag polar equation next to each of these curves, seen in Figure 7-1. The landing, gear down phase is the highest drag configuration, while the clean phase is the lowest drag configuration. The climb sizing is based on FAR 25 guidelines and requirements. These requirements are for One Engine Inoperative (OEI) and All Engines Inoperative (AEI) situations. The values for the wing area and lift coefficients are presented in Table 7.1.

Table 7.1: Wing and Powerplant Sizing Parameters

Parameter	Value
S	300 ft^2
$C_{L_{max,TO}}$	3.8
$C_{L_{max,clean}}$	1.3
$C_{L_{max,L}}$	5.2

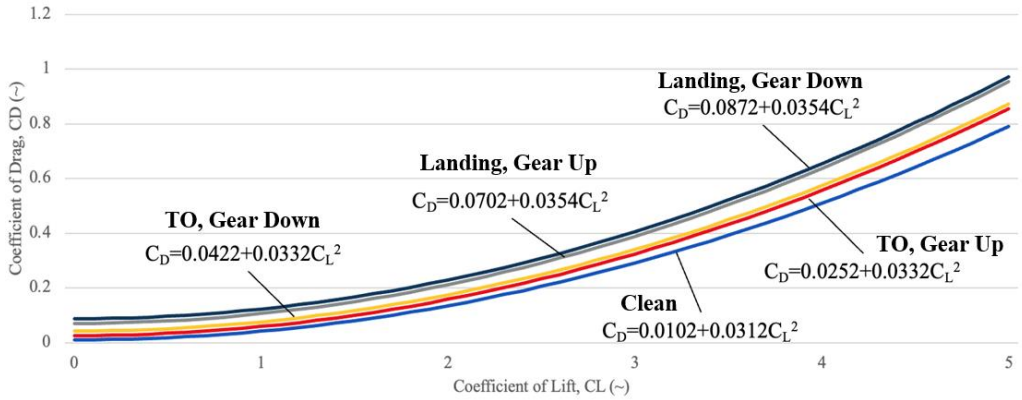

Figure 7-1: Meadowlark Drag Polars

7.3 Cruise Sizing

Cruise sizing is based on the altitude, density, speed and the drag polar for aircraft cruise configuration. The Meadowlark will be flying at 393.3 KTAS (Mach 0.67) in cruise. The given equations were used to find the thrust-to-weight ratio in cruise and the thrust at altitude.

$$\frac{T}{W} = (C_{D0} + \frac{(\frac{W}{\bar{q}S})^2}{\pi Ae})\bar{q}\frac{S}{W} \quad \textbf{Equation 7-5}$$

7.4 Powerplant

The engine selection is based on the boundaries and values found in the for the thrust-to-weight ratios in the sizing charts and the takeoff weight. The equations were used to find the required takeoff thrust of 11,520 lbf.

$$\frac{T}{W} = (C_{D0} + \frac{(\frac{W}{\bar{q}S})^2}{\pi Ae})\bar{q}\frac{S}{W} \quad \textbf{Equation 7-6}$$

7.5 Wing Fuel Volume

The wing fuel volume needed was calculated based on maximum capacity of fuel in gallons, given that one cubic foot is equivalent to 7.48 gallons. The wing fuel weight and volume was found using the equations above, and this is dependent on the thickness to chord ratios for the root and tip. The thickness to chord ratio is 15%. Since the same airfoil was used through the entire wing, τ_w is equal to one. The wing area is 300 ft^2 with a wing span of 60 feet, leading us to find 113 ft^3 of available volume, exceeding the 90.30 ft^3 of volume needed.

$$V_{WF} = 0.54\left(\frac{S^2}{b}\right)\left(\frac{t}{c}\right)_r\left((1+\lambda_w\tau_w^{\frac{1}{2}}+\lambda_w^2\tau_w)/(1+\lambda_w)^2\right) \quad \textbf{Equation 7-7}$$

$$\tau_w = (t/c)_t/(t/c)_r \quad \textbf{Equation 7-8}$$

Table 7.2: Fuel Volume

Fuel Weight, W_f	Fuel in Gallons	Fuel Volume Needed	Available Volume
4,580 lb	675.52 gal	90.30 ft^3	113 ft^3

7.6 Complete Sizing Chart

The carpet diagram depicting the wing loading and thrust-to-weight ratio at various lift coefficients is shown in Figure 7-2. The design point, depicted by the star in Figure 7-2, is located above and within the boundaries indicated on the plot. The vertical lines on the carpet diagram show the maximum landing $C_{L,}$ and the aircraft meets this requirement by being to the left of these boundaries. The diagonal lines represent the maximum take-off C_L, and the aircraft meets this requirement. Finally, the horizontal lines are the FAR 25 climb requirements, and the aircraft exceeds this requirement. There are eight aircraft shown on the diagram to compare with Meadowlark's design point. The descriptions of each line can be found on the right-hand side of the graph.

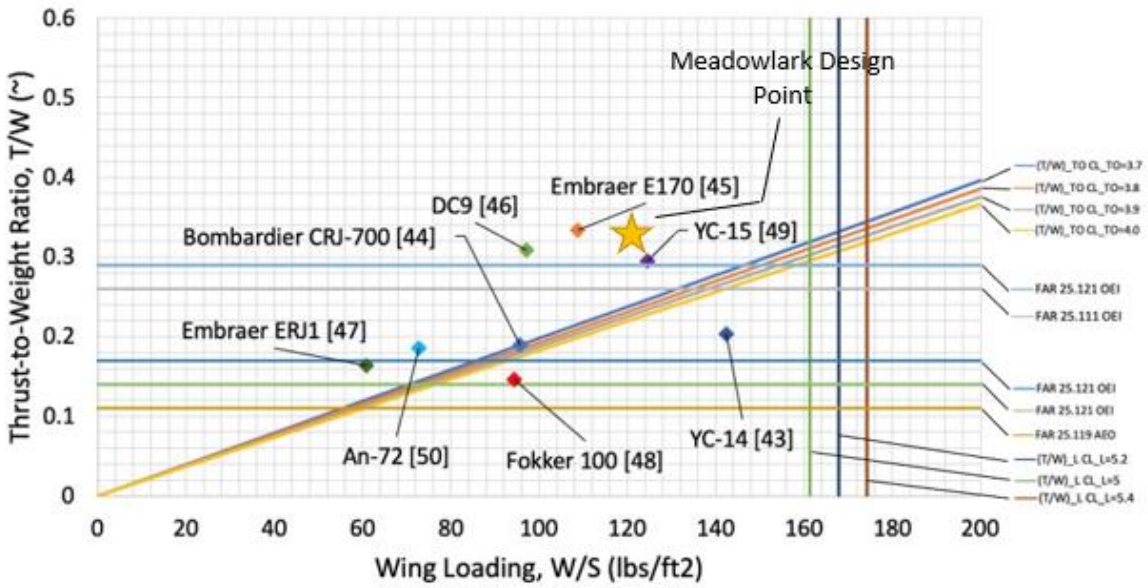

Figure 7-2: Meadowlark Sizing Chart

8 Configuration Sweep and Downselection

8.1 Configuration Matrix

After preliminary sizing, twelve configurations were selected to run through the design optimization function, seen in Figure 8-1.

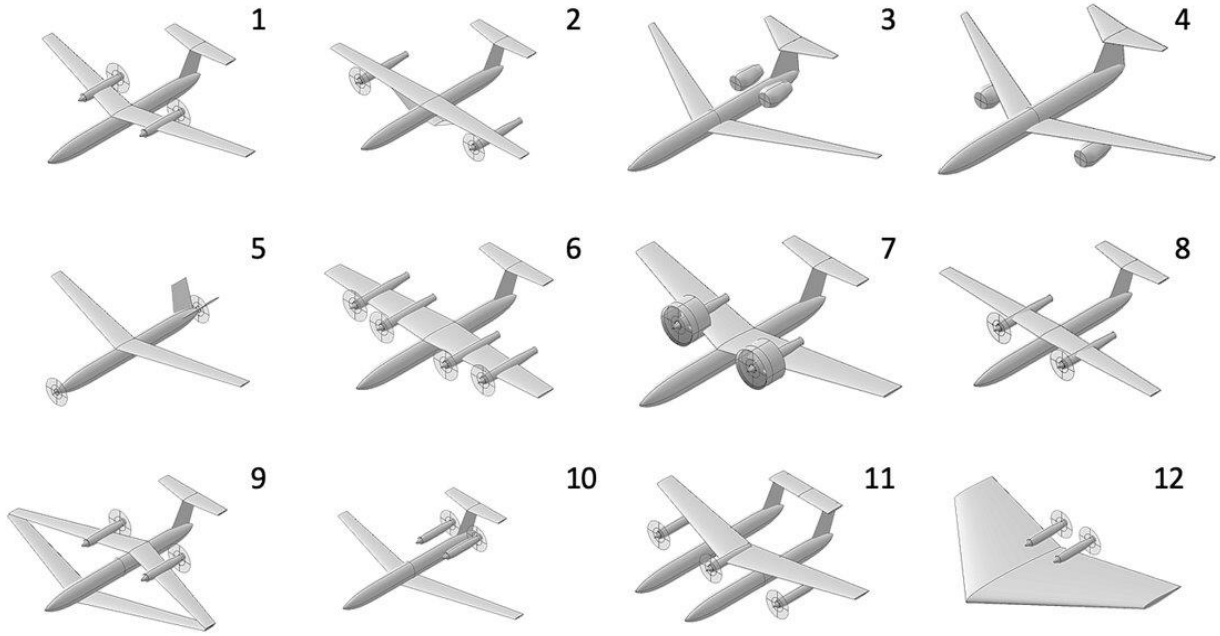

Figure 8-1: Configuration Sweep

8.2 Application of Optimization Function and Downselection

Every configuration is evaluated first on whether it will have the capabilities to meet the requirements as outlined in the RFP. The first twelve configurations are chosen based on the ability to meet the requirements. The requirements are part of the equation to decide on a final configuration, also seen in Equation 1. For a configuration to move on in the process of down selection it must receive a sore of one for each requirement outlined, shown in Table 8.1. The only configuration to not score a one for the design requirements was Configuration Twelve. The next step in the process is to score each of the configuration based on the RFP given objectives. They are ranked from best to worst with a score of zero being the worst and one being the best. The ancillary objectives are then scored based on the mission and goals of the team. The ancillary objectives are then weighted to decide on configurations that better meet the goals of the team. The final rankings of both the objectives and ancillary objectives are combined to choose a configuration as seen in Table 8.2.

Table 8.1: Design Requirements

Label	Requirement
R_1	50 +0/-4 in a single class arrangement with 30 inch seat pitch
R_2	1,000 nmi range (R) with full passengers
R_3	Seat width (W_s) >17.2 inches
R_4	Arm rest width (W_{ar}) >2 inches
R_5	Aisle stand up height similar to competitive aircraft
R_6	Baggage compartment tall enough for ergonomic servicing
R_7	Aisle width (W_i) >18 inches
R_8	Wingspan (b) <36 m
R_9	Able to be certified by 2035
R_{10}	Capable of flight in known icing conditions
R_{11}	Takeoff field length (TOFL) <4,500 ft over 50 ft obstacle dry pavement
R_{12}	Landing field length (LFL) <4,500 ft over 50 ft obstacle dry pavement
R_{13}	Performance should be shown 5,000 ft above mean sea level
R_{14}	Distance to climb <200 nmi to initial cruise altitude
R_{15}	Approach speed (V_{at}) category C, <141 kts
R_{16}	Cruise altitude >FL280
R_{17}	Cruise speed (V_{cr}) >275 KTAS
R_{18}	20% reduction in block fuel on 500 nmi mission
R_{19}	Meet 14 CFR 25.121 Climb Gradient Requirements
R_{20}	2 pilots and 1 cabin crew member for every 50 passengers

Table 8.2: Objectives Evaluation

	Configuration Number											
	1	**2**	**3**	**4**	**5**	**6**	**7**	**8**	**9**	**10**	**11**	**12**
												
O_1 : 350 KTAS cruise speed	1	1	1	1	1	1	1	1	1	1	1	0
O_2 : > 18” seat width	1	1	1	1	1	1	1	1	1	1	1	1
O_3 : < 24 m. wing span	1	1	1	1	1	1	1	1	1	1	1	1
O_4 : Systems and avionics that will enable autonomous operations	1	1	1	1	1	1	1	1	1	1	1	1
SUM	4	4	4	4	4	4	4	4	4	4	4	3
WEIGHTED SUM	1	1	1	1	1	1	1	1	1	1	1	0.75
AO_1 : Door width large enough for standard wheelchair	1	1	1	1	1	1	1	1	1	1	0	0
AO_2 : Large tray-tables for an average laptop	1	1	1	1	1	1	1	1	1	1	1	1
AO_3 : Fast ground turn (<8 min.)	0	0	0	0	1	1	1	1	0	0	0	0
AO_4 : European standards for cargo bay	1	0	0	0	1	1	1	0	0	0	1	1
AO_5 : Multiple doors for simultaneous loading and off boarding docks	1	1	0	1	1	1	1	1	0	0	1	0
AO_6 : Allow for engine diameter growth and powerplant upgrades	1	1	0	1	0	1	1	1	1	0	0	1
AO_7 : Minimal interference with ground traffic	1	0	1	1	1	0	1	1	0	1	0	0
AO_8 : Batteries are on outer mold line of fuselage	1	1	1	1	1	1	1	1	1	1	1	1
AO_9 : Allow for battery pack changes as they improve over time	1	1	1	1	1	1	1	1	1	1	1	1
AO_{10} : Ease of meeting Stage 5+ noise regulation	0	0	1	1	0	0	1	0	0	0	0	0
AO_{11} : Aesthetic appeal (surveyed by multiple non-engineers, ranked 0-1, 1 as best)	0.5	0.42	1	0.67	0.17	0.33	0.83	0.58	0.083	0.91	0.25	0.75
WEIGHTED SUM	6.5	5.22	5.6	6.87	6.17	6.83	8.73	6.88	4.28	4.61	3.95	4.85
TOTAL WEIGHTED SUM	0.74	0.60	0.64	0.79	0.71	0.78	1	0.79	0.49	0.53	0.45	0.56
COMPLETE WEIGHTED TOTAL	0.74	0.60	0.64	0.79	0.71	0.78	**1**	0.79	0.49	0.53	0.45	0.42

Configuration 7 is the selected configuration through the objective evaluation and is seen in Figure 8-2. The final objective function score is 1, meaning in a direct comparison to the other twelve configurations, this configuration is found to align with the Meadowlark goals and values most directly. The calculation of the objective function score is seen below.

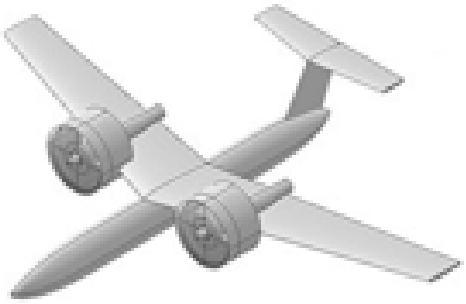

Figure 8-2: Selected Configuration

$$OF = (\prod_{i=1}^{20} R_i)(\sum_{n=1}^{4} O_j)\,(\sum_{k=1}^{7}(AO_k * weight)) = (1)(1)(1) = 1 \qquad \textbf{Equation 8-1}$$

8.2.1 Comparison of Selected Configuration with Popular Configuration

Below is a diagram that compares a recent, popular configuration, with a more detailed Configuration 7, seen in Figure 8-3.

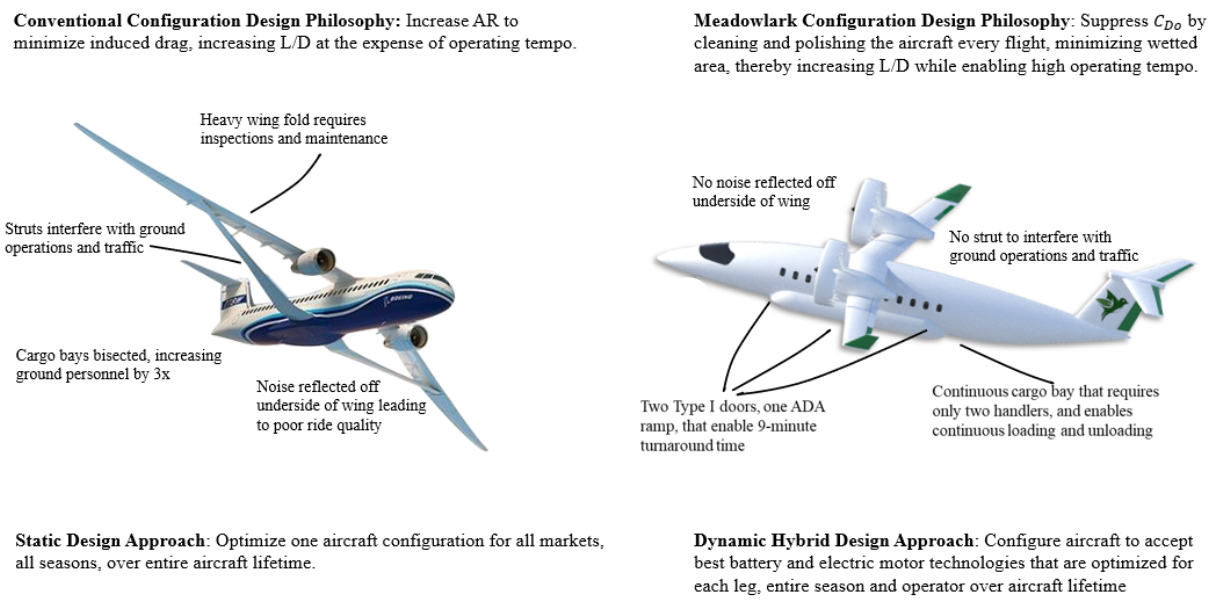

Figure 8-3: Configuration 7 vs. Popular Configuration

The issues indicated in Figure 8-3 lead to other problems with this configuration. For example, the engine noise reflected off of the underside of the wing leads to a much poorer ride quality than that of the selected configuration of the Meadowlark. Additionally, the popular configuration has few movements per year, leading to lower profits and higher ticket prices. This popular configuration also has a much larger fleet requirement given the route structure, leading to an adverse environmental impact [34].

9 V-n Gust and Maneuver Diagram

The gust and maneuver V-n diagram for the aircraft was generated and based on FAR 25 requirements. The graph shows the limits of the aircraft by showing different load factors being applied at different speeds. The speeds analyzed are seen in Table 9.1 and the diagram can be found in Figure 9-1.

Table 9.1: Speeds Analyzed

Speed Type Analyzed	Speed (kts)
+1g Stall Speed (V_{S1})	177
Cruise Speed (V_C)	375
Dive Speed (V_D)	469
Maximum Gust Intensity Speed (V_B)	291
Maneuver Speed (V_A)	286.5

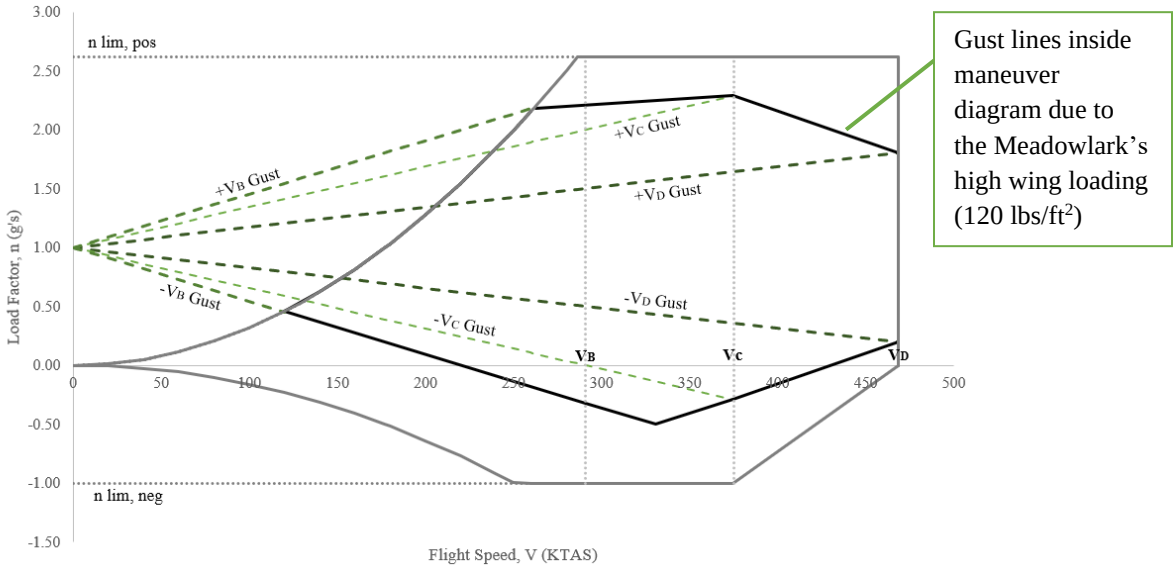

Figure 9-1: V-n Gust and Maneuver Diagram

The high wing loading of the Meadowlark leads to the gust lines being lower than the maneuver diagram lines. This leads to greater passenger comfort and less fatigue to the airframe. A lower fatigue is important due to the Meadowlark goal of increasing legs per day for each aircraft.

10 Payload-Range Diagrams and Fuel Burn

10.1 Payload-Range Diagrams

Payload-range diagrams use parameters that change aircraft efficiency and ranges based on various payloads. Figure 10-1 shows various percentages of electric and combustion payload-ranges at Mach 0.67, FL 300. The plot includes maximum zero fuel weight, maximum takeoff weight at maximum payload with full tanks, and maximum

ferry. Within the figure, between the 79% combustion and 100% combustion, the ACES and iGOAT are needed to maintain natural laminar flow.

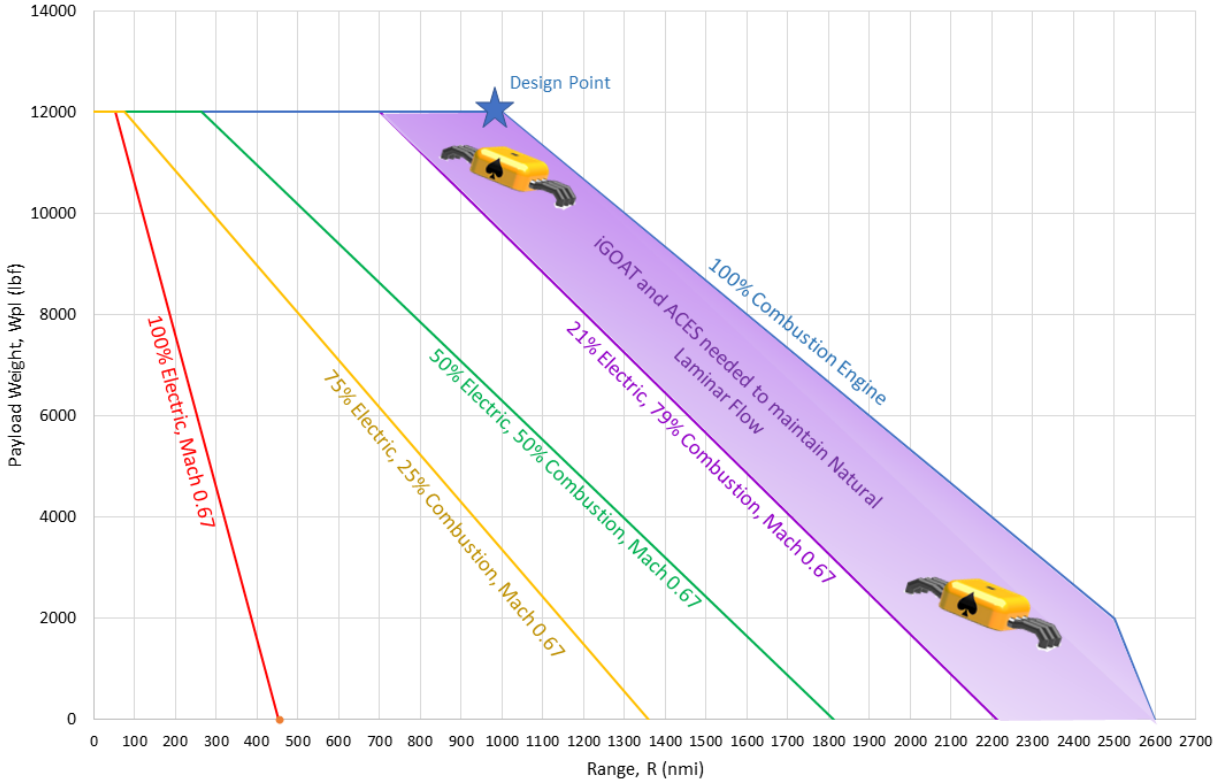

Figure 10-1: Meadowlark Payload-Range Diagram

To determine the current market ranges for regional aircrafts, the frequency of flights for several American regional commercial airlines were examined, as shown in Figure 10-2[a]. These airlines include Delta Connections, American Eagle, and United Express. For the data collected, a selected date, June 1, 2023, was examined for each airline. Along with the date, economy class and non-stop flights were examined. Although the frequency of the flights depended on these aspects, it was influenced on the aircraft type: regional turboprop and regional turbojets. Some of these aircrafts include Embraer 170 and Canadair Regional Jet 700. The frequency of flights was examined for every 50 nmi. Examining the data, between 100 nmi to 400 nmi, 53% of the flights are flown.

In Figure 10-2[b], the American average loading factor, along with the standard deviation, are shown for the various electric-combustion percentages examined. The average American loading factor is 79%, with a standard deviation of 18%. For each loading factor point, along with the maximum ferry, three components were examined:

the battery weight, fuel weight, and battery pack configuration. As the percentage of electric power decreases, the battery weight decreases. For example, at 100% electric power, 0% combustion for the average standard deviation, the battery weight is 6,274 lbf, however, decreases to 0 lbf at 0% electric, 100% combustion. Similarly, the fuel weight increase as the electric percentage decreases. The fuel specified is not the total fuel burn for the mission because it also includes the extra necessary fuel for FAR 25 requirements. The fuel amount is total fuel weight at takeoff. With the weights, different battery size packs were created to fit the payload-range. There are five types: Type A, B, C, D, and E, weighing 4,000 lbf, 2,000 lbf, 1,000 lbf, 500 lbf, and 250 lbf, respectively.

Examining Figure 10-2[a] and Figure 10-2[b], the percentage of total flights served can be determined for each electric power-combustion percentage for Meadowlark and Sugar Volt. In all electric power percentages, the Meadowlark can achieve 10.4% to 100% of the total flights served for average loading factor and average loading factor minus one standard deviation. The aircraft can accomplish these flight percentages due to the maximum ranges at these points. However, the Meadowlark for average loading factor plus one standard deviation in all electric power percentages achieves a smaller percentage of total flights served. For example, at 100% electric power, Meadowlark achieves 1% of the total flights achieved. Compared to Meadowlark in loading factor and electric power, the Sugar Volt achieves less of the total flights served due to the aircraft having a lower maximum range. Figure 10-3 portrays a direct comparison between the Meadowlark and the Sugar Volt load factor and fight effects.

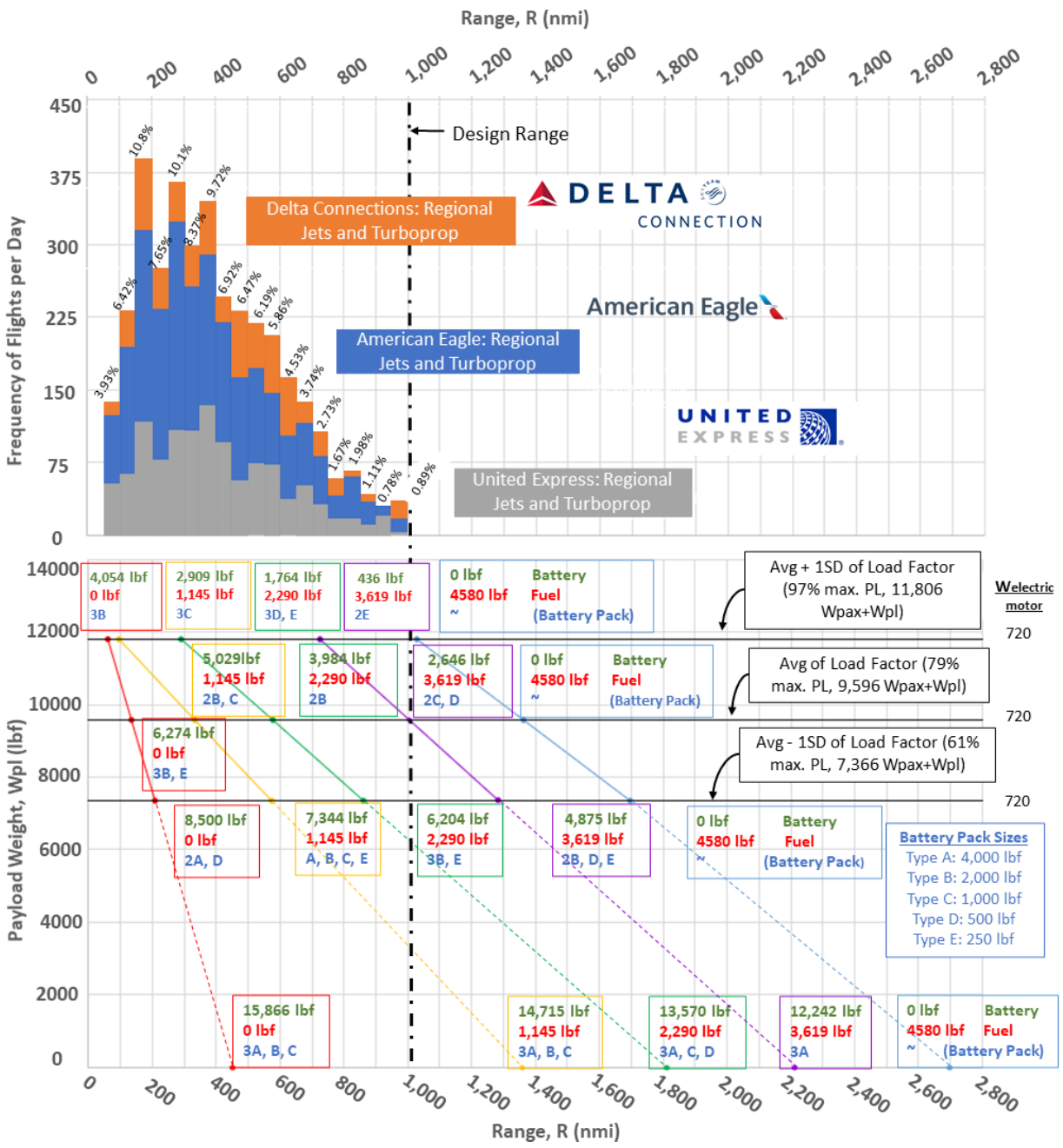

Figure 10-2[a]: Frequency of Flights for United States Regional Commercial Airlines

Figure 10-2[b]: Dynamic Battery Configuration Throughout Different Electric Power Percentages

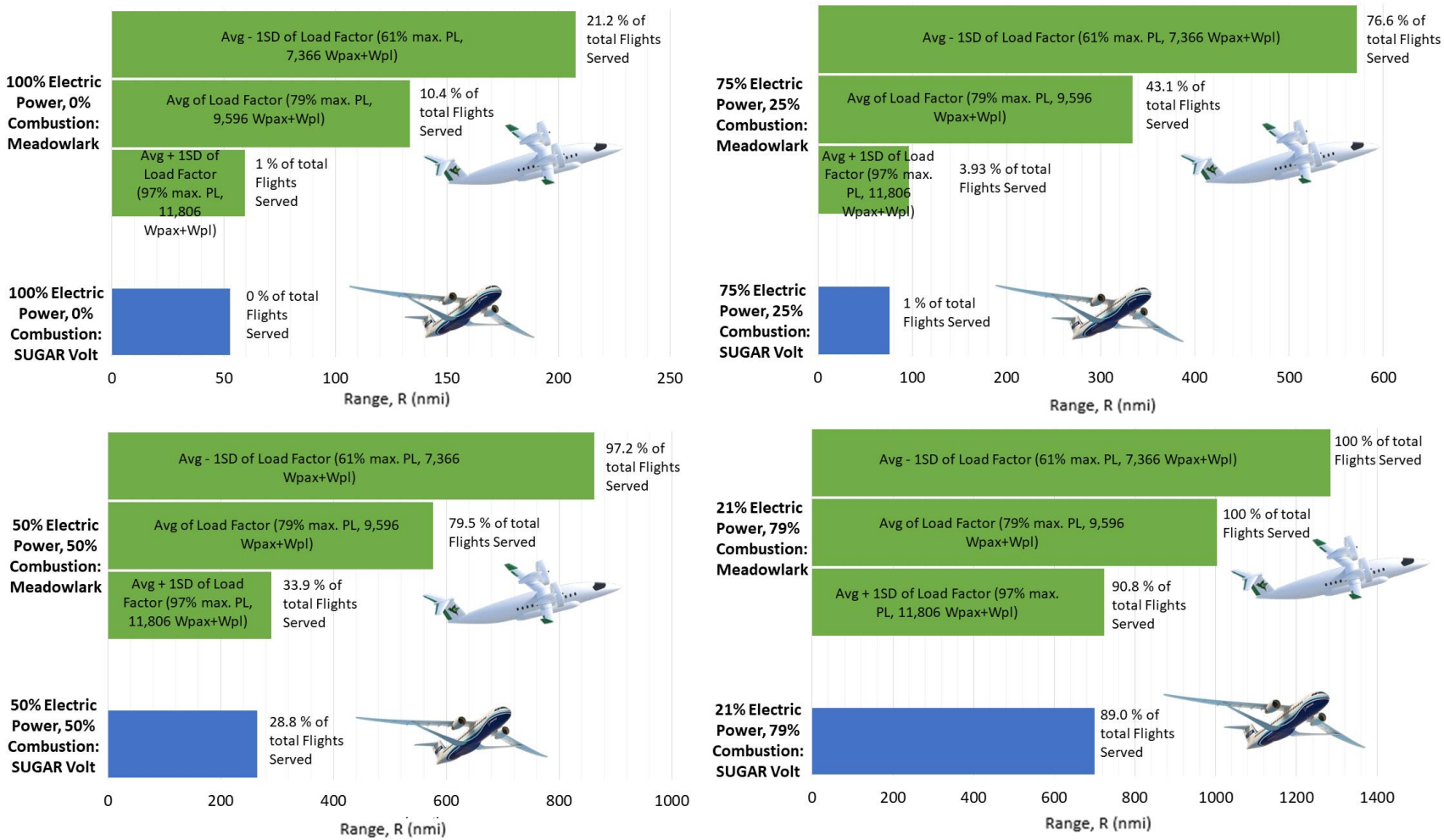

Figure 10-3: Percentage of Total Flights Served Between Meadowlark and SUGAR Volt

10.2 Fuel Burn

Fuel fractions determined using Roskam's *Airplane Design Part I* [35] are used to calculate the amount of fuel used during each stage of the mission profile under full combustion engine use. These calculations do not account for any percentage of electric propulsion, and are tabulated in Table 10.1 below.

Table 10.1: Fuel Weight Fractions

W_{i+1}/W_i	Segment	Fuel Fraction [R]-Roskam Estimation [E]- Estimation [C]- Calculated	State Weight (lbf)	lbf used
W_1/W_{TO}	Engine Start, Warm Up	1 [iGOAT powered] [E]	36,000	0
W_2/W_1	Taxi	1 [iGOAT powered] [E]	36,000	0
W_3/W_2	Take-off	0.996 [R]	35,856	144
W_4/W_3	Climb	0.985 [R]	35,318	538
W_5/W_4	Cruise	0.97 [C]	34,258	1,059
W_6/W_5	Climb to Alternate	0.98 [E]	33,573	685
W_7/W_6	Divert to Alternate	0.98 [E]	32,902	671
W_8/W_7	Loiter	0.993 [C]	32,672	230
W_9/W_8	Descent	1 [Battery powered] [E]	32,672	0
W_{10}/W_9	Landing, Taxi, Shutdown	1 [iGOAT powered] [E]	32,672	0
M_{ff}	Mission Fuel Fraction	.9075 [C]	32,672	3,328

From the payload-range diagram, it is estimated that 36% electric propulsion would be used for a 500 nmi range and 12,000 lb payload. Multiplying the 100% combustion fuel burn (3,328 lbs) by 64% gives the estimated fuel burn for a 500 nmi mission, as projected by the generated payload-range diagrams. The Meadowlark's fuel burn at a 500 nmi range is calculated to be 2,130 lbs. This is compared to two of the most common, current, 50 passenger turboprops—the ATR 42-600 and the Dash 8-300 –and total fuel consumption over a 500 nmi range. The Meadowlark has a 20% or greater reduction in block fuel when compared to both of these aircraft, as shown in Table 10.2 below.

Table 10.2: Block Fuel Reduction Comparison

	Meadowlark	ATR 42-600 [37]	Dash 8-Q300 [38]
Fuel Burn/Trip – 500 nmi (lbf)	2,130	2,761	3,288
Fuel Burn/Seat – 500 nmi (lbf)	42.6	44.2	65.8
Block Fuel Reduction (%)	-	22.9%	35.2%

11 Design and Sizing

The final design characteristics and specifications are shown in Table 11.1.

Table 11.1: Salient Characteristics

	Wing	Horizontal Tail	Vertical Tail
Area	300 ft^2	90 ft^2	81.05 ft^2
Span	60 ft	22.5 ft	10 ft
MGC	5 ft	4.66 ft	8.1 ft
Aspect Ratio	12	5.6	1.23
Sweep Angle	10°	20°	30°
Taper Ratio	0.4	0.5	0.75
Thickness Ratio	15%	9%	9%
Airfoil	NACA 65415	NACA 0009	NACA 0009
Dihedral	-3°	0°	90°
Incidence	1°	0°	0°
Control Chord Ratio	30%	30%	30%
Control Span Ratio	80%-95%	0%-90%	20%-80%
Flap Chord Ratio	30%	-	-
Flap Span Ratio	20%-80%	-	-
	Fuselage	**Cabin**	**Overall**
Length	75 ft	37 ft	75.7 ft
Width	8.8 ft	8 ft	62.7 ft
Height	9.3 ft	7.5 ft	21.1 ft

11.1 Cockpit Layout and Design

The cockpit was sized to ensure compliance with pilot compatibility and FAR 25 visibility requirements. These were found using Roskam's *Airplane Design Part III*. [39] Even though NLF poses a challenge of room towards the nose of the aircraft, this design allows for pilots to sit in a conventional, side-by-side configuration, seen in Figure 11-1 and Figure 11-2. This will allow for easier wiring and communication between the pilots.

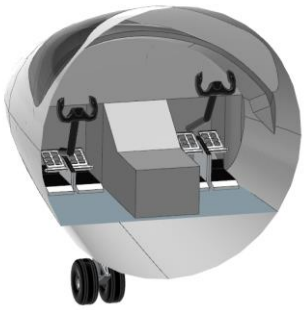

Figure 11-1: Cockpit Layout

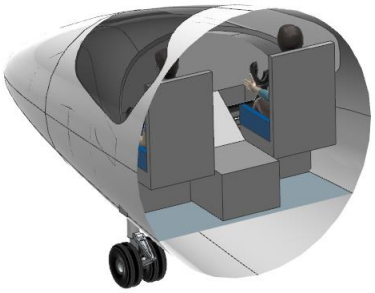

Figure 11-2: Pilot Setup

From the side view, it can be seen that the pilots' eyeline is the same. This is important when looking at the visibility chart. The angles of the pilots' visibility are shown in Figure 11-3. The Meadowlark visibility is better or equal to the FAR 25 recommended viewing angles, shown in Figure 11-4.

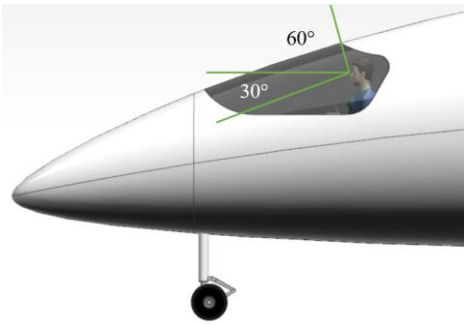

Figure 11-3: Cockpit Side View Visibility

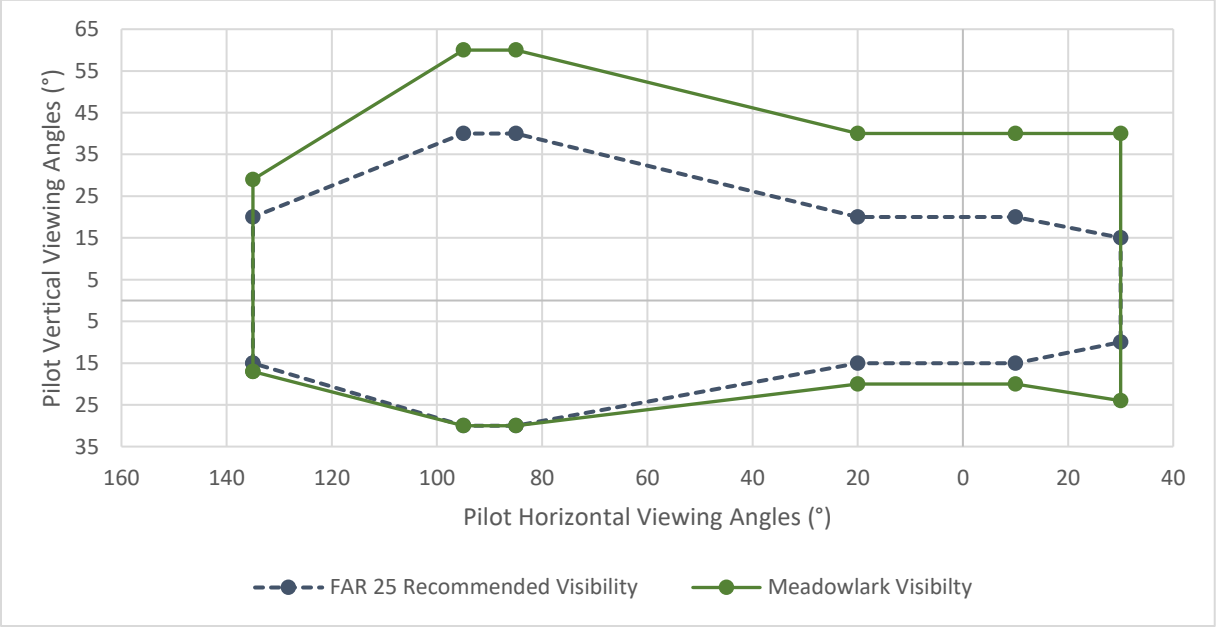

Figure 11-4: Meadowlark vs. FAR 25 Recommended Cockpit Viewing Angles

11.2 Fuselage Layout

The fuselage dimensions were sized with fuselage fineness ratio, which is the ratio of the total fuselage length (l_f) to the maximum fuselage diameter (d_f). Generally, a fineness ratio from 4 to 10 is good. The Meadowlark is designed to have a fuselage fineness ratio of 8.04 given the length of 75.6 ft and a widest diameter of 9.4 ft. The fuselage was designed to make sure that 50 passengers could comfortably sit. The fuselage was also made with a

$$Fuselage\ Fineness\ Ratio = \frac{l_f}{d_f}$$ **Equation 11-1**

desire to keep natural laminar flow and the initial design lines were similar to the Piaggio P180 fuselage. Another goal was to decrease the amount of fuselage wetted area to increase the L/D and efficiency. The fuselage layout and cross section can be found in Figure 11-5 and Figure 11-6.

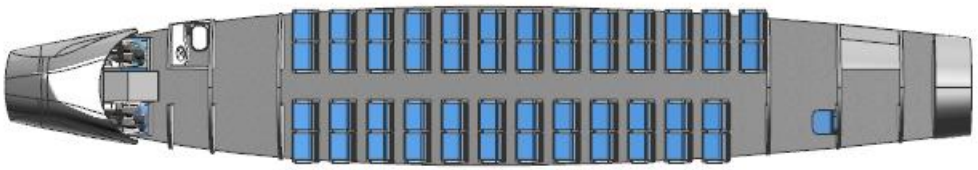

Figure 11-5: Fuselage Layout

Figure 11-6: Cross Section of Aircraft

A two and two configuration were chosen for the seat layout to maximize fuselage fineness ratio. A two and one would result in a long, slender fuselage and a three and one would result in a short, stubby fuselage. The cabin is able to accommodate passengers up to 7.5 ft tall. The interior contains one bathroom and a galley with one crew member seat. These are all seen below in Figure 11-7 and Figure 11-8.

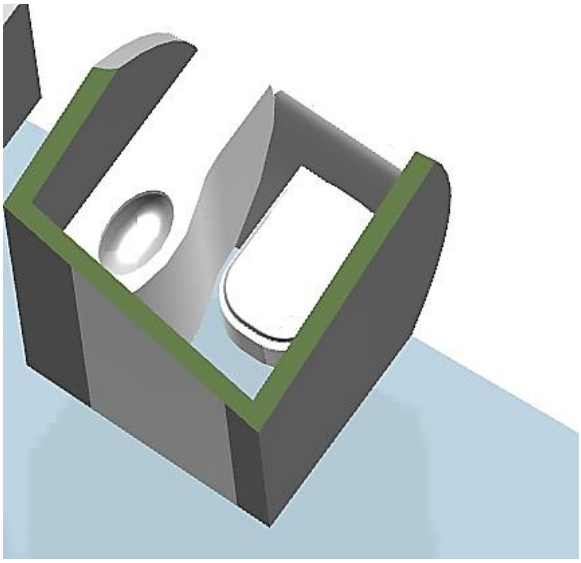

Figure 11-7: Lavatory

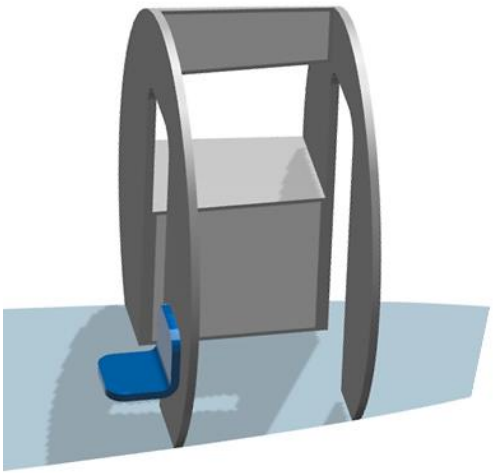

Figure 11-8: Galley

The seats have an 18 in. width and a 2 in. arm rest width for maximum comfort. While there are 50 traditional aircraft seats, there is also room for two extra passengers. This row is saved for passengers in wheelchairs. While at this time, an FAA-certified in-flight wheelchair option does not exist for passengers who use them, there are strides being made in that direction. Leaving this row open allows for some hardware to be installed into the floor to allow for passengers to take their own personal wheelchairs into the cabin. Another option would be to install something similar to what Molon Labe Freedon Seat is attempting to accomplish. [40] While this function might not be integrated at the start of the Meadowlark's life, there will still be a space for these to be implemented in the future as they are FAA approved.

11.3 Combustion Engine Selection

Using Roskam's *Aircraft Design Part II*, a starter combustion engine was selected. The required power at takeoff is 3,900 hp for a takeoff weight of 36,000 lbs. Each engine must provide at least 1,950 shp. From these values, the Pratt & Whitney PW121 turbo-propellor engine was chosen as shown in Figure 11-9. Properties of the PW121 are listed in Table 11.2.

Figure 11-9: PW121 Engine [41]

Table 11.2: PW121 Engine Specifications [40]

Introduction Year	1987
Length (ft)	6.99
Width (ft)	2.1
Weight, Dry (in)	933
Max TO Power (hp)	2,150
Max Continuous Power (hp)	1,950
TO Specific Fuel Consumption (lbf/hp·hr)	0.48

Although the PW121 was first introduced over 30 years ago, it was chosen as a starter combustion engine for the Meadowlark because it is already certified and used on current regional turboprops—the ATR 42-320 and DeHavilland Canada Dash 8-100 series. These turbo-prop regional aircraft have comparable takeoff weights to the Meadowlark. In addition, according to Turbine Options aviation agency PW100 engines produce up to 50% less CO_2 emissions than other similar-sized aircrafts" [41]. Due to the Meadowlark's dynamic design, the combustion engine used will still be able to easily adapt to new, cleaner combustion engine options released in future years. In December 2022, Pratt & Whitney Canada (P&WC) accomplished their first hybrid-electric demonstrator with intents to flight test the system on a Dash 8 later this year. The overall power output was 2MW, equivalent to 2682 hp for a twin hybrid-electric engine configuration. This program is aiming for a 30% reduction in fuel burn and carbon dioxide emissions [43]. New engines such as the P&WC hybrid engine could be easily integrated onto the Meadowlark as soon as they are certified.

11.4 Engine Convergence

Performance of turboprops have been improving over the last few decades. These improvements bring the performance of turboprops closer to that of turbofans. By ducting a turboprop, the similarities between the two are even closer. Ducting the turboprop will result in gaining extra thrust, enhanced high speed performance, and noise suppression, which is key when the engines are close to the fuselage.

11.5 Electric Motor Selection

As part of P&WC's regional hybrid-electric flight demonstrator program, Collins Aerospace is developing an electric motor and controller powered by a turbogenerator and battery system as shown in Figure 11-10 [44]. Pratt & Whitney is also partnering with Swiss based company H55 S.A. to supply battery packs for the project. The Collins electric motor provides 1341 hp (1 MW) and is combined with the P&W combustion engine in a 50/50 power split, parallel hybrid configuration. The hybrid configuration is also being designed to use 100% Sustainable Aviation Fuel, leading to further decrease in emissions [45].

Figure 11-10: Collins Aerospace Electric Motor [44]

11.6 Wing Layout

The wing characteristics that were used to develop the wing design are listed in this chapter. The Meadowlark aircraft features a high wing design, which allows for high visibility but can struggle with high landing gear weight and increased interference drag. Based on gate requirements, objectives, historical data, and STAMPED data, the characteristics of the wing are found in Table 11.3. To maintain natural laminar flow, the airfoil used was NACA 65_2-415 (a=0.5). It indicates that the area of minimum pressure is 50% of the chord, maintaining a low drag 0.2 below and above the lift coefficient of 0.4, has a maximum thickness of 15% of the chord, and maintains laminar flow over 50% of the chord. The wing area and aspect ratio were determined by STAMPED data. Other characteristics were modeled after the Bae 146 such as the tamper ratio and twist angle. The front and isometric view of the wings are shown in Figure 11-11.

Table 11.3: Wing Characteristics

Characteristics	Value
Airfoil	NACA 65_2-415 (a = 0.5)
Wing Area, S	300 ft^2
Aspect Ratio, A	12
Quarter Chord Sweep Angle $\Lambda_{c_{1/4}}$	10 degrees
Thickness Ratio, t/c	0.15
Taper Ratio, λ	0.40
Incidence Angle, i_w	3 degrees

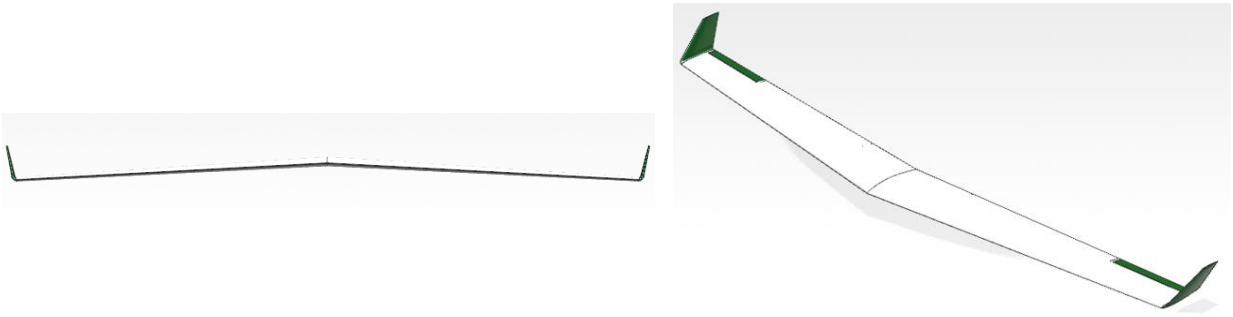

Figure 11-11: Wing Front and Isometric View

11.7 High Lift Devices

High lift devices were chosen and sized based on Roskam's *Airplane Design Part II*. [46] Ultimately, Fowler flaps were chosen. Fowler flaps allow more lift, which is important for the amount of C_L necessary for the takeoff the landing conditions the Meadowlark has. The characteristics of the designed Fowler flaps are seen in Table 11.4. Other beneficial features of the Fowler flaps are that they are relatively easy to manufacture, reducing manufacturing costs, and they increase wing area. An image of the wing system is seen in Figure 11-12.

Table 11.4: Fowler Flap Characteristics

Characteristics	Value
Weight and $C_{L_{max}}$	9,353 lbf, 26% off $C_{L_{max}}$
Change in $C_{L_{max}}$	2.2
Change in $C_{L_{max}}$ at take-off needed	0.042
Change in $C_{L_{max}}$ at landing needed	2.88
Required $C_{L_{max}}$ with flaps down	2.02
Wing Area to Wing Flap Area	0.8
Flap Chord to Wing Chord	0.3
Flap Angle	28.03°

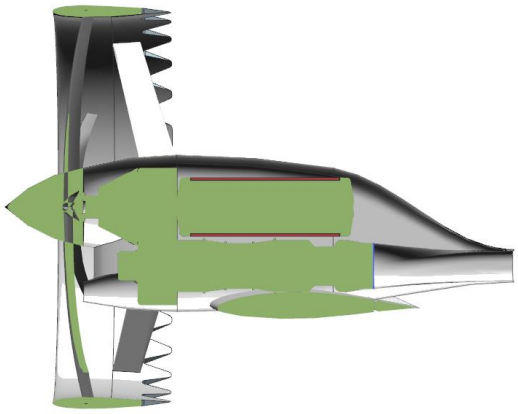

Figure 11-12: High Lift Device System

11.8 Empennage Sizing

The projected empennage characteristics for the Meadowlark aircraft are shown below in Table 11.5. These are the initial sizing values estimated through Roskam techniques. The approximate center of gravity (CG)

locations of the horizontal and vertical tail was estimated with a three-view CAD drawing of the Meadowlark. The areas of the tails were calculated given the wing area, wing span, and mean geometric chord of the wing.

Table 11.5: Projected Empennage Characteristics

Projected Characteristics	Meadowlark
Horizontal Tail Volume Coefficient, $\bar{V}_h$	1.20
CG to the Quarter-Chord of the MGC on the Horizontal Tail, X_h (ft)	42.4
Horizontal Tail Area, S_h (ft^2)	70
Incidence Angle of the Horizontal Tail, i_h (°)	0
Sweep Angle of the Horizontal Tail, Λ_h (°)	20.5
Vertical Tail Volume Coefficient, $\bar{V}_v$	0.08
CG to the Quarter-Chord of the MGC on the Vertical Tail, X_v (ft)	42.4
Vertical Tail Area, S_v (ft^2)	60
Dihedral Angle of the Vertical Tail, Ψ_h (°)	90
Sweep Angle of the Vertical Tail, Λ_v (°)	30

The sweep angle of the horizontal tail, 20.5°, is much greater than the wing's sweep of 10°. This ensures that the horizontal tail does not stall before the wing. This remains true for the vertical tail, which has a sweep of 30°. Table 11.6 contains Meadowlark's selected sizing values using Figure 11-13 and Figure 11-14 and the Munk shift values were calculated using Multhopp Integration. There are some slight changes made to ensure level 1 handling qualities identified later on.

Table 11.6: Empennage Selected Sizing Values

Sizing Characteristics	Values
Lift Coefficient due to Angle of Attack on the Wing, $C_{L_{\alpha w}}$ (rad^{-1})	4.1
Lift Coefficient due to Angle of Attack for the Wing-Fuselage, $C_{L_{\alpha wf}}$ (rad^{-1})	4.1
AC Wing Location from the LE of the Wing MGC, $\bar{\bar{X}}_{ac_w}$ (fr. $\bar{c}$)	.25
Lift Coefficient due to Angle of Attack on the Horizontal Tail, $C_{L_{\alpha h}}$ (rad^{-1})	3.37
AC Horizontal Tail Location from the LE of the Wing MGC, $\bar{\bar{X}}_{ac_h}$ (fr. $\bar{c}$)	7.206
Horizontal Tail Area, S_h (ft^2)	90
Downwash on the Horizontal Tail due to Angle of Attack, $\partial\varepsilon_h/\partial\alpha$	.0233
Change in AC Location due to Fuselage (Munk Shift), $\Delta\bar{X}_{ac_f}$ (fr. $\bar{c}$)	-0.22
AC Location of the Aircraft from the LE of the Wing MGC, $\bar{\bar{X}}_{ac_A}$ (fr. $\bar{c}$)	.7365
Vertical Tail Area, S_v (ft^2)	81.05
Yawing Moment Coefficient due to Sideslip for the Wing-Fuselage, $C_{n_{\beta wf}}$ (deg^{-1})	-.0016
Yawing Moment Coefficient due to Sideslip, C_{n_β} (deg^{-1})	.0041

Figure 11-13 tracks the aerodynamic center (AC) and CG locations as a function of horizontal tail area with the forwardmost and aftmost CG location lines superimposed to visualize the static margin range. Horizontal tail area was selected based on the intersection of the most aft CG line for neutral stability. A flight controller will be utilized with this targeted static margin to maintain stability. A more neutral stability point allows for a more

efficient flight, reducing fuel and emissions. Figure 11-14 tracks yawing moment coefficient as a function of vertical tail area.

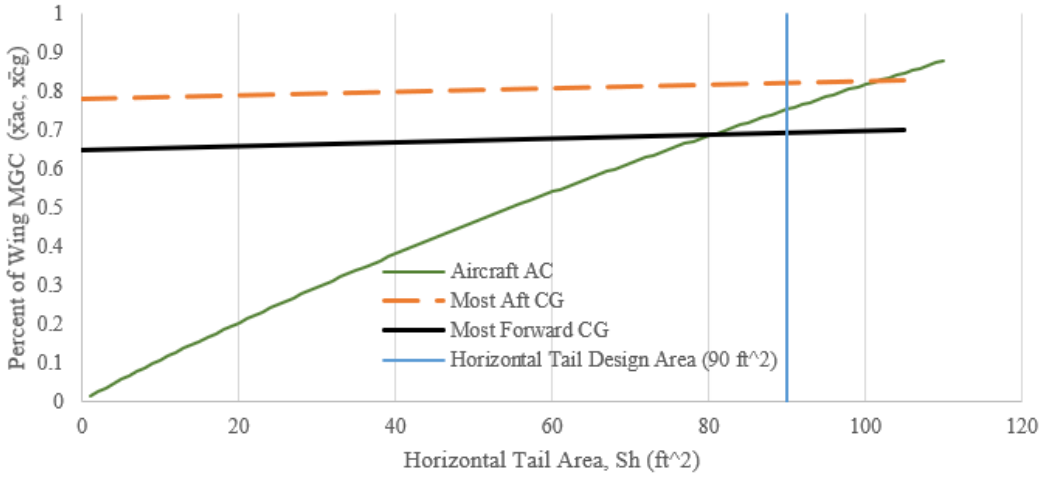

Figure 11-13: AC and CG Location Plot with Horizontal Tail Area

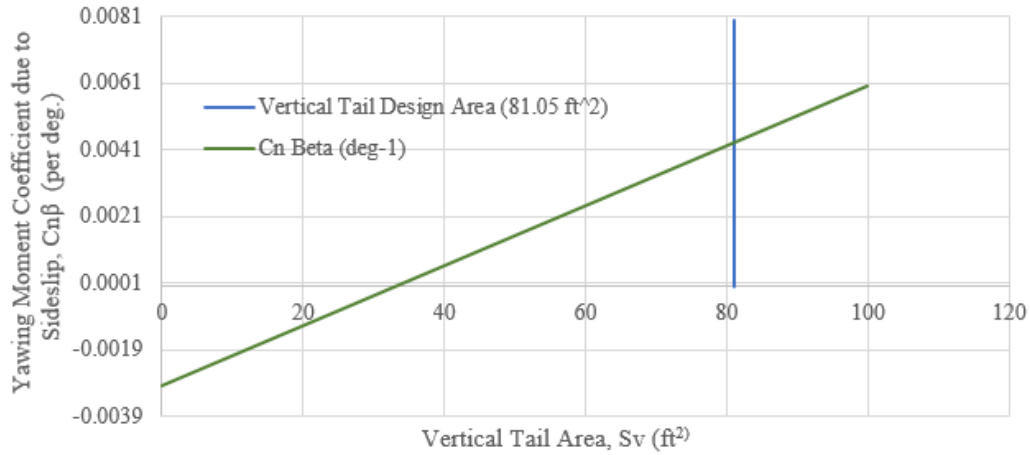

Figure 11-14: Yawing Moment Coefficient Plot with Vertical Tail Area

An important note is that the empennage design is not limited by engine out yawing moment, but instead was sized for inherent stability and a Cn_{β} value which induces lateral-directional stability. The engines of the Meadowlark are cross-shafted, which mitigates the engine out yawing moment effects. Cross-shafting allows for a transfer of power to keep both engines alive even if not at full power. A full image of the empennage is seen below in Figure 11-15.

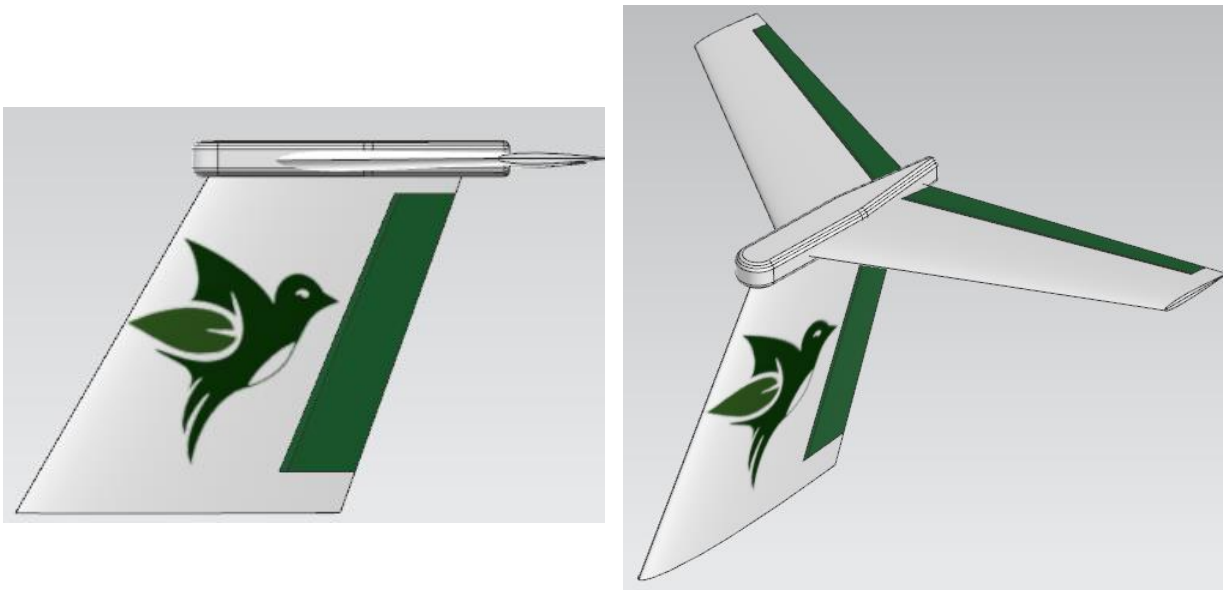

Figure 11-15: Empennage Design

11.9 Landing Gear Designs

The landing gear chosen for the Meadowlark is a retractable, tricycle landing gear, seen in Figure 11-16. The nose gear assembly have two wheels on the nose gear, and the main gear assembly has two sets of wheels on each gear, with a total of four wheels on the main landing gear. The size of the wheels for both the nose gear and main gear are shown in Table 11.7. The longitudinal placement of the main gear allows the Meadowlark to achieve 10° of takeoff clearance, shown in Figure 11-18. The main landing gear was placed using a 35° half-angle shown in Figure 11-17. This was designed to account for the longitudinal stability of the aircraft. This placed the main gear 68.5 inches off of the centerline of the aircraft. The lateral ground clearance was design to have an angle of 10°, placing the main landing gear at FS507. The takeoff angle is able to be this low due to the fact that the Meadowlark has both fowler flaps and blown wings to help with takeoff rotation. The nose gear is located at the bulkhead that separates the cockpit and the main cabin area.

Table 11.7: Landing Gear Wheel Dimensions

	Nose Gear	Main Gear
Wheel Diameter (in.)	14.5	26
Wheel Thickness (in.)	5.5	6.6

Figure 11-16: Landing Gear Front View

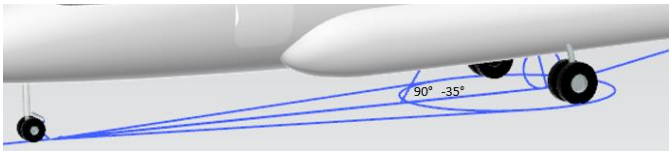

Figure 11-17: Landing Gear Placement Method

Figure 11-18: Seater Side View and Clearance Angle

The landing gear configuration was designed on several aspects. The Meadowlark landing gear will have one strut for the nose gear and two struts for the main gear. Each strut will hold two tires, with a total of six tires for the aircraft. Table 11.8 shows the landing gear loads and components such as the length of the main gear from the CG (l_m) and length of the nose gear from the CG (l_n). The dynamic and static tire loads were determined for the aircraft, as shown in Table 11.9. For the aircraft, the maximum tire loads were more critical for the tire selected.

Table 11.8: Landing Gear Loads

Loads	Meadowlark
W_{to} (lb)	36,000
l_m (in)	28.6
l_n (in)	330
h_{cg} (in)	125
P_m (lb)	32,400
P_n (lb)	3,600

Table 11.9: Determined Static and Dynamic Loads

	Meadowlark
Maximum Static Main Gear Load, PM_{max} (lbf)	34,700
Maximum Static Nose Gear Load, PN_{max} (lbf)	3,850
Minimum Static Main Gear Load, PM_{min} (lbf)	5,500
Minimum Static Nose Gear Load, PN_{min} (lbf)	3,400
Dynamic Main Gear Load, Pm_{dynt} (lbf)	6,870
Dynamic Nose Gear Load, Pn_{dynt} (lbf)	4,260

Table 11.10 contains the tire and landing gear defections calculated, along with components that influence the deflections. The touchdown rate was determined by the FAR 25 requirements, thus having a rate of 12 feet per second. The landing gear load factor and shock absorption efficiency for the tires were determined through *Jan Roskam's Aircraft Design: Part IV*. Since the Meadowlark aircraft will use oleo-pneumatic struts, the shock absorption efficiency is known.

Table 11.10: Landing Gear Strut and Tire Deflection

	Main Gear	Landing Gear
Touchdown Rate, w_t (ft/s)	12	
Landing Weight, W_L (lbf)	36,000	
Touchdown Kinetic Energy, Kt (ft-lbf)	965,000	
Allowable Tire Deflection, s_t (in)	2	1.5
Shock Absorption Efficiency for oleo-pneumatic, η_s	0.80	
Shock Absorption Efficiency for tires, η_t	0.47	
Landing Gear Load Factor, Ng	2.0	
Strut Stroke Deflection, ss (in)	18.5	16.9

Table 11.11 shows the tire selection and specifications for the main gear and nose gear. The tires were selected from several tables in *Roskam's Aircraft Design: Part IV*. The tables listed the tire dimensions, type, maximum loading, and uninflated tire pressure, which were considered for tire selection. To finalize the selection, the weight and minimum size available was examined. Along with these specifications, the clearance radius and width were calculated.

Table 11.11: Tire Selection and Specifications

	Main Gear	Nose Gear
Manufacturer	Goodrich	
Tire Outer Diameter, Do (in)	24	18
Tire Width, w_{tire} (in)	7.7	5.5
Tire Type	VII	
Maximum Loading, Pmax (lbf)	9,725	4,000
Unloaded Inflation Pressure (psi)	165	140
Static Loaded Radius, rsl (in)	10	7.5
Clearance Radius, rcl (in)	1.31	1.22
Clearance Width, wd (in)	3.4	2.8

The landing gear strut shown in Figure 11-19 shows the landing gear in full extended position. Instead of completely retracting into the sponsons, the landing gear will be squatted, leaving it partially exposed.

Figure 11-19: Nose-Wheel Strut Layout

12 Emissions, Solar Farms, and Batteries

12.1 Emissions

The Meadowlark utilizes batteries and electric motors in combination with two PW121 engines. A driving force in the development and use of hybrid-electric turboprops is the decreased fuel burn and CO_2 emissions. Based on studies, a typical hybrid-electric turboprop design would experience approximately 28% less mission fuel and CO_2 emissions [47]. As discussed in Chapter 11, De Havilland Canada is working with Pratt & Whitney Canada to develop hybrid-electric aircraft propulsion technology. This technology is to be integrated onto the Dash 8-100, and the target fuel and emissions reduction is 30% compared to other regional turboprop aircraft [48].

The Meadowlark aims to support the industry-wide goal of net-zero carbon emissions by 2050. Table 12.1 below lists some common causes of emissions and how the Meadowlark design works to reduce them.

Table 12.1: Emission Mitigation [49]

Cause of Emissions	Meadowlark Solution
Idling on airport tarmac & fuel use during taxi adds up to over 200 million gallons of excess fuel burn	Engines shutdown on tarmac and iGOAT used to taxi—electric taxiing could save 77,000 gallons of fuel per aircraft per year.
Dust and dirt collection reduce efficiency	ACES remove debris, leading to a 0.025% reduction in fuel use and saving $22,000 per aircraft per year.
Drag reduces efficiency	NLF fuselage and blended winglets reduce drag. Winglets alone can save 83,000 gallons of fuel per aircraft per year.
Congestion in landing zones, causing aircraft to circle in holding patterns and waste fuel	High wing loading leads to greater gust resistance and maintains safe high operational tempos, even in extreme conditions.
100% aviation fuel	Emission-free recharging of batteries from airport-based solar farms.

The dynamic design of the Meadowlark allows for continuous improvements in engine technology, and can easily adapt to new technologies. As propulsive technology develops to decrease emissions over the lifespan of the aircraft (with an EOS date predicted at 2085), the Meadowlark can accommodate new engine designs and smaller battery sizes. This is a huge advantage over static aircraft designs, as demonstrated in Figure 12-1 below.

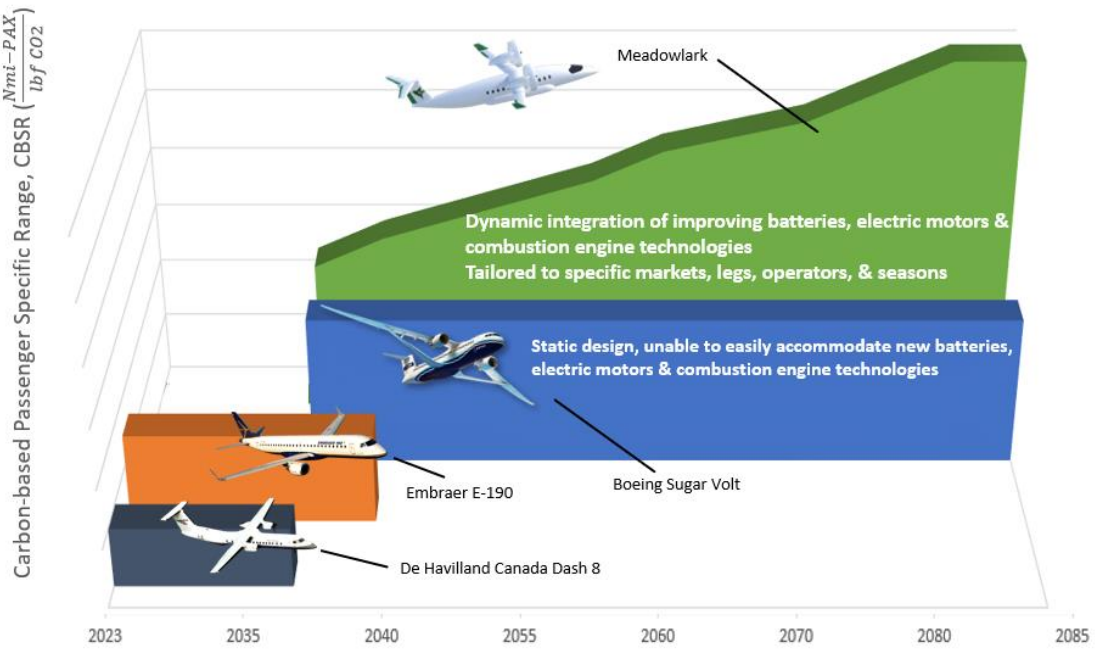

Figure 12-1: Propulsion System Adaptability

12.2 Solar Farms

As seen in Figure 1-1, the CONOPS features a solar farm on the outskirts of the airport. This solar farm, much like the one seen in Figure 12-2, will provide energy to the iGOAT and ACES chargers. 20% of public airports from 2010 to 2020 adopted the use of solar energy [50]. The use of solar power has rapidly decreased over time. A decade ago, a single solar module cost approximately $2.50 per Watt, while as of 2021, an entire utility-scale photovoltaic system costs approximately $1 per Watt [51]. This rapid decrease in price is leading to the development of solar farms in areas that are not the ideal location.

Figure 12-2: Solar Farm [51]

When the Meadowlark is introduced in 2035, it will have a limited number of airports to utilize due to the need of a solar farm to power the iGOAT and ACES chargers. The airports the Meadowlark will first begin to fly into are locations with significant open land, such as dessert areas like Arizona and Nevada. By the year 2050, solar farms will be more widespread across airports, allowing the Meadowlark to continue to expand for decades.

12.3 Batteries

As mentioned in Chapter 10, the Meadowlark will use different battery pack types, as shown in Table 12.2. Depending on the payload-range, the aircraft can use different pack types. For example, if the maximum battery weight is 3,400 lbf, the battery pack configuration can be Type B, Type C, and Type E.

Table 12.2: Battery Pack Types

Battery Pack Type	Weight (lbf)
A	4,000
B	2,000
C	1,000
D	500
E	250

At the required altitude and cruise speed, the determined shaft power is 1.31 MW. Figure 12-3 shows the volumetric energy density of Lithium-ion batteries increasing between 2008 to 2020. The increase in the volumetric energy density allows for the size of the battery pack specified to remain the same, allowing for the aircraft to travel further. For example, in 2008, lithium-ion batteries had a volumetric energy density of 55 watt-hours per liter. By 2022, the density increases to 450 watt-hours per liter. By 2035, the volumetric energy density of the batteries will increase, with the size remaining constant. Thus, allowing for the batteries packs to adapt over time.

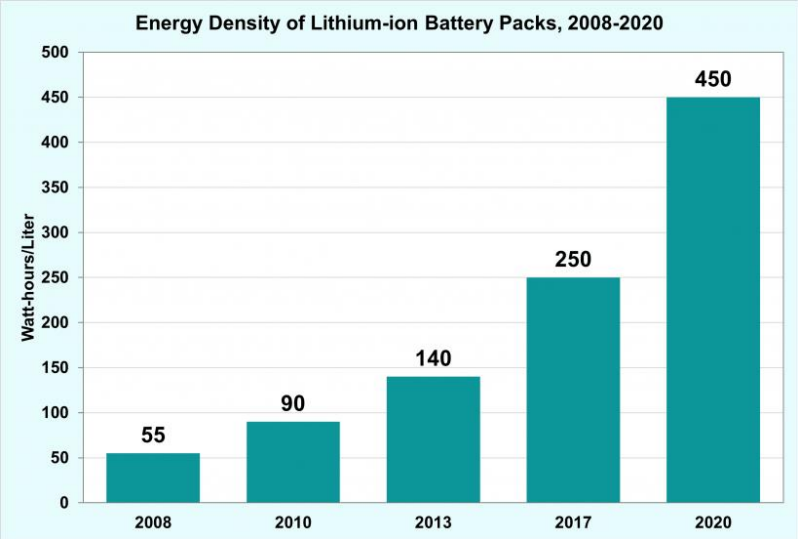

Figure 12-3: Volumetric Energy Density of Lithium-Ion Batteries from 2008 to 2020 [50]

13 Weight and Balance

The following chapter shows the Class II balance analysis and CG excursion diagram.

13.1 Center of Gravity Excursion

For the final weight and balance calculations, methods from *Roskam's Airplane Design Part V: Component Weight Estimation.*[53] Table 13.1 displays the weight of each component, the weight fraction of each component, which is the weight of the component divided by the aircraft take-off weight, the CG location along the x-axis, and that center of gravity location multiplied by the weight of each component. The sum of the weight fractions totals up to equal 100%. The initial calculations showed that the Meadowlark was within 5% of the overall takeoff weights and preliminary weight and balance. Using the values from Table 13.1 and Table 13.2, the final CG excursion diagram was created, as shown in Figure 13-1. This diagram shows that the main landing gear is located behind the centers of gravity for each weight case. The vertical lines of the CG excursion diagram indicate the Meadowlark is utilizing ballast tanks to store fuel; the CG does not move when fuel is added or removed.

Table 13.1: Class II Weight Sizing

Weight Sizing		
Component	Weight (lb)	Weight Fraction
Takeoff	37090	
Empty	16901	45.6%
Fuel	4580	12.3%
Payload	12660	34.1%
TOTAL		1.00

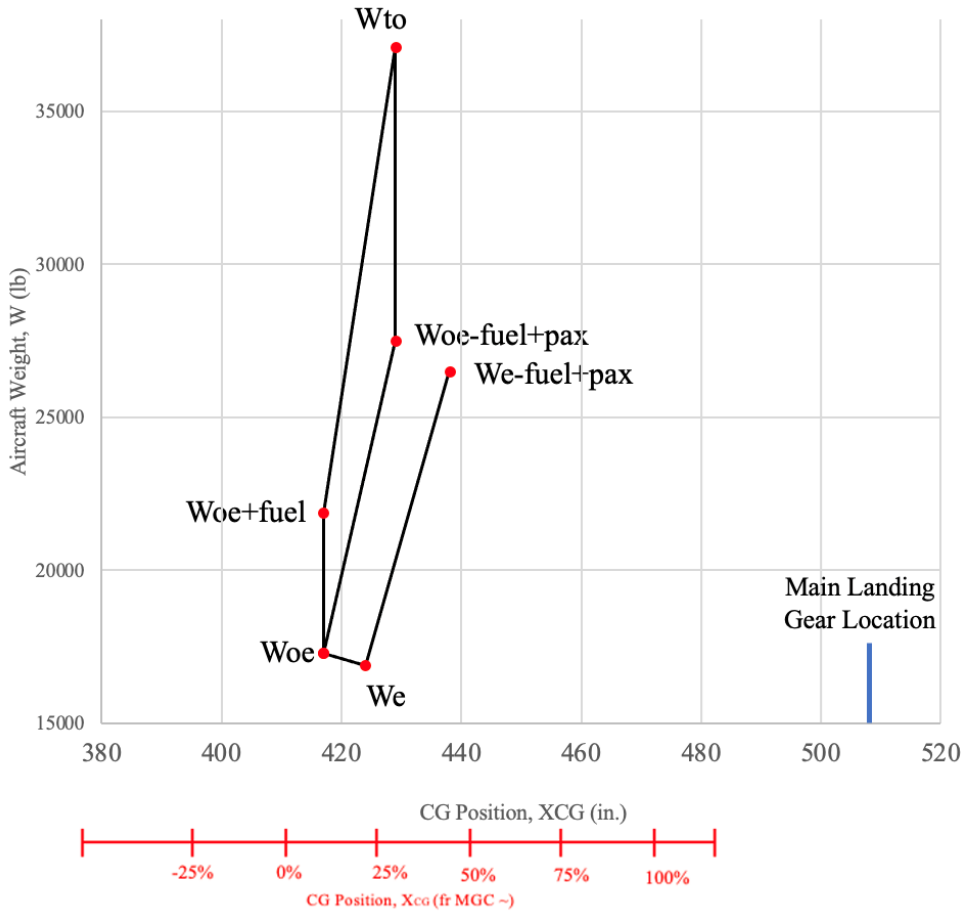

Figure 13-1: CG Excursion Diagram

The different specific load cases' CG excursions and weights are seen in Table 13.2.

Table 13.2: CG Excursions and Weights for Load Cases

Load Case CGs			
Load Case	Weight	W*Xcg (lb-in)	Xcg (in)
We	16901	7166024	424
Woe	17299	7213683	417
Woe + Fuel	21879	9123543	417
Wto	37090	15911610	429
Woe + Pass	26598	11649924	438
Woe	17299	7213683	417

13.2 Accounting for Static Margin and Center of Gravity Excursion

The center of gravity excursion for the Meadowlark is 35.8 feet and the static margin remains positive.

Table 13.3 displays the location of items with respect to their CG in order to balance the Meadowlark.

Table 13.3: Weight and Balance Sizing

Balance Analysis					
Component		Weight Fraction	Weight (lb)	Xcg (in)	W*Xcg (lb-in)
STRUCTURE	Wing	3.9%	1433	402	575743.575
	Horizontal Tail	0.5%	170.2	916	155911.1994
	Vertical Tail	0.3%	125	892	111492.5625
	Fuselage	7.6%	2816	424	1192582.457
	Nacelle	3.2%	1188	418	496584
	Landing Gear (Main)	3.6%	1344	434	583296
	Landing Gear (Nose)	0.9%	318.6	104	33134.4
	Cargo Carpet	2.7%	1000	340	340000
FUEL	Fuel System	1.8%	676	450	304200
	Trapped Oil and Fuel	0.0%	18	402	7236
	Max Fuel Capacity	12.3%	4580	402	1841160
POWERPLANT	Engine	7.9%	2931	418	1225158
FIXED EQUIPMENT	Propulsion System	1.2%	461	418	192698
	Avionics & Instrumentation	0.0%	3.6	121	435.6
	Surface Controls	1.3%	468	424	198432
	Hydraulic System	8.7%	3240	424	1373760
	Pneumatic/Electrical System	1.9%	720	424	305280
	Electronics	0.1%	36	121	4356
	Air Conditioning System	2.9%	1080	424	457920
	Anti-Icing System	0.0%	18	418	7524
	Furnishings	4.9%	1800	458	824400
	Auxiliary Gear	0.0%	3.6	424	1526.4
PAYLOAD	Pilot (2 Pilots, 1 Crew)	1.0%	380	145	55100
	Passengers + One Crew (50 Max)	27.5%	10190	458	4667020
	Baggage 1 (40lbs / Passenger)	5.4%	2000	458	916000
	Baggage 2 (30 lbs / Crew)	0.2%	90	659	59310
	TOTAL	1.00			

14 Advanced CAD

A three-view of the Meadowlark aircraft is seen in Figure 14-1.

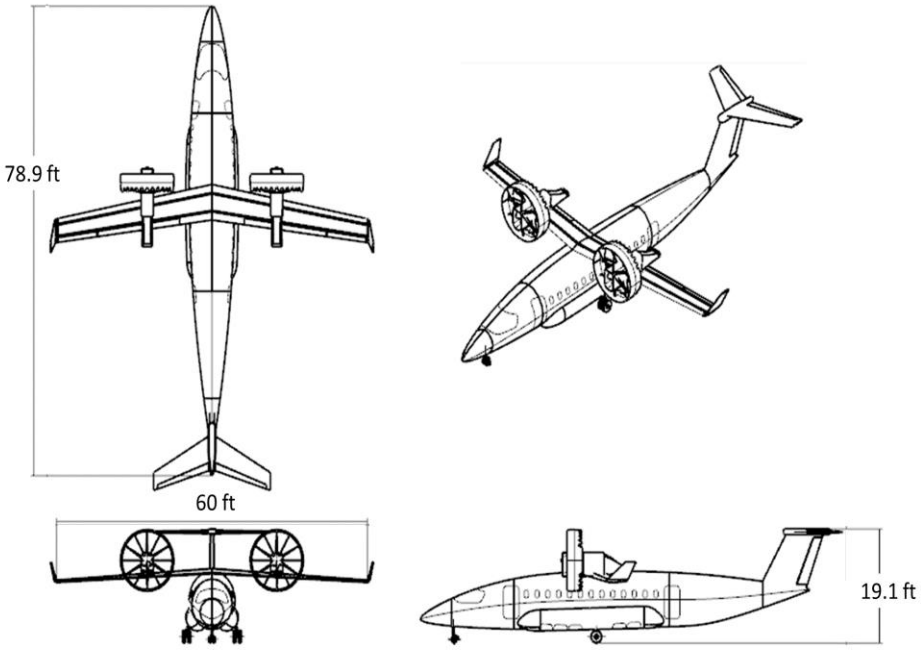

Figure 14-1: Meadowlark Three-View

A situational rendering of the Meadowlark is seen in Figure 14-2 in a hangar environment. The materials applied to the CAD components are listed in Table 14.1.

Figure 14-2: Meadowlark Situational Rendering

Table 14.1: CAD Model Materials

Airframe/Exterior	
Skin	Carbon-PEEK Composite
Ribs	Aluminum
Spars	Carbon-PEEK Composite
Fuselage Frames	Aluminum
Engine Structural Support	Titanium
Landing Gear Strut	Steel
Landing Gear Wheel	Steel
Landing Gear Tire	Rubber
Forward Bulkhead	Carbon-PEEK Composite
Aft Pressure Bulkhead	Carbon-PEEK Composite
Interior	
Windows	Plexi Glass
Seat	Leather
Floor	Carpet
Interior Walls	Plastic

14.1 Substructure

The Meadowlark substructure are seen in Figure 14-3. Details of the substructure are outlined in following subsections.

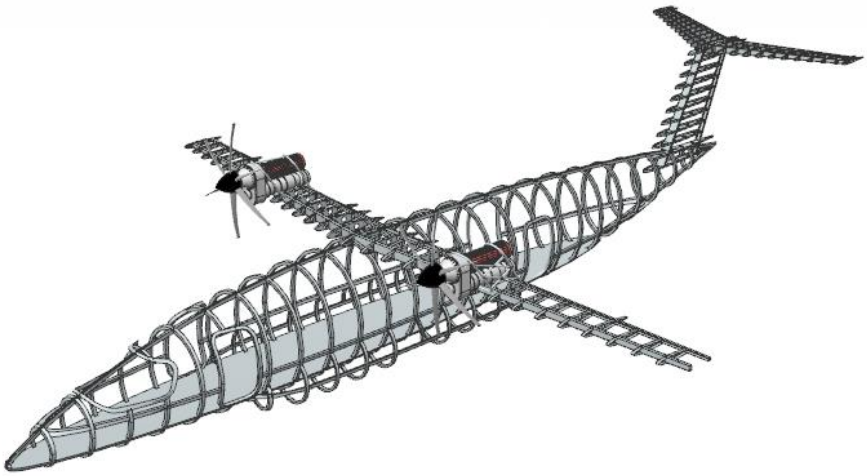

Figure 14-3: Meadowlark Substructure

14.1.1 Fuselage Substructure

The fuselage substructure can be seen in Figure 14-4. and characteristics can be found in Table 14.2.

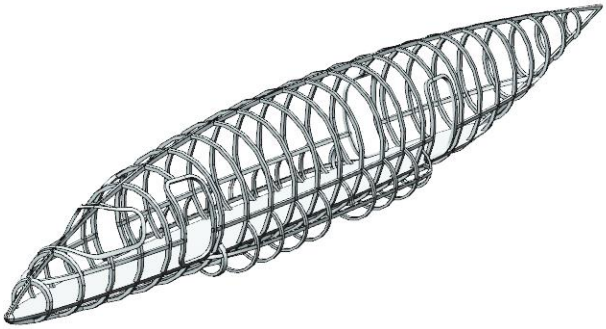

Figure 14-4: Fuselage Substructure

Table 14.2: Fuselage Characteristics

Frame Depth	3 in.
Frame Spacing	25 in.
Longeron Spacing	24 in.

14.1.2 Wing Substructure

The wing substructure, seen in Figure 14-5, has a two-spar design. Characteristics of this substructure can be found in Table 14.3.

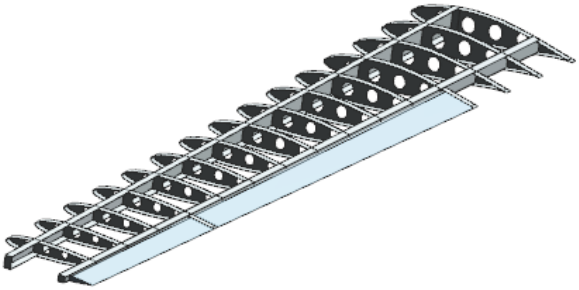

Figure 14-5: Wing Substructure

Table 14.3: Wing Characteristics

Rib Spacing	18 in.
Spar Thickness	0.125 in.
Front Spar Location (% chord)	30%
Rear Spar Location (% chord)	70%

14.1.3 Horizontal Tail Substructure

The horizontal tail also has a two-spar design with the only control surface being the elevator, seen in Figure 14-6. Characteristics of this substructure can be found in Table 14.4.

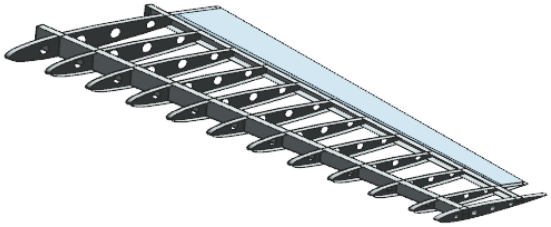

Figure 14-6: Horizontal Tail Substructure

Table 14.4: Horizontal Tail Characteristics

Rib Spacing	12 in.
Spar Thickness	0.125 in.
Front Spar Location (% chord)	30%
Rear Spar Location (% chord)	70%

14.1.4 Vertical Tail Substructure

The vertical tail also has a two-spar design with the only control surface being the rudder, seen in Figure 14-7. Characteristics of this substructure can be found in Table 14.5.

Table 14.5: Vertical Tail Characteristics

Rib Spacing	12 in.
Spar Thickness	0.125 in.
Front Spar Location (% chord)	30%
Rear Spar Location (% chord)	70%

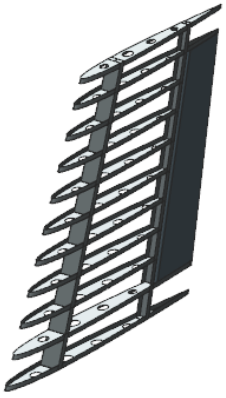

Figure 14-7: Vertical Tail Substructure

14.1.5 Engine Substructure

The structural provisions for the hybrid turboprop engines of the Meadowlark consist of engine cradles which attach to both wing spars. These cradles are made of titanium tubing and support the engine and motor

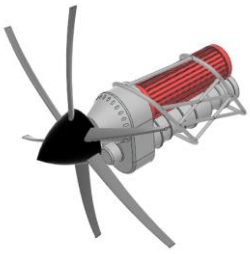

Figure 14-8: Engine Mount Substructure

assembly from above and below. While costly, titanium tubing offers excellent specific strength and is less intensive to manufacture compared to composite elements. The engine cradle can be seen in Figure 14-8.

15 Aircraft Systems

The following sections outline all aircraft systems integrated on the Meadowlark.

15.1 Flight Control Systems

The flight control system layout is shown below in Figure 15-1. This diagram pictures how many actuators are on each control surface and how they are connected to the controllers and computer systems. To ensure redundancy, the rudder and elevators have three actuator systems, the ailerons, Fowler flaps, and Krueger flaps have two actuator systems, and the slats have one actuator system as they will use electro hydrostatic actuators.

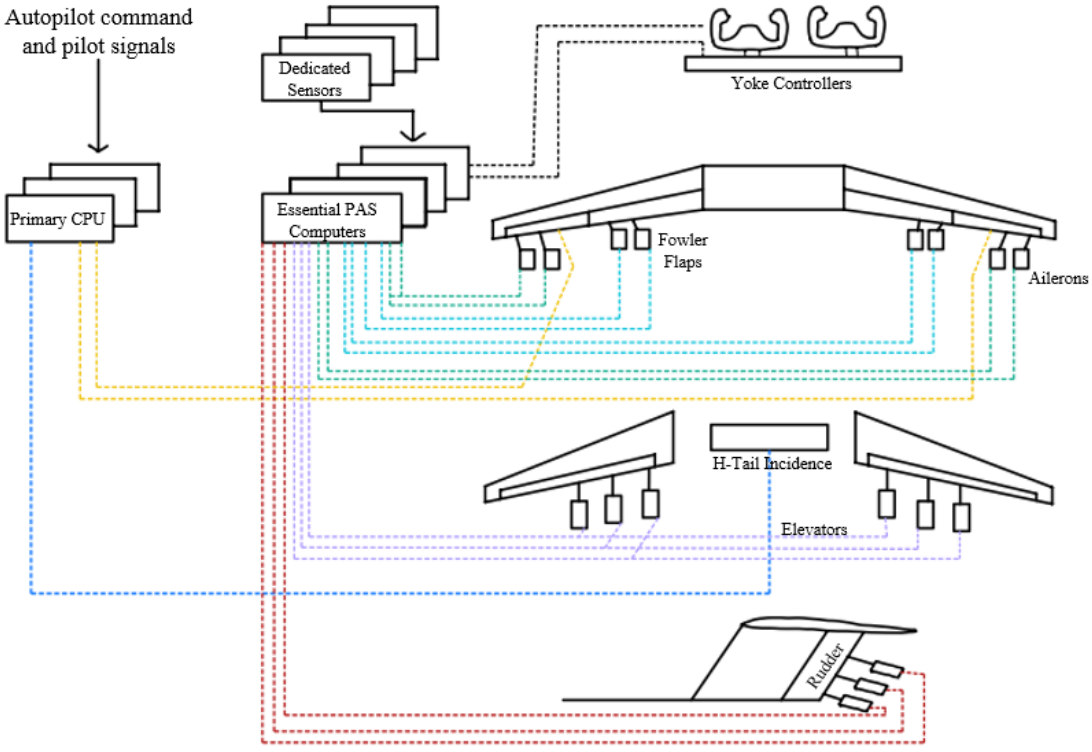

Figure 15-1 Flight Control System

15.2 Fuel Systems

The fuel system will have four tanks: one in each wing, one in the left sponson, and one ballast tank at the back of the plane. All tanks will be interconnected with pumps to allow the entirety of the 4,580 lbs of necessary fuel to flow. To store the 90.30 ft^3 of fuel volume, the two wing tanks will store 21 ft^3 each, the sponson will hold 50 ft^3, and the ballast tank will hold 21 ft^3 of fuel. As the wing has anhedral, gravity will feed the wing-housed fuel towards the wingtips. The pumps will be at the intersection of the winglets and the wing. These wing pumps will either pump to the engine or to the ballast tank. There will be pumps at the bottom of the sponson tank that will pump to the wings' fuel tanks. The winglets will act as surge tanks for the fuel and they will allow fuel to flow in them if needed. There will be a vent at the top of the winglets and at the top the empennage for the ballast tank. There is no vent for the sponson tank because the fumes will travel to the wing tanks. There is one refueling port at the left sponson. The fuel will be immediately pumped from the sponson refueling site to the wings for them to fill first. Then, the sponson will be filled until the necessary fuel is reached. Pumps will act to move any fuel weight to the ballast tank for CG/balance purposes. The left side and right sides of the fuel system can be seen in Figure 15-2 and Figure 15-3.

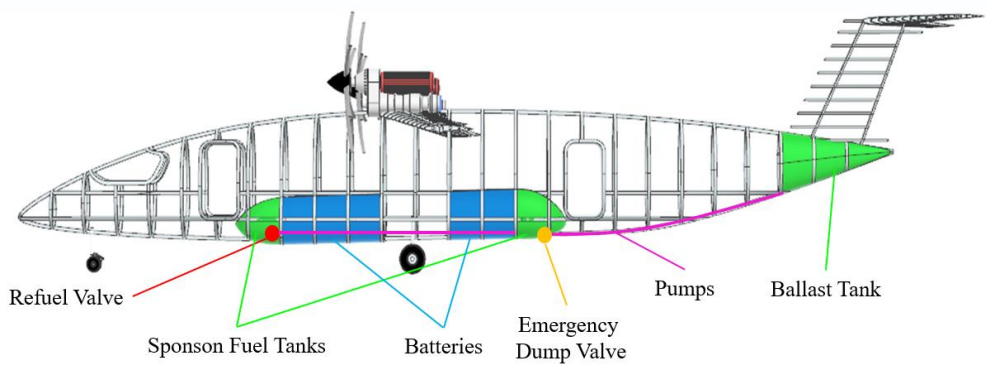

Figure 15-2: Left Side Fuel System

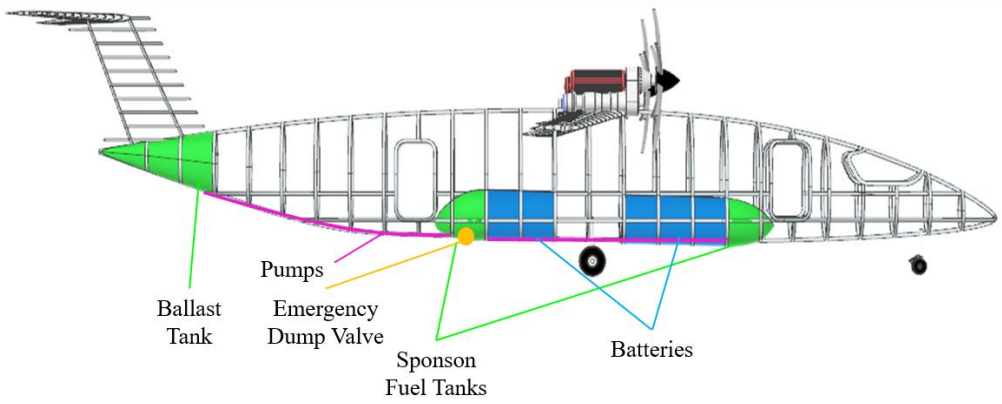

Figure 15-3: Ride Side Fuel System

Eight ultrasonic fuel level sensors will be used: two in each of the wings, two in the ballast tank, and two in the sponson tank. This will measure the height of the fuel in the tank. For crash worthiness, 50 ft^3 of fuel will be pumped to the sponson tanks, which is 55.4% of the total fuel. These sponson tank can act like drop tanks and can be jettisoned in case of emergency. There will also be a valve at the bottom of two of the sponson tanks that can be opened to let out increments of fuel. The entire system can be seen from the top in Figure 15-4.

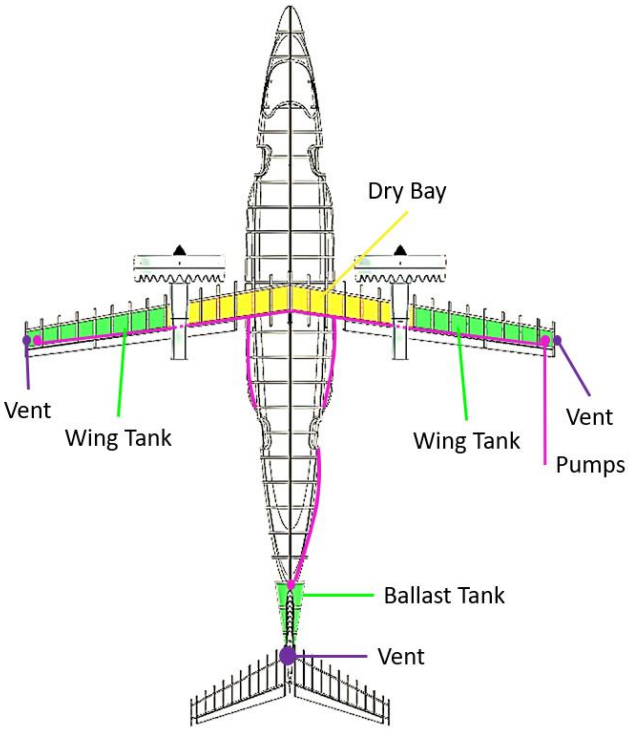

Figure 15-4: Fuel System Layout Top View

15.3 Hydraulic System

The hydraulic system is shown below in Figure 15-5. The system includes the connections to the breaks and the landing gear.

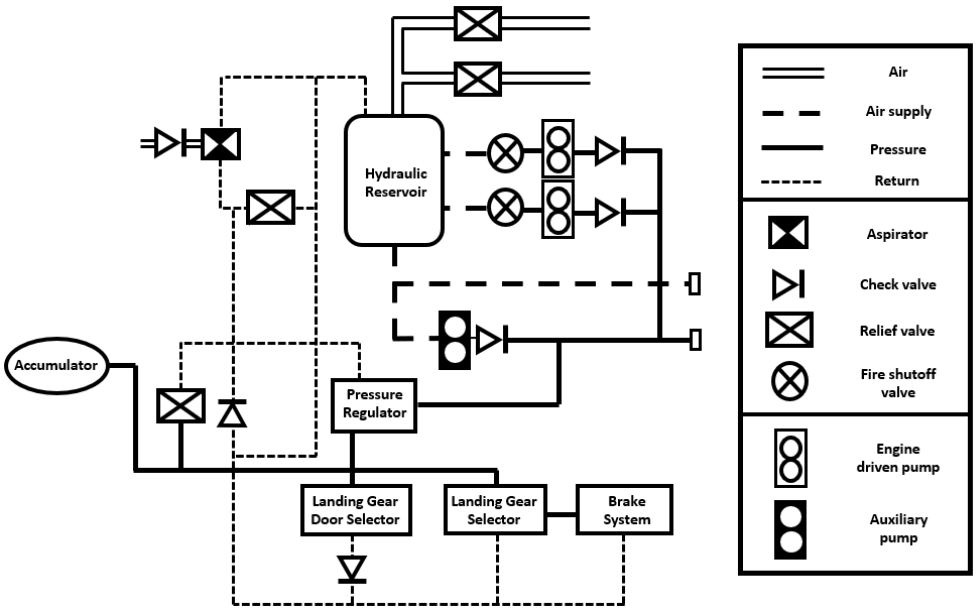

Figure 15-5: Hydraulic System Layout

15.4 Electric System

The Meadowlark electrical system, specifically for propulsion, is seen in Figure 15-6 and Figure 15-7. There is a base electrical system common in most aircraft, and a separate electrical system for the hybrid portion. The two systems are designed to be separate with one for the fuel propulsion starter, and one for the electric motors. The larger voltage utilized in the electric propulsion system allows for a huge reduction in wire diameter and volume. The systems show the batteries from the sponsons supplying power to the motors and the starters for the engines. The electric motor count, battery count, and ESC count all are to meet FAR 25 safety regulations through redundancy. The systems have two main bus components, the primary used for main ignition and heat, with the secondary bus being utilized to power the avionics, flight computer, and will house the instrumentation.

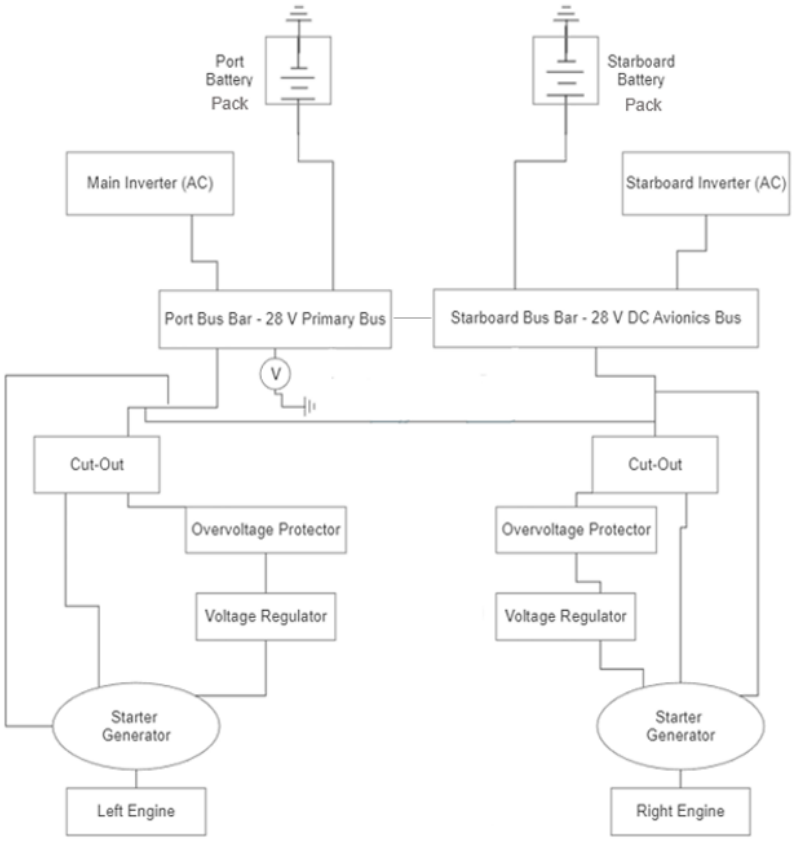

Figure 15-6: Base Electrical System Layout Schematic

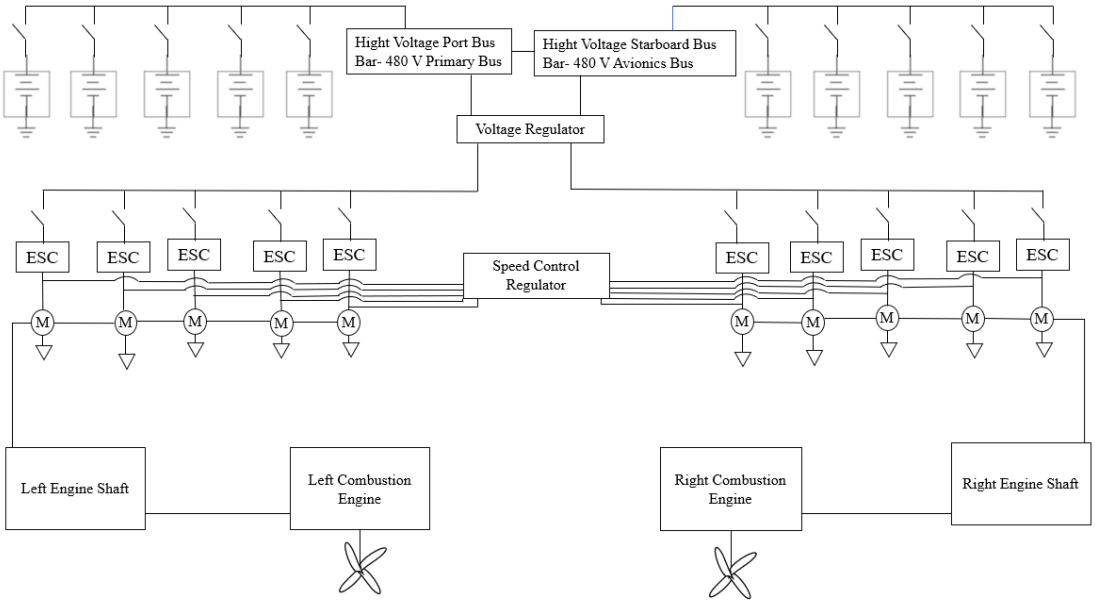

Figure 15-7: Electric Propulsion Schematic

15.5 Escape System, Fire Detection and Suppression System

Because the Meadowlark is a 50-passenger aircraft, there must be at least one Type 1 door or larger on each side of the fuselage. The Meadowlark will have two Type 1 doors on the left side for ingress and egress and one Type 1 door and one Type 2 doors on the right side for servicing and emergency egress. The escape system can be seen in Figure 15-8. This layout also shows the location of the fire detection, protection, and suppression system. There will be thermal switches in the baggage bay and lavatory, smoke detectors to measure for smoke ionization, and dry chemical fire extinguishers. The suppression system will be in the engine cowlings and the baggage bay.

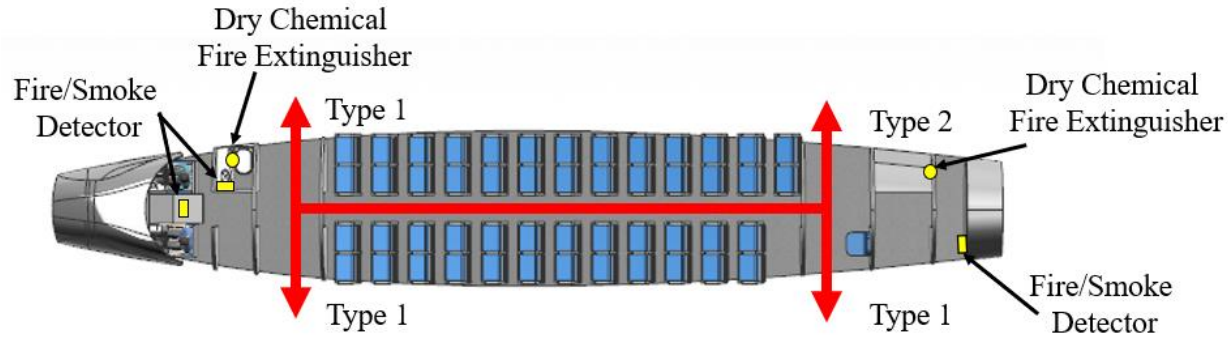

Figure 15-8: Escape System and Fire Extinguishers

15.6 Pressurization System

The pressurization system utilizes high-pressure air from the engine, ambient pressure input, and cockpit control and monitoring system. Positive or negative pressure can be used to protect the integrity of the structure that will change with altitude. This is seen in Figure 15-9.

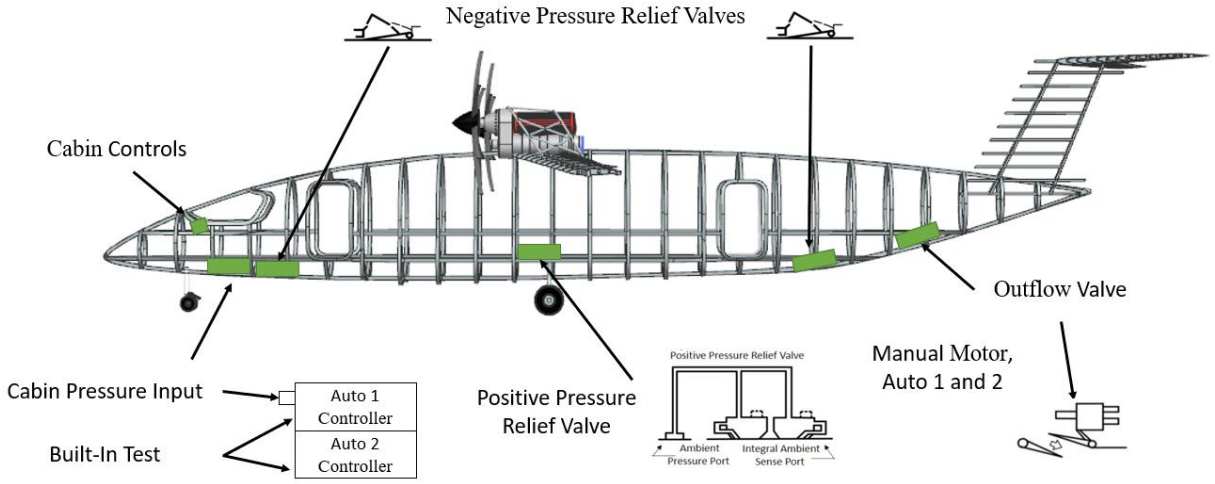

Figure 15-9: Pressurization System Layout

15.7 Pneumatic System

There is no auxiliary power unit (APU) required for the Meadowlark aircraft because of the battery power. The battery power will assist with ice protection system. The iGOAT will function as the huffer cart to assist with any necessary ground starts, all seen in Figure 15-10.

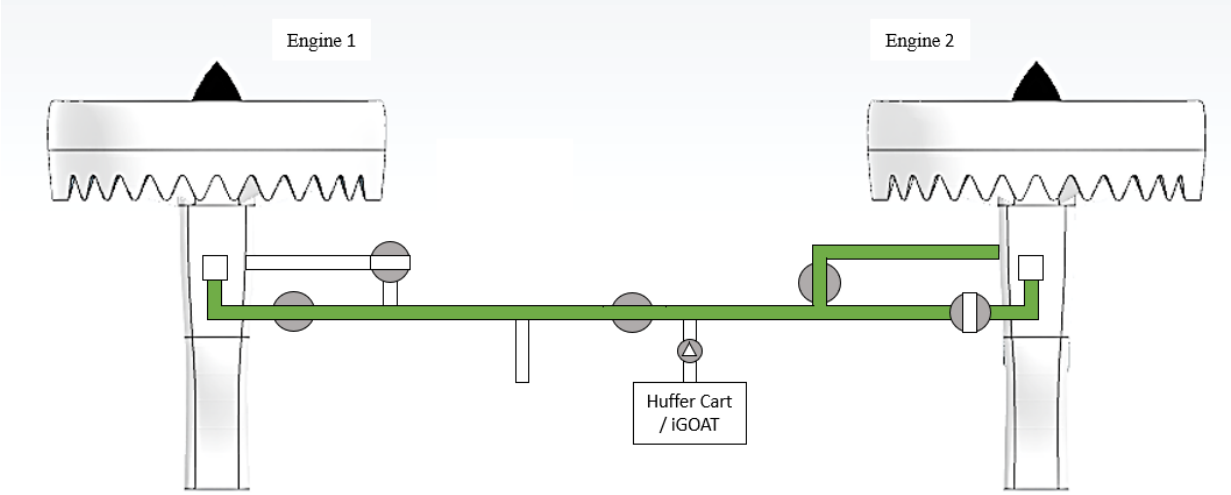

Figure 15-10: Pneumatic System Schematic

15.8 Oxygen System

There will be a crew oxygen system and passenger oxygen system. The crew system is from a gaseous source, shown in Figure 15-11. As there are far more passengers than crew, the passenger system is from a chemical source that will lessen fire hazards because there will not be common oxygen cylinder replacement.

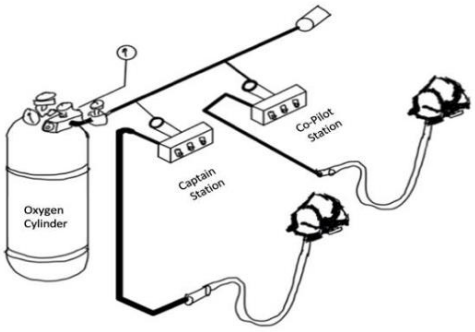

Figure 15-11 Oxygen System [36]

15.9 Cabin Sterilization System

Figure 15-12 RAY System [54]

The cabin will be sterilized using a UV light disinfection system: the Aero Hygenx RAY system. UV light disinfection has been used in hospitals and water-treatment plants for years and this more recent implementation of the systems in aircraft has been directly related to the Covid-19 pandemic. The cart will roll along the aircraft aisle and are 99% effective for eliminating harmful bacteria and viruses without the use of chemicals. There is also no personal protective equipment needed with the RAY system and no dry time like with normal disinfectant sprays. [54] The RAY system is seen in Figure 15-12.

15.10 Cockpit Instrumentation

The Meadowlark cockpit is designed to accommodate a maximum of two pilots. However, according to the market survey, about a third of total operation costs are related to salaries and benefits. To work towards decreasing operation costs, the Meadowlark provides an avionics system that supports growing levels of aircraft autonomy.

Figure 15-13 Honeywell Anthem Flight Deck System [55]

Launched in 2021, Honeywell Anthem is "the aviation industry's first cloud-connected cockpit system" [55], seen in Figure 15-13. This new flight deck system can automate tasks, leading to single-pilot operation compatibility for the Meadowlark. Honeywell Anthem allows third-party applications and websites to run, allowing integration with and control of the iGOAT and ACES system from the cockpit.

15.11 De-Icing, Anti-Fog, Rain Removal Systems

Two types of ice removal systems used on the aircraft: anti-icing and de-icing. Anti-icing will occur prior to flights from heating and through the ACES. With de-icing, the system will be used after there has been a large amount of ice buildup. The system focuses on sending engine air through airducts (specifically for de-icing). The ducts are located in the leading edge of the wing. The method can also be used for the engine. To prevent fogging and rain removal, hydrophobic coating will be used on the window. It will repel any form of water and will utilize the wipers. This system is seen in Figure 15-14. Another way to remove ice and snow on the wing is using the ACES. The ACES will operate on the trailing edge of the wing to remove these issues, which cannot be reached using the methods mentioned above.

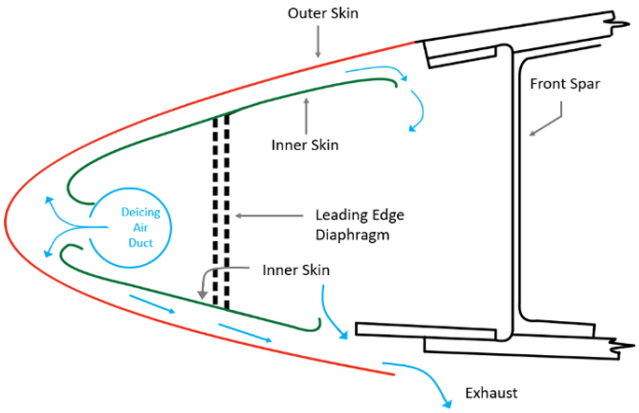

Figure 15-14 De-Icing Method for Wing and Engine [34]

15.12 Lavatory, Galley, Water, and Waste Systems

The galley will be equipped with a beverage service cart, cabinets and room for the crew member's baggage, and counter space. Locks will be on every door and cabinet for safety. The lavatory is large enough to accompany a standard size wheelchair, with two levels of sinks for different height needs. There will be around a half of gallon of water for a self-contained flush with help from the cabin pressurization. The waste will be combined with chemicals to disinfect with a catalytic process and the tanks themselves will be flushed with blue disinfectant. The waste system will be serviced after each flight from the lowest point waste drain

15.13 Safety and Survivability

The Meadowlark will be equipped with certain systems and antenna to ensure the best safety and survivability for the crew and passengers. Like most general aviation aircraft, the Meadowlark will have an emergency locator transmitter (ELT) to transmit a distress signal in the event of an aircraft accident. The Meadowlark will also possess a Traffic Alert and Collision Avoidance System (TCAS). This system will be integrated into the flight controls and

used for collision avoidance. The system will notify air traffic control of any incoming traffic. This system will use two antennas: one on the belly of the aircraft and one on the top of the aircraft.

15.14 Checked Baggage Handling System

The Meadowlark will utilize an automatic luggage carpet to decrease the amount of personnel needed to unload checked bags, decreasing the cost, and to decrease the time it takes to unload. The carpet will be installed from nose to tail in the sponsons of the aircraft. The luggage will be loaded from the right side of the back end of the aircraft and unloaded on the right side near the nose. Some things need to be taken into consideration when determining where the luggage carpet will be located. Batteries will need to be stored in the sponsons, and the storage of these will depend on passenger ingress and egress. Figure 15-15 is a plot made from Telair data that compares loading times of manual luggage loading versus the automatic carpet the Meadowlark implements. The system can be found in Figure 15-16.

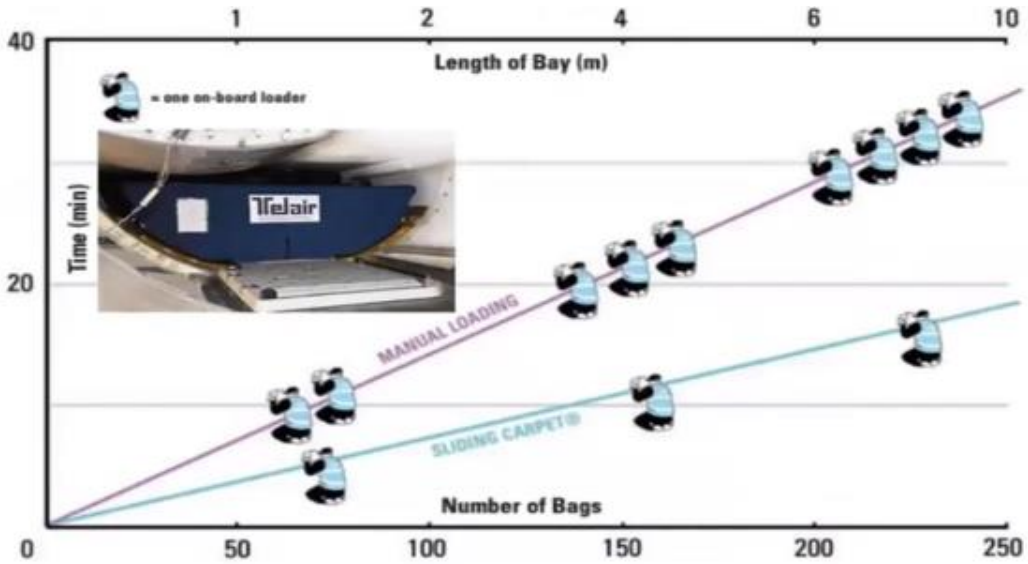

Figure 15-15: Number of Baggage Unloaders with Manual vs Sliding Carpet [56]

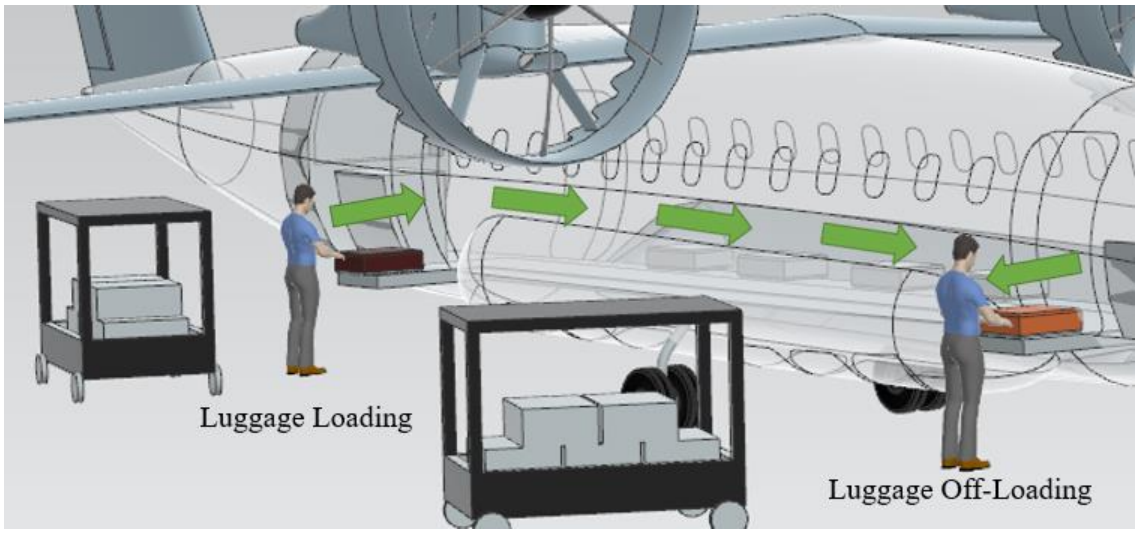

Figure 15-16: Checked Baggage Handling System

15.15 Cabin Baggage Accommodations

There will be overhead bins that span the length of the cabin, not including the wing-fuselage intersection, doors, or lavatories. These bins will be able to carry baggage with a volume of 4 ft^3, shown in Figure 15-17.

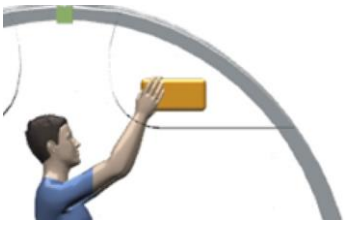

Figure 15-17: Cabin Baggage Accommodation

15.16 Ground Equipment and Servicing Vehicles Compatibility

The Meadowlark's high wing configuration allows for plenty of clearance for ground vehicles. This is a main advantage of the high wing configuration. Though the engines do protrude past the lower surface of the wings and the Meadowlark will keep the engine core running for a hot turn, the props will not be turning, so it will be safe for any ground vehicles and stairs to come near. Air stairs will be utilized for the two entrance doors to speed up passenger ingress and egress. The magic carpet allows for smoother loading and unloading while simultaneously taking up less space. The lavatory service is all completed towards the rear of the aircraft, while the galley is loaded near the front in each respective location. The cleaning services are quickly completed through the galley access door as well. Important additions to the flight line are the iGOAT and the battery loader.

Because of the small wing span of the Meadowlark and ability to have closer ground equipment vehicles, the flight line footprint will be smaller compared to other regional aircraft. The high wing configuration also allows for increased maneuverability around the aircraft during ground operations. Figure 15-18 shows a comparison of the two flight line footprints for the Meadowlark and the Embraer EMB 190. The Meadowlark flight line is 550 m^2 which is a reduction of 1260 m^2.

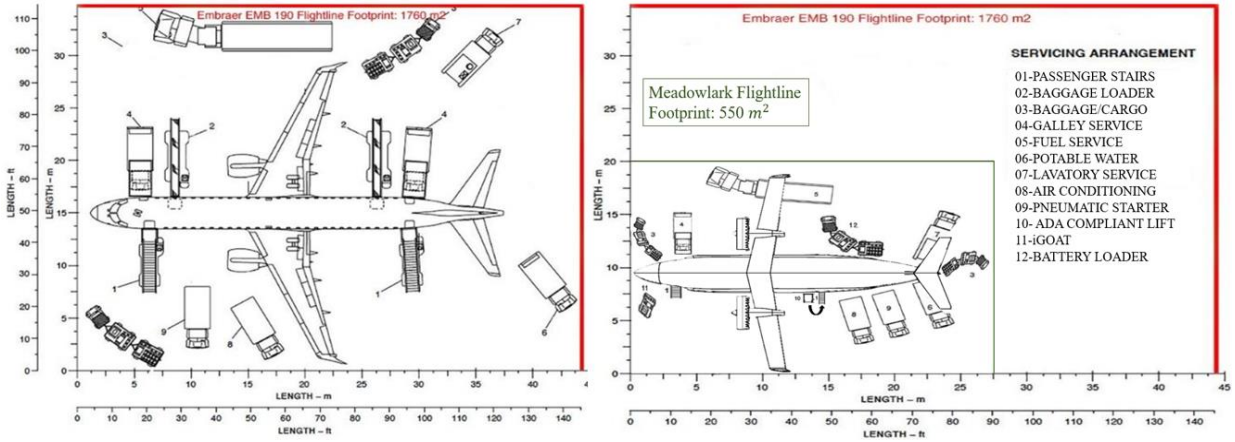

Figure 15-18: Embraer 190 vs. Meadowlark Flight Line Footprint Comparison

Although the EMB is larger than the Meadowlark, the Meadowlark has a vast advantage in turnaround time and fleet size. The Meadowlark ground operations footprint will allow for a larger fleet size and an increase in productivity as well as profit. Meadowlark will have the capability to capture both the turboprop market and the jet market through improvements like these. A terminal layout can be seen in Figure 15-19 comparing Meadowlark to competition.

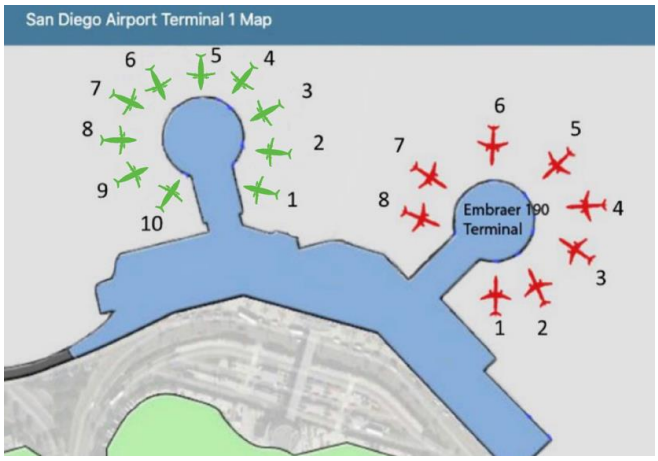

Figure 15-19 Meadowlark vs. Embraer 190 Terminal Packing

16 Class II Stability and Control

Advanced Aircraft Analysis (AAA) dynamic modeling software was used to preform stability and control analysis for the Meadowlark. The calculated metrics for longitudinal and lateral-directional stability are seen in Table 16.1. These can be compared to the requirements for short period and phugoid damping ratios for different handling qualities and flight phases are seen in Table 16.2 and

Table 16.3, and time to double amplitude for roll mode and spiral mode at flight phases are seen in Table 16.4 and Table 16.5. Meadowlark meets all of the level one handling qualities.

Table 16.1: Meadowlark AAA Stability Metrics

	Meadowlark
Load Factor per Angle of Attack, $^{n}/_{\alpha}$, (g's/rad)	7.39
Short Period Natural Frequency,$\omega_{n_{sp}}$, (rad/s)	1.4648
Short Period Damping Coefficient, ζ_{sp}	0.367
Phugoid Natural Frequency, $\omega_{n_{ph}}$, (rad/s)	0.1515
Phugoid Damping Coefficient, ζ_{ph}	0.04
Dutch Roll Natural Frequency, $\omega_{n_{dr}}$, (rad/s)	2.309
Dutch Roll Damping Coefficient, ζ_{dr}	0.082
Roll Mode Time to Double Amplitude, t_R, (s)	0.69
Spiral Mode Time to Double Amplitude, t_{2S}, (s)	54.09

Table 16.2: Allowable Short Period Damping Ratios for Dynamic Longitudinal Stability

Handling Qualities	Category A and C Flight Phases	Category B Flight Phases
Level 1	$0.35<\zeta_{sp}<1.30$	$0.30<\zeta_{sp}<2.00$
Level 2	$0.25<\zeta_{sp}<2.00$	$0.20<\zeta_{sp}<2.00$
Level 3	$0.15<\zeta_{sp}$	$0.15<\zeta_{sp}$

Table 16.3: Allowable Phugoid Damping Ratios for Dynamic Longitudinal Stability

Handling Qualities	Phugoid Stability Requirement
Level 1	ζ_{ph}>0.04
Level 2	ζ_{ph}<0
Level 3	t_2>55 s

Table 16.4: Time to Double Amplitude for Roll Mode Lateral-Directional Stability

Flight Phase	Class	Level I	Level II	Level III
A	I, IV II, III	t_R<1.0 s t_R<1.4 s	t_R<1.4 s t_R<3.0 s	-
B	All	t_R<1.4 s	t_R<3.0 s	t_R<10 s
C	I, II-C, IV II-L, C	t_R<1.0 s t_R<1.4 s	t_R<1.4 s t_R<3.0 s	-

Table 16.5: Time to Double Amplitude for Spiral Mode Laterial-Directional Stability

Flight Phase and Category	Level 1	Level 2	Level 3
A and C	t_{2S}>12 s	t_{2S}>8 s	t_{2S}>4 s
B	t_{2S}>20 s	t_{2S}>8 s	t_{2S}>4 s

The final longitudinal stability and lateral-directional stability and control values are seen in Table 16.6 and Table 16.7, respectively.

Table 16.6: Meadowlark Class II Longitudinal Stability and Control Derivatives

	Meadowlark
Lift Coefficient due to Forward Velocity, C_{L_u}	0.334
Drag Coefficient due to Forward Velocity, C_{D_u}	0.08
Pitching Moment Coefficient due to Forward Velocity, C_{m_u}	0.5912
Lift Coefficient due to Angle of Attack, C_{L_α}, (rad^{-1})	4.922
Drag Coefficient due to Angle of Attack, C_{D_α}, (rad^{-1})	0.244
Pitching Moment Coefficient due to Angle of Attack, C_{m_α}, (rad^{-1})	-1.2638
Lift Coefficient due to Angle of Attack Rate, $C_{L_{\dot{\alpha}}}$, (rad^{-1})	3.01
Drag Coefficient due to Angle of Attack Rate, $C_{D_{\dot{\alpha}}}$, (rad^{-1})	0
Pitching Moment Coefficient due to Angle of Attack Rate, $C_{m_{\dot{\alpha}}}$, (rad^{-1})	-20.3
Lift Coefficient due to Pitch Rate, C_{L_q}, (rad^{-1})	15.07
Drag Coefficient due to Pitch Rate, C_{D_q}, (rad^{-1})	0
Pitching Moment Coefficient due to Pitch Rate, C_{m_q}, (rad^{-1})	-97.52
Lift Coefficient due to Elevator Deflection Angle, $C_{L_{\delta_e}}$, (rad^{-1})	0.3533
Drag Coefficient due to Elevator Deflection Angle, $C_{D_{\delta_e}}$, (rad^{-1})	0.0077
Pitching Moment Coefficient due to Elevator Deflection Angle, $C_{m_{\delta_e}}$, (rad^{-1})	-2.376

Table 16.7: Meadowlark Class II Lateral Directional Stability and Control Values

	Meadowlark
Side Force Coefficient due to Side Slip Angle, C_{y_β}, (rad^{-1})	-0.9407
Rolling Moment Coefficient due to Side Slip Angle, C_{l_β}, (rad^{-1})	-0.1165
Yawing Moment Coefficient due to Side Slip Angle, C_{n_β}, (rad^{-1})	0.278
Side Force Coefficient due to Side Slip Rate, $C_{y_{\dot{\beta}}}$, (rad^{-1})	-0.25
Rolling Moment Coefficient due to Side Slip Rate, $C_{l_{\dot{\beta}}}$, (rad^{-1})	0.0004
Yawing Moment Coefficient due to Side Slip Rate, $C_{n_{\dot{\beta}}}$, (rad^{-1})	-0.134
Side Force Coefficient due to Roll Rate, C_{y_p}, (rad^{-1})	0.184
Rolling Moment Coefficient due to Roll Rate, C_{l_p}, (rad^{-1})	-0.439
Yawing Moment Coefficient due to Roll Rate, C_{n_p}, (rad^{-1})	-.14
Side Force Coefficient due to Yaw Rate, C_{y_r}, (rad^{-1})	0.74
Rolling Moment Coefficient due to Yaw Rate, C_{l_r}, (rad^{-1})	0.302
Yawing Moment Coefficient due to Yaw Rate, C_{n_r}, (rad^{-1})	-0.384
Side Force Coefficient due to Aileron Deflection Angle, $C_{y_{\delta_a}}$, (rad^{-1})	0
Rolling Moment Coefficient due to Aileron Deflection Angle, $C_{l_{\delta_a}}$, (rad^{-1})	0.0558
Yawing Moment Coefficient due to Aileron Deflection Angle, $C_{n_{\delta_a}}$, (rad^{-1})	-0.006
Side Force Coefficient due to Rudder Deflection Angle, $C_{y_{\delta_r}}$, (rad^{-1})	0.22
Rolling Moment Coefficient due to Rudder Deflection Angle, $C_{l_{\delta_r}}$, (rad^{-1})	0.007
Yawing Moment Coefficient due to Rudder Deflection Angle, $C_{n_{\delta_r}}$, (rad^{-1})	-0.13

Figure 16-1 contains the trim diagram in cruise flight condition for the Meadowlark. The trim diagram was developed utilizing AAA. The design point is the open red circle.

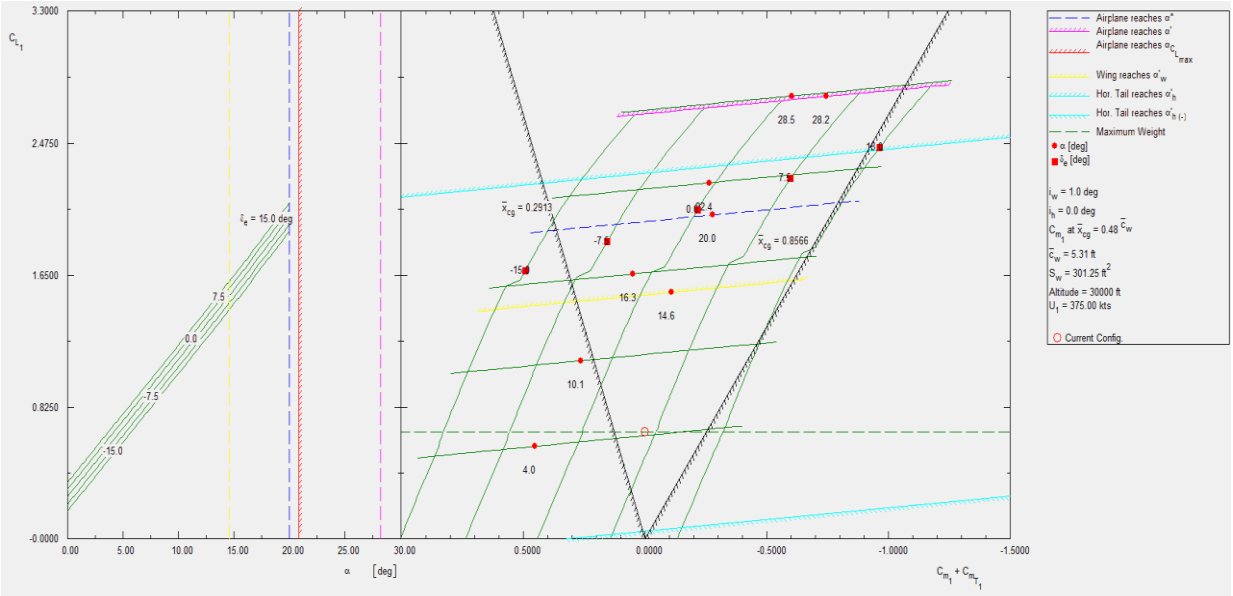

Figure 16-1: Meadowlark AAA Trim Diagram During Cruise

Figure 16-2 shows the longitudinal handling qualities during cruise through and evaluation of the short period frequency response. Meadowlark meets level one handling qualities during cruise conditions.

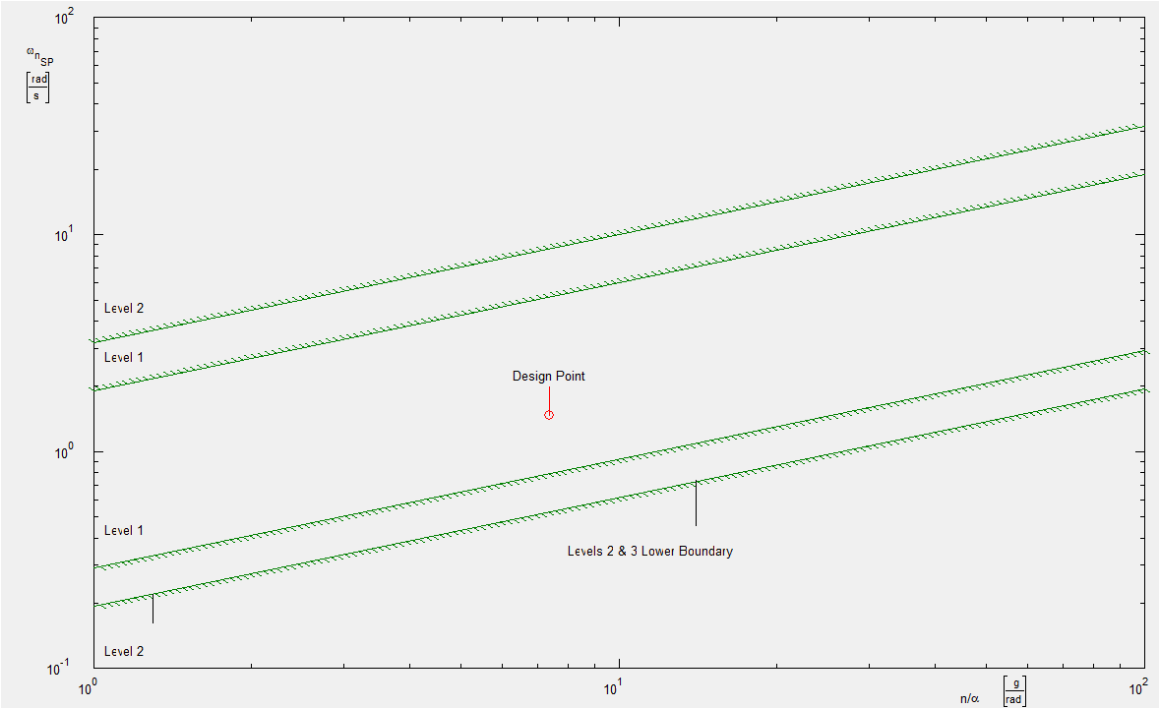

Figure 16-2: Meadowlark AAA Short Period Frequency Requirements During Cruise

Figure 16-3 shows the Dutch roll frequency and damping requirements AAA analysis of the Meadowlark. Meadowlark meets level one handling qualities for Dutch roll in cruise conditions.

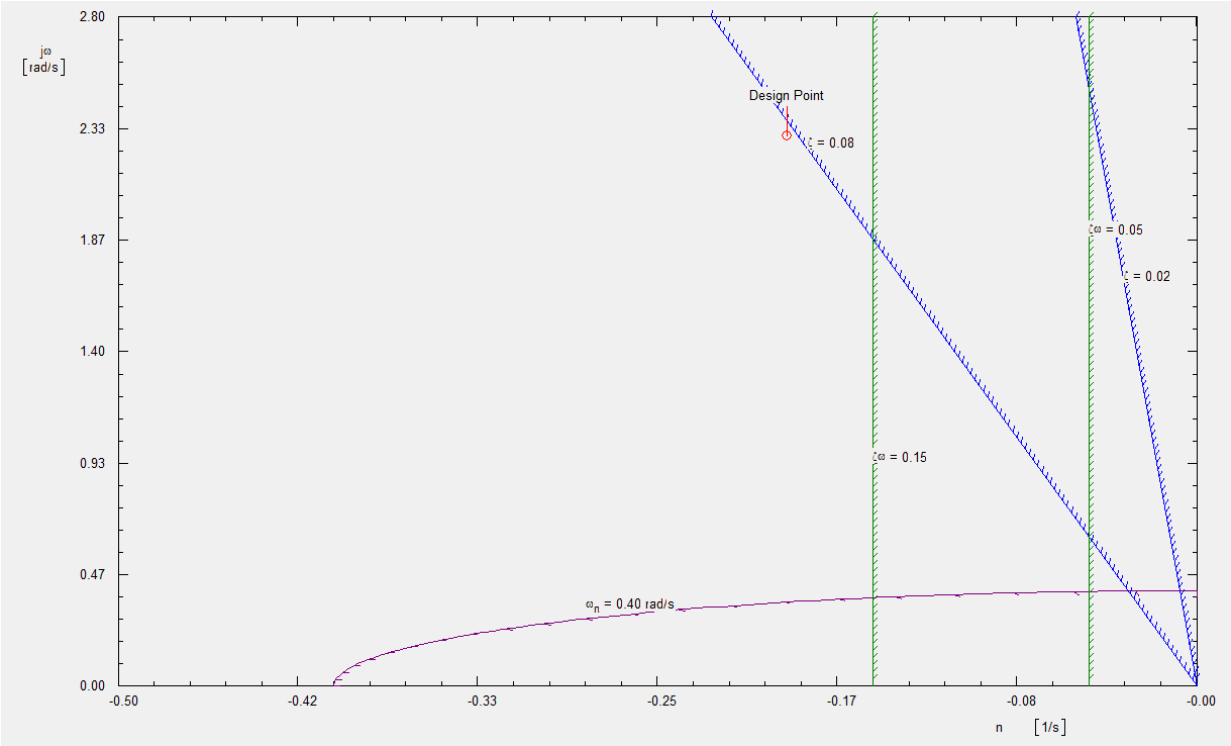

Figure 16-3: Meadowlark AAA Dutch Roll Frequency and Damping Ratio Requirements During Cruise

17 Ride Quality and Comfort

Gust sensitivity and ride quality are crucial for customer acceptance and minimization of crew and aircraft fatigue. These, in turn, maximize the aircraft's life, have an associated reduction of DOC, and can safely operate in more extreme conditions. Mathematical modelling can be done to analyze ride and comfort characteristics, as found in Roskam's *Airplane Design Part VII*. The ride comfort index, C_{ride}, is a function of lateral and vertical acceleration, a_{lat} and a_{vert} respectively. These equations can be seen below.

$$a_{vert} > 1.6a_{lat} \qquad C_{ride} = 2 + 18.9a_{vert} + 12.1a_{lat}$$

$$a_{vert} < 1.6a_{lat} \qquad C_{ride} = 2 + 1.62a_{vert} + 38.9a_{lat}$$

As seen from Figure 17-1, 50% of passengers are satisfied with a C_{ride} of 5.9 or lower. To calculate C_{ride}, the equations for vertical and lateral acceleration are substituted in, getting the following equation, which assumes an isotropic gust, σ_w.

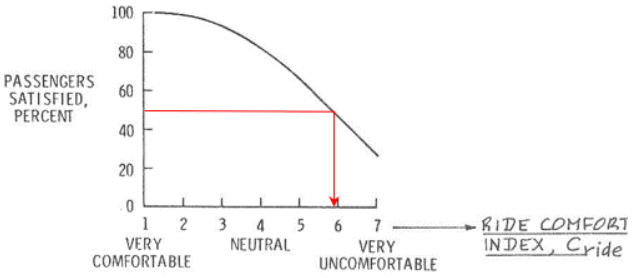

Figure 17-1: Ride Comfort Index and Customer Satisfaction

$$C_{ride} = 2 + \frac{\rho U_1 \sigma_w}{2\left(W/S\right)}\left(18.9C_{L\alpha} + 12.1C_{Y\beta}\right)$$

From known geometries and basic assumptions based off of their design, the following characteristics of the Meadowlark, Boeing's SUGAR Volt, and the EMB 190 are found, seen in Table 17.1

Table 17.1: Characteristic Comparison

	Meadowlark	SUGAR Volt	EMB 190
C_{L_α}	4.9	6.4	5.1
$C_{L_{\alpha\,dyn}}$	2.6	6.4	5.1
C_{Y_β}	-0.94	-1.5	-0.92
W/S	120	129	109

Based on these characteristics, the velocity due to turbulence can be calculated for the same three aircraft, seen below in Table 17.2.

Table 17.2: Velocity Due to Turbulence

Altitude, h (ft)	Density, r (slug/ft^3)	U_1 (ft/s)	Meadowlark	SUGAR Volt	EMB 190	U_1 (kts)
0	0.002378	350	18.6	8.7	12.0	207
5000	0.002048885	377	20.0	9.4	13.0	223
10000	0.001756153	407	21.6	10.1	14.0	241
15000	0.001496238	441	23.4	11.0	15.2	261
20000	0.001266998	479	25.5	11.9	16.5	284
25000	0.001065582	523	27.8	13.0	18.0	310
30000	0.00088961	572	30.4	14.2	19.7	339
35000	0.000736942	629	33.4	15.6	21.6	373

These amplitudes of turbulence can be graphed on top of lines that indicate what level of gusts (light, moderate, or severe) will cause what level of altitude change. The three aircraft can be seen in Figure 17-2.

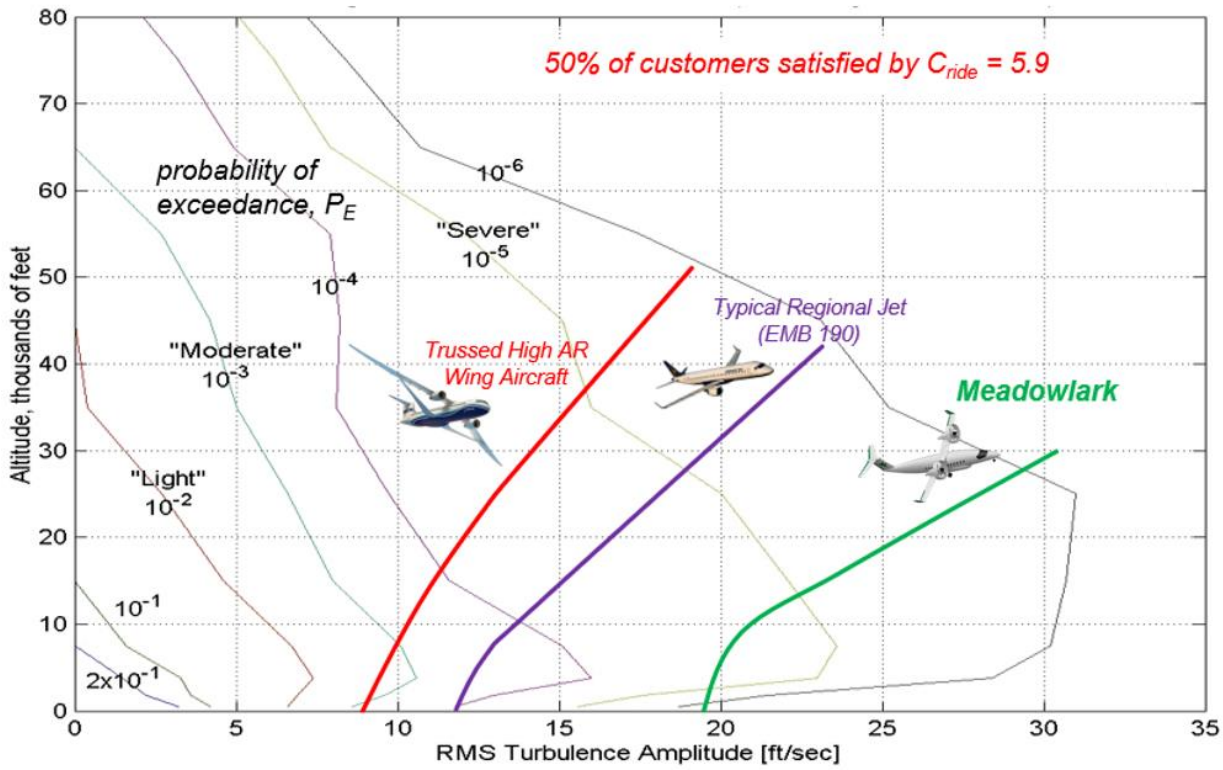

Figure 17-2: Turbulence Intensities

As seen in the figure, the SUGAR Volt and EMB 190 have much less resistance to gusts the Meadowlark. The Meadowlark also has less altitude change than the other aircraft when the same gusting occurs. The Meadowlark's ride quality will be superior to these jets. The Meadowlark provides customers with a smoother ride than new jets and highly used jets. Operational tempos are key to the Meadowlark's mission and success. The Meadowlark's high resistance to gust reactions allows it to maintain safe high operational tempos in more extreme conditions. This feature, along with the fast turn time, allows for more flights per day and more revenue generated.

18 Performance and Acoustics

18.1 Takeoff Performance

Meadowlark initial design for takeoff requirements is to meet the takeoff distance of 4,500 ft over a 50 ft obstacle to a runway with dry pavement (ISA + 18°F). The Meadowlark takeoff performance when further analyzed accounting for ground affect during takeoff effectively taking away induced drag. The Meadowlark landing values are the same as the takeoff. Meadowlark's takeoff and landing distances shown in Table 18.1 prove opportunity for STOL applications as well.

Table 18.1: Class II Takeoff Performance for Meadowlark

Performance Metric	Meadowlark
Takeoff Distance, s_{to} (ft)	3300
Takeoff Ground Distance s_{TOG} (ft)	640
Balanced Field Length, BFL (ft)	3810

18.2 Drag Polar and Wetted Area

The wetted area of all Meadowlark components is calculated to a higher accuracy to in turn increase the accuracy of the drag polars. The components analyzed are the fuselage, engine nacelles and ducts, wing, and empennage.

18.2.1 Fuselage Wetted Area

For finding the fuselage wetted area, two methods can be implemented. The first is to use the equation to the right. Assuming the fuselage has a circular cross-section, the wetted area of the fuselage was found by using an average of the equation in AAA, and the wetted area was found to be 1940 ft^2.

$$S_{wetFus} = \pi D_f l_f (1 - 2/(\frac{l_f}{D_f})^{\frac{2}{3}}(1 + (\frac{D_f}{l_f})^2) \quad \textbf{Equation 8-1}$$

The second, and more accurate, method of finding the fuselage wetted area is the perimeter method. The peak shown in Figure 18-1 is where the sponsons are integrated into the aircraft. Using the cross section shown in Figure 18-1, the perimeters were found and plotted, leading to a wetted area of 2,084 ft^2, seen in Figure 18-2. When comparing the values from the perimeter plot and AAA, there is a 7% difference. The error can be attributed to accounting for the sponsons. The wetted area used for the drag polar calculation is the area found from the perimeter method.

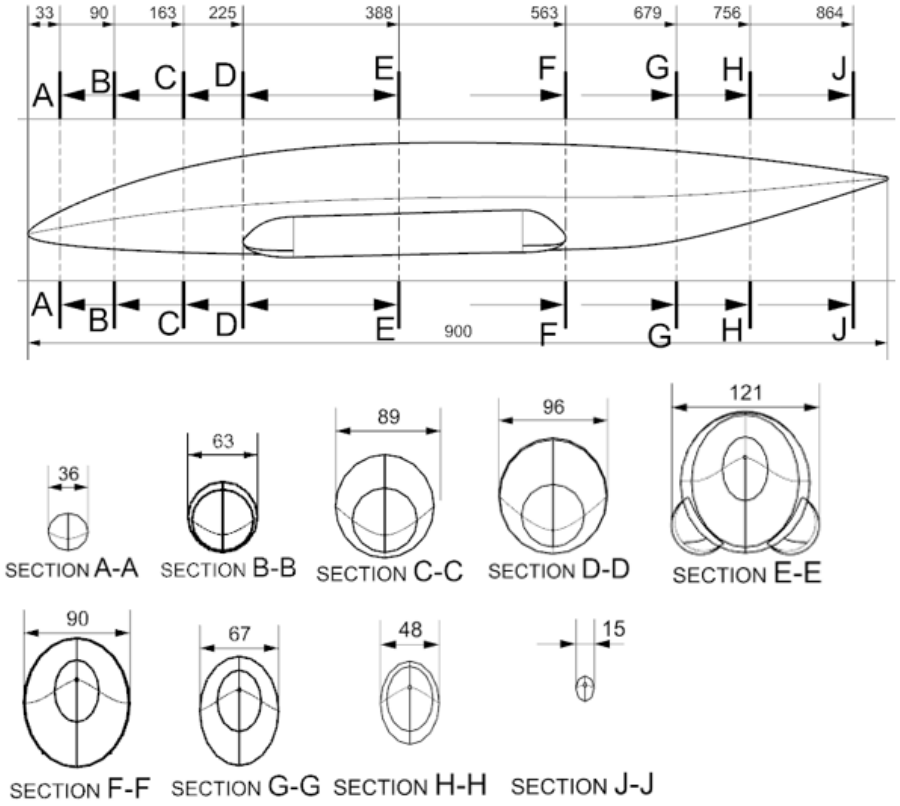

Figure 18-1: Perimeter Cross-Section Analysis

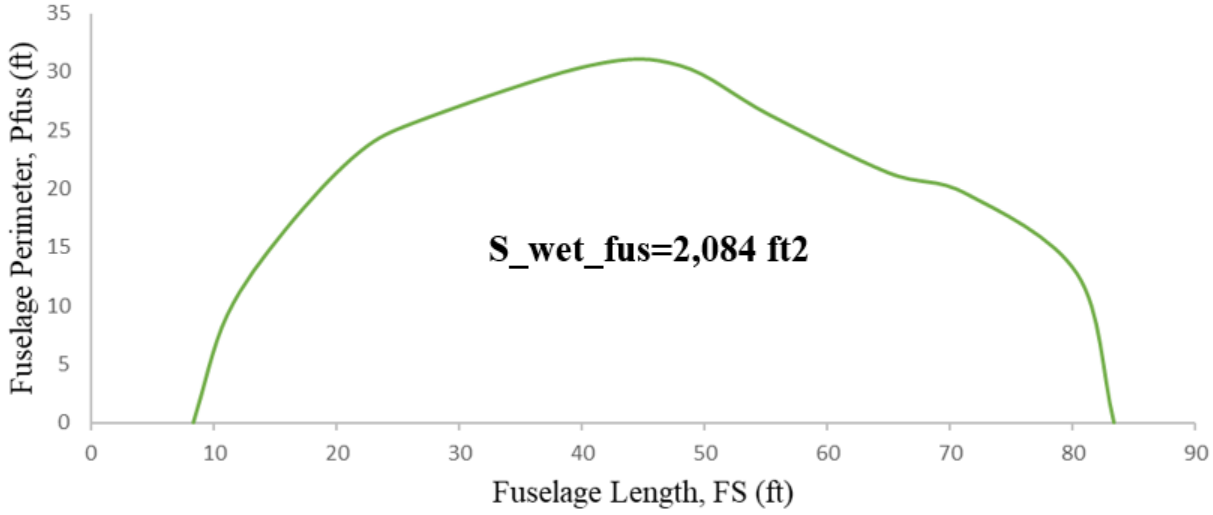

Figure 18-2: Perimeter Plot and Wetted Area

18.2.2 Engines Wetted Area

The contributors to the engine wetted area include the engine nacelle and the propellor ducts. The combination of these two wetted areas are calculated to a final value of 263.9 ft^2, seen in Table 18.2.

Table 18.2: Engine Wetted Area

$S_{wet,propulsion}$ (ft^2)		
Nacelles	**Ducts**	**Total Area**
75.4	188.9	263.9

18.2.3 Wing Wetted Area

The geometry of the wing is used to find the wetted area of the wing. The final wetted area of the wing is found to be 490.4 ft^2 as seen in Table 18.3.

Table 18.3: Wing Wetted Area

Root Chord, c_r (ft)	7.14
Root Thickness, t_r (ft)	0.99
Tip Chord, c_t (ft)	2.86
Tip Thickness, t_t (ft)	.05
S_{wet} (ft^2)	490.4

18.2.4 Empennage Wetted Area

The characteristics used to calculate the wetted area of the empennage are seen in Table 18.4. The final wetted area for the empennage is a summation of the vertical tail and horizontal tail wetted area. The empennage wetted area is calculated to be 213.36 ft^2.

Table 18.4: Empennage Wetted Area

Characteristic	Horizontal Tail	Vertical Tail
Root Chord, c_r (ft)	6	9.21
Root Thickness, t_r (ft)	0.72	1.1
Tip Chord, c_t (ft)	3.5	7
Tip Thickness, t_t (ft)	0.42	0.84
Swet (ft^2)	111.38	101.98

18.2.5 Aircraft Wetted Area

The total aircraft wetted area is found by summing the component wetted areas. The total aircraft wetted area is 3052 ft^2 and is found in Table 18.5.

Table 18.5: Total Aircraft Wetted Area

Component	Wetted Area
Fuselage (ft^2)	2084
Engine Nacelle and Duct (ft^2)	263.9
Wing (ft^2)	490.4
Horizontal Tail (ft^2)	111.38
Vertical Tail (ft^2)	101.98
TOTAL (ft^2)	3052

18.3 Acoustics

Principles of acoustic suppression were thought of when thinking of the design of the Meadowlark. As the Meadowlark has a ducted propeller, the acoustics will be compared to that of a jet engine. By ducting the propeller, noise is reduced for side line observers. This is important because of how close the engines are to the cabin. As the Meadowlark has a high wing design, the high engines allow for acoustic waves to be reflected upwards. This is unlike the EMB 190, as the lower wing, lower engine design reflects noise downward. The comparison can be seen in Figure 18-3 and Figure 18-4.

Figure 18-3: EMB 190 Acoustic Refraction

Figure 18-4: Meadowlark Acoustic Refraction

19 Cost Analysis

The cost of the aircraft is analyzed utilizing the AAA cost analysis tool as well as utilizing a few assumptions. The team wanted to look further into the lifecycle of the Meadowlark as this is where it will have established itself in the market and have the required infrastructure for maximum productivity. The Meadowlark team chose to keep the configuration of the aircraft similar to those already in market to reduce the cost of maintenance. The cost is also only evaluated for the aircraft not the advanced technologies during ground operations. The cost and price can be seen in Table 19.1. A visual of aircraft price related to how many aircraft a company can manufacture can be seen in Figure 19-1.

Table 19.1: Meadowlark Cost and Price

Acquisition Cost ($ in Millions)	Price Per Aircraft ($ in Millions)
34.2	39.3

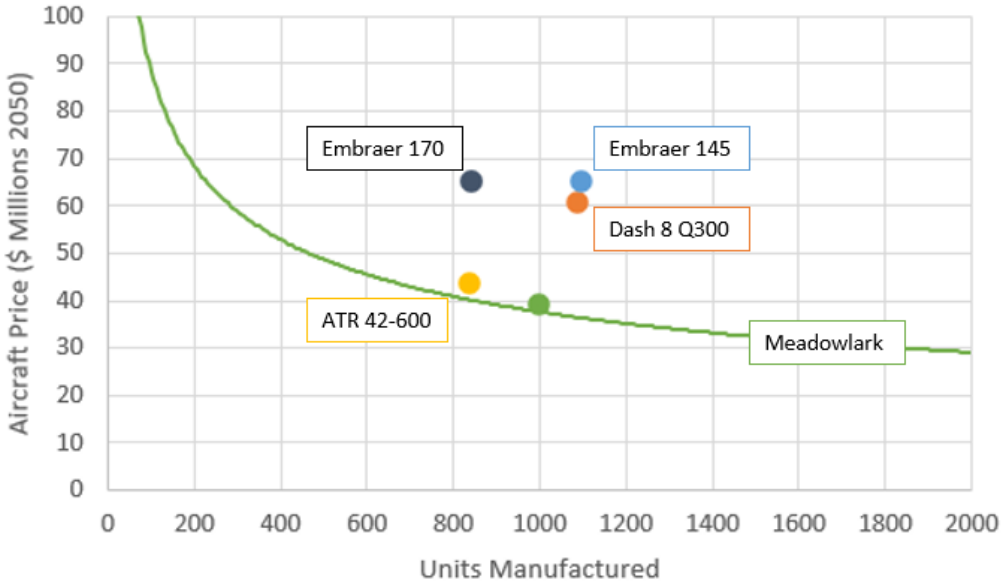

Figure 19-1: Aircraft Price vs. Units Manufactured [36] [57] [58]

References

[1] AIAA, "Hybrid-electric Regional Turboprop RFP," 2022, [Online].

[2] "ATR 42-600 The ideal local commuter", *ATR Aircraft,* 2023. https://www.atr-aircraft.com/our-aircraft/atr-42-600/.

[3] "ATR 42, ATR 72 production list," *RZJets*, 2023. https://rzjets.net/aircraft/?typeid=310.

[4] "ATR 72-600: The most fuel efficient regional aircraft," *ATR Aircraft*, 2023. https://www.atr-aircraft.com/our-aircraft/atr-72-600/.

[5] "Who we are," *ATR Aircraft*, 2023. https://www.atr-aircraft.com/about/who-we-are/.

[6] "Everything You Need To Know About The Fokker F27," *Simple Flying*, 2021. https://simpleflying.com/fokker-f27/.

[7] "Fokker F-50 Turboprop Passenger Airliner," *Aerospace Technology*, 2023. https://www.aerospace-technology.com/projects/fokker-f50/.

[8] Jackson, P., "EADS CASA – Aircraft: Spain," *Jane's All the World's Aircraft 2007-2008,* Jane's Information Group Limited, Surrey, 2007, pp. 551-552.

[9] "Bae ATP/J61," *BAe Systems*, 2023. https://www.baesystems.com/en/heritage/british-aerospace----atp---jetstream-61.

[10] "30 Years of Flight: The Story Of The Saab 2000," Simple Flying, March 2022. https://simpleflying.com/saab-2000-30-years-story/.

[11] Jackson, P., "CANADA: Aircraft – Bombardier," *Jane's All the World's Aircraft 2007-2008,* Jane's Information Group Limited, Surrey, 2007, pp. 70.

[12] "Bombardier to discontinue Q200/Q300 in 2009", *Flight Global*, April 2008. https://www.flightglobal.com/bombardier-to-discontinue-q200/q300-in-2009/79686.article.

[13] "Q Series" (PDF). Bombardier. 2017. Archived from the original (PDF) on April 16, 2018.

[14] "Avro 748 & Avro 748MF," *BAe Systems*, 2023. https://www.baesystems.com/en/heritage/avro-748---avro-748mf.

[15] "Hawker Siddeley HS 748", Royal Australian Navy. https://www.navy.gov.au/aircraft/hawker-siddeley-hs-748.

[16] "Hermes: Bristol Hercules: 1960: 2695: Flight Archive." *Flight Archive*, 2016. https://web.archive.org/web/20160306094314/https:/www.flightglobal.com/pdfarchive/view/1960/1960%20-%202695.html.

[17] "Handley Page H.P.R.3 Herald / H.P.R.7 Dart Herald," Avia Deja Vu, https://aviadejavu.ru/Site/Crafts/Craft21767.htm.

[18] "EMB-120 Cargo Conversion," *Worldwide Aircraft Services, Inc*., WASI Publications, Missouri, Sept. 5, 2000, pp. 3-5.

[19] "Embraer EMB-120 Brasilia specs," *Aviation Safety Network*, 2023. https://aviationsafety.net/database/types/Embraer-120-Brasilia/specs.

[20] "Embraer ERJ-145," *Aerospace Technology*, 2023. https://www.aerospacetechnology.com/projects/erj145/#:~:text=The%20ERJ%2D145%20is%20Embraer's,operational%20with%2027%20airlines%20worldwide.

[21] "Light Passenger Jets: Bombardier CRJ 700," *Aerocorner*, 2023. https://aerocorner.com/aircraft/bombardiercrj-700/

[22] "Embraer 170," *Aerospace Technology*, 2023. https://www.aerospace-technology.com/projects/embraer_170/

[23] "Airline Pilot Forums," MH Sub I, LLC dba Internet Brands, 2017.

[24] Barrett-Gonzalez, R., 2021. *AE 522 Regional Jet Lecture*, April 8, 2021.

[25] Airfleets, 2023. https://www.airfleets.net/home/

[26] Lewis, P., "SkyWest pursues expansion plans."

[27] “SkyWest – Facts,” *Skywest Airlines*, 2023. https://skywest.com/about-skywest-airlines/facts.
[28] “So – How Does It Work?,” *Mototok*, 2023. https://www.mototok.com/how-does-it-work.
[29] “Autonomous Electric Tow Tugs Could Cut Handling Costs”, *AIN Online*, Nov. 13, 2020. https://www.ainonline.com/aviation-news/business-aviation/2020-11-13/autonomous-electric-tow-tugs-could-cut-handling-costs.
[30] “How to Clean a Plane,” *Aviation Pros*, Feb. 8, 2017. https://www.aviationpros.com/gse/blog/12303102/how-to-clean-a-plane.
[31] “Composicean Products Page,” *Composiclean*, https://composiclean.com/products.html.
[32] 罗元建, “Green airport intelligence aircraft tractor,” CN Patent 202022069426, Jan. 8, 2021.
[33] Hinman et al., “Aircraft Charging Unit,” US Patent 11433775B1, Sep. 6, 2022.
[34] Hafenrichter, J., Georgeson, G., “Walking Robot,” US Patent 10773761B2, Sep. 15, 2020.
[35] Roskam, J., *Airplane Design, Part I: Preliminary Sizing of Airplanes*, DARcorporation, Kansas, 1985.
[36] Jackson, L., Scharf, O., Nilaweera, B., et al., “Skyblazer,” University of Kansas, Kansas, May 13, 2021.
[37] “ATR 42-600: The ideal local commuter,” *ATR Aircraft*, 2023. https://www.atraircraft.com/wpcontent/uploads/2022/06/ATR_Fiche42-600-3.pdf.
[38] “Bombardier DASH 8 Q300,” *Airlines Inform*. https://www.airlines-inform.com/commercial-aircraft/dash-8q300.html/.
[39] Roskam, J., *Airplane Design, Part III: Layout Design of Cockpit, Fuselage, Wing and Empennage: Cutaways and Inboard Profiles*, DARcorporation, Kansas, 1986.
[40] “Introducing the Freedom Seat,” *Molon Labe Seating*, 2019. https://www.airlineseats.biz/how-it-works.
[41] “PW121,” *Turbine Options*, 2023. https://turbineoptions.com/home/pw100/pw121/#.
[42] “PW121,” *Aircraft database*, 2021. https://aircraft-database.com/database/engine-models/pw121.
[43] “Pratt & Whitney Runs First Hybrid-Electric Engine Ground Test,” *AINonline*, Dec. 20, 2022. https://www.ainonline.com/aviation-news/air-transport/2022-12-20/pratt-whitney-runs-first-hybrid-electric-engine-ground-test.
[44] “ATR, P&WC Reveal ATR 42/72 Upgrade Plan,” *Aviation Week Network*, Nov. 15, 2021. https://aviationweek.com/shownews/dubai-airshow/atr-pwc-reveal-atr-4272-upgrade-plan.
[45] “Collins Aerospace completes preliminary design of 1MW electric motor for Pratt & Whitney Canada’s Regional Hybrid-Electric Flight Demonstrator,” *Collins Aerospace*, July 18, 2022. https://www.collinsaerospace.com/news/news/2022/07/collins-complete-preliminary-design-of-1mw-electric-motor-for-pratt-whitney-canada.
[46] Roskam, J., *Airplane Design, Part II: Preliminary Configuration Design and Integration of the Propulsion System*, DARcorporation, Kansas, 1985.
[47] Voskuijl, M., van Bogaert, J. & Rao, A.G. “Analysis and design of hybrid electric regional turboprop aircraft,” *CEAS Aeronaut J* Vol. **9**, Oct. 2017, pp. 15–25. https://doi.org/10.1007/s13272-017-0272-1.
[48] “De Havilland Canada Working with Pratt & Whitney Canada to Support the Development of Sustainable Hybrid-Electric Aircraft Propulsion Technology,” *De Havilland Aircraft of Canada Limited*, July 15, 2021. https://dehavilland.com/en/news/posts/de-havilland-canada-working-with-pratt-whitney-canada-to-support-the-development-of-sustainable-hybrid-electric-aircraft-propulsion-technology.
[49] “These 7 simple airplane fixes could cut carbon emissions in half at little to no cost,” *PBS*, Nov. 2013. https://www.pbs.org/newshour/science/these-7-simple-airplane-fixes-could-halve-carbon-emissions-at-little-to-no-cost.
[50] “CU Denver Researcher Analyzes the Use of Solar Energy at U.S. Airports: 20% of U.S. Airports Have Adopted Solar Power in the Last Decade,” *CU Denver News*, Sep. 2020. https://news.ucdenver.edu/cu-denver-researcher-analyzes-the-use-of-solar-energy-at-u-s-airports/.
[51] “Seeking Space for Solar Farms, Cities Find Room at Their Airports,” *New York Times*, Dec. 2021. https://www.nytimes.com/2021/12/07/business/airports-solar-farms.html.

[52] “FOTW #1234, April 18, 2022: Volumetric Energy Density of Lithium-ion Batteries Increased by More than Eight Times Between 2008 and 2020,” *Office of Energy Efficiency & Renewable Energy*, April 2022. https://www.energy.gov/eere/vehicles/articles/fotw-1234-april-18-2022-volumetric-energy-density-lithium-ion-batteries.
[53] Roskam, J., *Airplane Design, Part V: Component Weight Estimation*, DARcorporation, Kansas, 1985.
[54] “RAY: Hospital-Grade UVC Disinfection,” *Aero Hygenx*. https://www.aerohygenx.com/products/ray.
[55] “Honeywell Unveils Anthem, The Aviation Industry’s First Cloud-Connected Cockpit System,” *Honeywell*, Oct. 2021. https://www.honeywell.com/us/en/press/2021/10/honeywell-unveils-anthem-the-aviation-industry-s-first-cloud-connected-cockpit-system
[56] Anon., “Telair.pdf,” *Telair International.*
[57] “ATR 42-600 Specs, Interior, Cockpit, and Price,” *Airplane Update*, https://www.airplaneupdate.com/2019/08/atr-42-600.html#:~:text=The%20price%20of%20the%20latest%20ATR%2042-600%20aircraft,27%20ATR%2042-320%20for%20FedEx%20are%20in%20conversion.
[58] “Bombardier Dash 8 Q300 Specs, Interior, Cockpit, and Price,” *Airplane Update*, https://www.airplaneupdate.com/2019/10/bombardier-dash-8-q300.html#:~:text=The%20price%20of%20the%20latest%20Bombardier%20Dash%208,Q300%20aircraft%20is%20around%20US%20%24%2017%20Million.